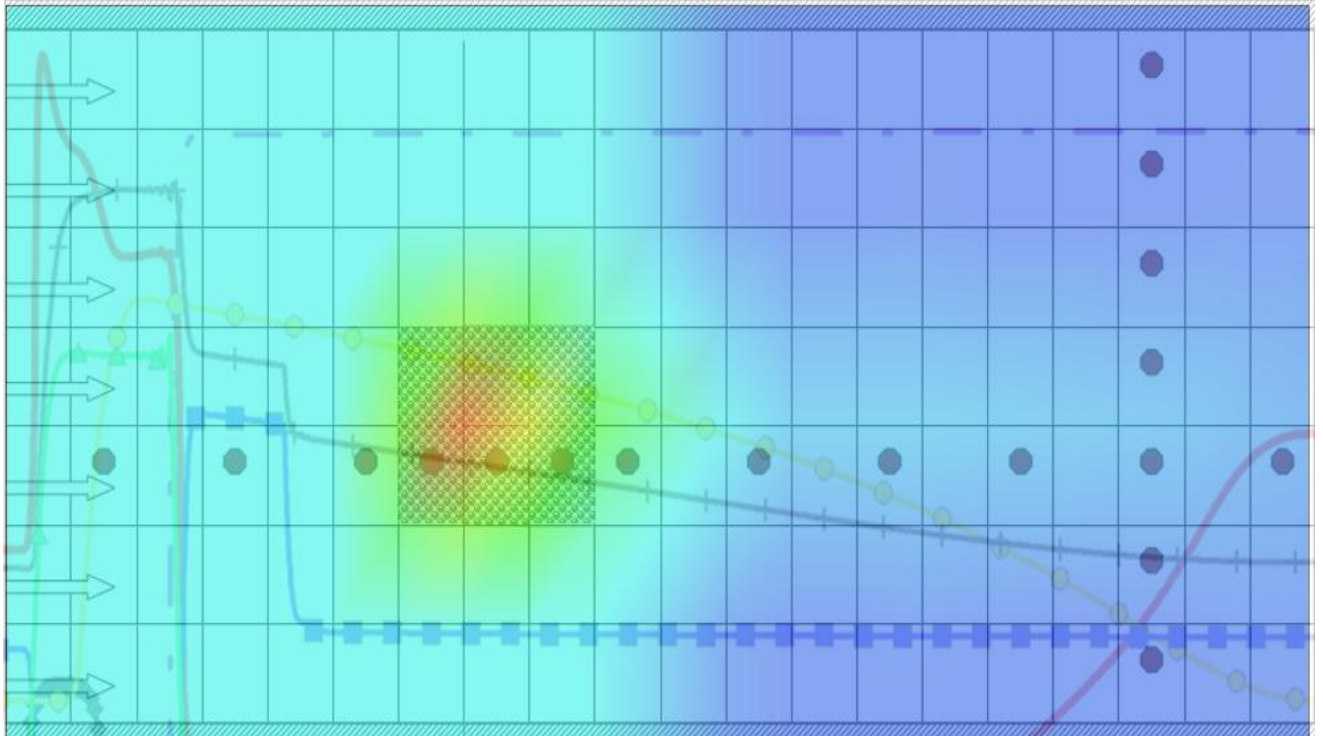# Modeling feedback driven remediation

A modeling study for the monitoring of efficiency, during KMnO$_4$-based in-situ chemical oxidation of PCE contamination

Status	**[Definitive]**

Title	**Modeling feedback driven remediation**

Subtitle	**A modeling study for the monitoring of efficiency, during KMnO$_4$-based in-situ chemical oxidation of PCE contamination.**

Graduation thesis	Master Hydrology track: Environmental Hydrogeology Department of Earth Sciences Faculty of Geosciences University Utrecht

Organization	Deltares Department Soil & Groundwater systems Princetonlaan 6, 3584 CB, Utrecht

Project	UPSOIL Seventh Framework Program 6th Work Package

Author	Frank Versteegen Graduation intern Deltares MSc student Environmental Hydrogeology University Utrecht 　　　E: f.g.versteegen@gmail.com 　　　T: +31611401984

Supervisors	Dr. Niels Hartog (Utrecht University; Deltares) Dr. Johan Valstar (Deltares) Prof. Dr. Ruud Schotting (Utrecht University)

Date	10-08-2011

Content

List of figures

List of tables

.

List of appendices

Preface

The report lying in front of you is the result of a graduation internship performed at Deltares, Utrecht. More than that, it is the culmination of the two years research master Environmental Hydrogeology, followed at the University Utrecht.

This research has been carried out during a six months internship at Deltares, a Dutch-based research institute specialized in a wide range of water, soil and subsurface related topics. As one of the main goals is to develop knowledge, Deltares participates in many European projects in which it cooperates with universities and other research institutions. This report adds to the UPSOIL project. One of the goals of this project is to increase efficiency of existing remediation techniques such that contaminated soil and groundwater sites can be cleaned up more cost-effective.

The remediation technique investigated in this study is In Situ Chemical Oxidation (ISCO). This technique involves the injection of an oxidant that converts hazardous contaminants into less (or non-) hazardous components. It is widely used to clean up sites contaminated with chlorinated solvents. Efficiency related issues arise when it is not exactly known where the source zone is situated. Common practice often comes down to the injection of an oxidant, whereafter the change in contaminant concentration is measured. So knowledge of the ongoing process limits to the amount of oxidant injected and the change in contaminant concentration. Whether the target compound, i.e. the contamination, or the non-target compounds (such as pyrite or organic matter) are mainly oxidized is not known.

Subject of this study is the applicability of certain indicators, which can provide insight in the remediation efficiency during clean up. Main idea is that monitoring the concentration of certain components results in a better idea whether or not the remediation is efficient. Based on indicators interventions can be made to increase efficiency.

The results of this study are presented in this report, my master thesis. I would like to thank Deltares for giving me the opportunity to do this research and finish my master in a highly regarded research institute. I found the atmosphere in this company inspiring, and thanks to the numerous maps on the wall, I really felt at home here.

Furthermore, I would like to thank my two supervisors at Deltares, Dr. Niels Hartog and Dr. Johan Valstar. Without their help on geochemical processes and computer modeling I wouldn't have managed to do this research. I think that the knowledge acquired from you during the weekly meetings will prove to be a very welcome addition in my further career.

And, finally, I would like to thank my fellow interns at Deltares for making the six months a really joyful period. And yes, you international students, it often rains in the Netherlands!

Frank Versteegen

Summary

Over the past two decades, In Situ Chemical Oxidation (ISCO) has proved to be an effective remediation technique to clean up DNAPL contaminated sites. Previous studies concerning permanganate-based ISCO remediation show that focus now shifts from proof of concept towards efficiency related issues (a.o. Hood et al., 2000; Kao et al., 2008; Henderson et al.,2009). Efficiency losses of injected oxidants occur due to the presence of natural oxidant demand, as well as lack of exact information on the contamination source zone. In this study it is investigated if feedback driven remediation can improve the efficiency of permanganate-based ISCO technique. Feedback driven remediation implies the use of indicators to adjust remediation characteristics (such as injection rate, oxidant concentration, location) during the process.

In this study a two dimensional MODFLOW/PHT3D-based reactive multi-component transport model has been created. Focus of the model has been to find indicators amongst field parameters that could quantify the remediation progress during an ISCO process. The injected oxidant is potassium permanganate, the contamination consist of a tetrachloroethylene (PCE) source zone at residual saturation. The aquifer composition varies in organic matter content, pyrite and calcite presence.

From stoichiometric relations it is known that the oxidation of organic matter by potassium permanganate consumes H^+, which results in an increased pH. Oxidation of aqueous phase PCE by potassium permanganate, on the other hand, produces H^+, resulting in a decrease of the pH. Other indicators are: chloride, calcium, CO_2 species and sulfate.

From the different modeled scenarios, it followed that chloride is the strongest indicator for the oxidation of $PCE_{(aq)}$. Chloride fluxes have been used to determine efficiency of the $PCE_{(aq)}$ oxidation. Following previous work (a.o. Schnarr et al.,1998), the measured chloride concentration is used to determine the mass of $PCE_{(aq)}$ oxidized through the stoichiometric relation. In this manner, for all modeled scenarios the efficiency of the injected permanganate has been determined. Efficiencies found are low: <1% of the injected permanganate reacts with $PCE_{(aq)}$. The main reason for this low efficiency is found to be the mass transfer rate from the nonaqueous phase PCE into the aqueous phase.

The pH of the groundwater proved to be a strong indicator. Although the pH of groundwater is dependent on other factors, such as the aquifer mineralogy and the presence of potential pH buffering components like calcite, the oxidation of $PCE_{(aq)}$ reflected clearly in pH values within this study.

The calcium concentration, involved through the dissolution and precipitation of calcite, showed to effectively indicate the moment at which oxidation of the target compound was prevailing. Because calcium concentration depends on calcite dissolution and precipitation, which in turn depends on temperature, pH and CO_2 pressure in the soil it is considered a weak indicator.

The reflection of prevailing oxidizing processes on the CO_2 species concentration is weak, as both target and non-target compounds result in an increase of CO_2 concentration.

The indicators are finally used to conduct a feed back driven modeling scenario for which a 'rule of thumb', based on pH measurements, has been used to adjust the injection

1. Introduction

1.1 Background of in situ chemical oxidation (ISCO)

NAPL contamination

The subsurface plays an important role in many human activities as well as in natural/eco systems. For food production, drinking water supply as well as for a healthy environment the quality of the soil and groundwater is of crucial importance. On the other hand the subsurface is intensively used for, from the quality point of view, potentially threatening human activities. These imply the storage of mass (think of (nuclear) waste, toxics, and recently the discussions on CO_2 storage), energy (like Aquifer Thermal Energy Storage), excavation of resources and construction of facilities and infrastructure (such as highways, pipelines and sewerage). These human activities should not come at the expense of the quality of soil and groundwater. However, either due to the lack of knowledge, accidents or due to conflicting interests numerous contaminated areas have been created when contaminants were released on or below the ground from drums, tanks and landfills. It is estimated that up to 250.000 contaminated sites are present within the European Economic Area which require clean up (UPSOIL Proposal, 2009), as they form a direct threat to soil and groundwater quality. The predominant group of contaminants at these sites is the organic contaminants.

Organic contaminants include hydrocarbons, such as chlorinated aliphatic hydrocarbons (CAH's) and polycyclic aromatic hydrocarbons (PAH), as well as BTEX (benzene, toluene, ethyl benzene and xylenes). These contaminants come in different forms: in the soil gas phase, the soil aqueous phase, adsorbed to the soil solid phase, and as non-aqueous phase liquid (NAPL) that can be either lighter (LNAPL) or denser (DNAPL) than water (Fetter, 2008). Once released on the surface these NAPL contaminants migrate through the subsurface, moving by gravity through the vadose zone until they reach the water table (figure 1.1). As it moves through the vadose, or unsaturated, zone it leaves behind residual levels of non-aqueous phase contaminant, held between the grains of the porous media by capillary forces. In the unsaturated zone of a contaminated site the pores are often filled with three phases: residual water/soil moisture, gas (air) and residual non aqueous phase liquid. Once the water table is reached LNAPL's will form a layer or pool that floats above the water table, thereby slowly dissolving into groundwater passing below it.

Chlorinated solvents are denser than water (DNAPL's) and will sink below the water table, possibly moving through cracks and joints or sinking through discontinuous clay layers (fig. 1.1) Thereby again leaving residual 'droplets' in the pore spaces, which now 'share' the pore space with only two phases, water and residual non aqueous phase liquids. DNAPL's will continue sinking until a low permeable layer is reached, where it will spread out creating a high saturation DNAPL "pool" (figure 1.1.) (Goltz et al., 2007) or until the total spilled volume has been spread out as residual droplets.

From a risk point of view the most important contaminants are the CAH's: a family of compounds that are commonly used as chlorinated organic solvents. The most prevalent of these CAH's are tetrachloroethylene (PCE), trichloroethylene (TCE) and trichloroethane (TCA). Within this research the cleanup of a (hypothetical) PCE contaminated site is subject.

Chlorinated organic solvents are widely used for dry cleaning processes in the textile industry (PCE is therefore also known as 'dry cleaning fluid'). But a wide range of industries uses chlorinated solvents. Actually, the three largest contributors to their use and their release into the environment are the electronic, instrument manufacturing, and the aerospace industries (Pankow and Cherry, 1996).
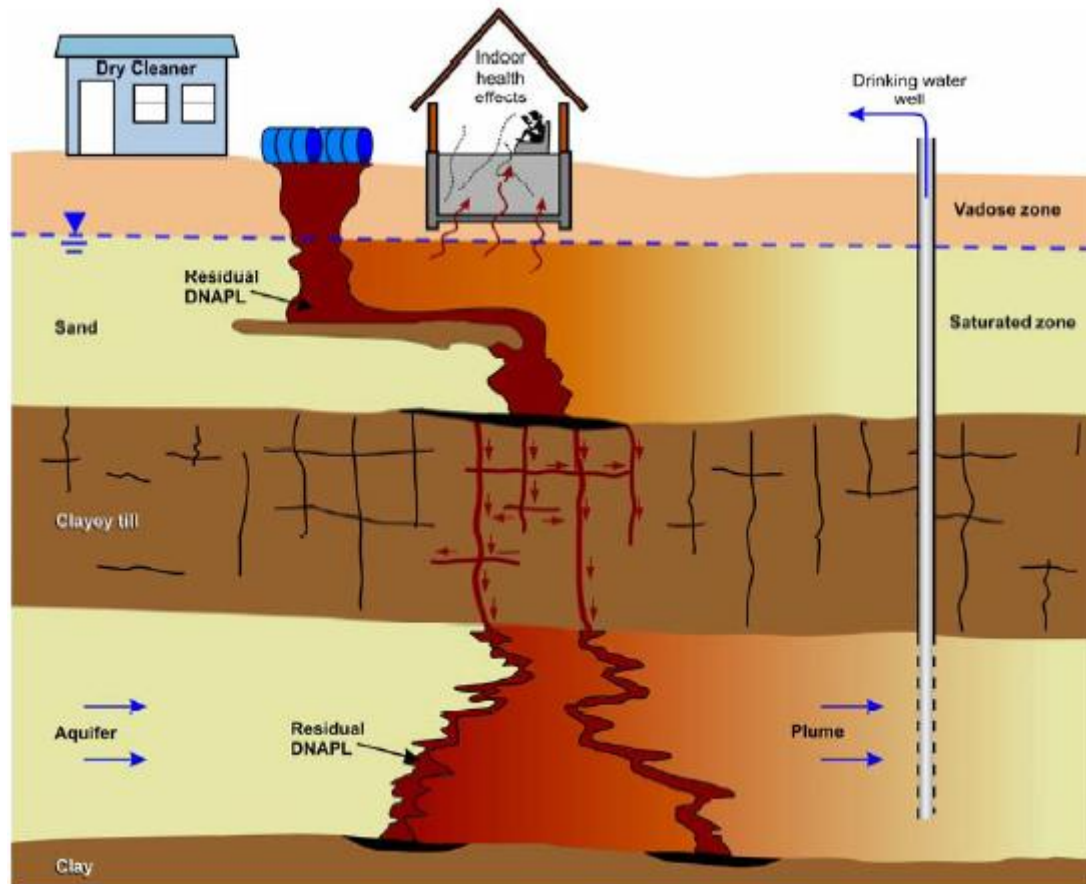
Figure 1.1   Distribution and migration of DNAPL contamination in subsurface (source: J. Hønning, 2007)

ISCO remediation

First awareness of the scale of the problem of soil and groundwater contamination by NAPL's began in the late 1970's to early 1980's (Mayer and Hassanizadeh, 2005). Since then intensive research efforts have led to 'an enhanced understanding of NAPL migration in subsurface, improved characterization of NAPL's as sources of groundwater contamination, appropriate site investigation techniques for assessing NAPL contamination, and better technologies and strategies for remediating NAPL-contaminated sites' (Mayer and Hassanizadeh, 2005). Several well-known remediation techniques are pump & treat, soil excavation and soil washing, monitored natural attenuation, air sparging, bioremediation and chemical oxidation. Subject of this research is the cleanup of a (hypothetical) PCE contaminated site using in situ chemical oxidation (ISCO).

ISCO involves the introduction of chemical oxidants into the soil to convert hazardous contaminants into nonhazardous or less toxic compounds (UPSOIL Proposal, 2009; Kao et al., 2008). One popular ISCO method for the treatment of aquifers contaminated with chlorinated solvents is chemical oxidation based on the injection of potassium permanganate ($KMnO_4$) (Heiderscheidt et al., 2008; Henderson et al., 2009; Hønning, 2007). Laboratory experiments as well as field scale projects have demonstrated effective NAPL mass removal by injecting this oxidant. Permanganate is, together with catalyzed hydrogen peroxide (Fenton's reagens), the most common oxidant used in ISCO applications (Xu and Thomson, 2008).

Permanganate

Permanganate (MnO_4^-) has been used for decades to treat wastewater. About 20 years ago the first in situ remediation was carried out using permanganate. There are two forms of permanganate which are commonly used for the in situ treatment of chlorinated solvents: potassium permanganate and sodium permanganate.

Potassium permanganate ($KMnO_4$) is a crystalline solid from which aqueous MnO_4^- solutions up to (40 g/l) permanganate saturation can be prepared on site. Sodium permanganate comes as a concentrated liquid, with higher permanganate saturation. But because liquids are more expensive to transport, potassium permanganate is the most widely used oxidant of these two (Hønning, 2007). Another advantage, especially in the light of this research, is that permanganate is applicable over a wide pH range and it is a very stable oxidant that can persist in the subsurface for months. Permanganate can auto decompose by reacting with water, resulting in non-productive depletion of permanganate, but this reaction expires at very slow rates.

UPSOIL project

Although in situ treatment of contaminated sites is widely used, there are some 'general key issues relating to the sustainability and cost-effectiveness due to (UPSOIL Proposal, 2009. p.16):

- loss of oxidant through reactions with the natural soil oxidant demand (e.g. components such as organic matter and iron sulphides),
- mitigation of potential adverse effects (e.g. mobilizing metals or formation of toxic by-products),
- reduced biological soil functions, including natural attenuation capacity, after ISCO application, and
- faster reaction rates complicate the monitoring of the remediation process.'

These and other processes cause that in-situ remediation techniques are not yet utilized to their full potential. To optimize biochemical remediation techniques a large international European project is founded: "Sustainable Soil Upgrading by Developing Cost effective, Biogeochemical Remediation Approaches" (project acronym UPSOIL). It is a collaborative project carried out by an international consortium of research institutions, amongst which Deltares in the Netherlands (www.upsoil.eu). The goal of the project is summarized as follows (UPSOIL Proposal, 2009. p.9):

"The project's aim is to make the required breakthrough in in-situ (bio)chemical remediation for organic contaminants, by developing robust technologies for fast, cost-effective, integrated source zone and plume treatment that result in both allowable (risk) levels and maximal use of the natural soil rehabilitation potential at a longer term."

To achieve these objectives the project is subdivided into seven work packages. In this research a contribution is made to the sixth work package of the UPSOIL project. The focus within this package is feedback driven remediation. It is believed that feedback driven remediation 'can further optimize the speed, cost-effectiveness and sustainability of the remediation efforts' (UPSOIL Proposal, 2009. p.23). This by using data about the progress made and adjusting the oxidant injection rates according to this data during the remediation process. Before focusing on feedback driven ISCO remediation, some more detail about conventional ISCO remediation is described.

Conventional ISCO

The conventional ISCO method is to first determine the size, volume and content of the contaminated area and then, depending on these characteristics, inject a certain amount of chemical oxidants into the system. After a certain time, measurements are performed to see if the concentration is below the maximum contaminant level (MCL). If this is the case, the project is considered successful. If this is not the case, oxidant injection is repeated until the concentration is below the MCL. Although this method might be effective, the efficiency of this

method – defined by Henderson et al. (2009) as 'the fraction of the injected oxidant which reacted with the contaminant'- can be rather low.

Other possible causes of consumption of the oxidant in the system include reaction with naturally present organic matter and/or with reactive solid phases such as pyrite. Though these reactions might be unavoidable, as naturally present oxidant demand is often both available and reactive, losses might be reduced to a minimum if one has better insight in what is going on during the remediation process.

Other efficiency related issues with the conventional ISCO technique are flushing of the dissolved contamination out of the system due to high injection flow rates and the effect of concentration rebound from remained pure phase NAPL's. In addition, some of the injected oxidant can persist as unreacted oxidant (Henderson et al., 2009).

Feedback driven ISCO

With feedback driven remediation information about field parameters, such as pH value, chloride-, sulfate- and calcium concentrations, redox potential, temperature, specific conductance, heavy metals concentrations and other water quality parameters are considered. This information can be used to adjust the oxidant concentrations and injection flow rate during the remediation process. One method to do so is to use a segmented well, with which various injection rates and oxidant concentrations can be added at various depths, based on breakthrough observations of chemical components downstream of the contaminated site. However, because many measurements need to be done in order to be able to use this technique it is expensive and considered an elaborate technique.

1.2 Research objectives

Previous studies concerning permanganate-based ISCO remediation show that focus shifts from proof of concept towards efficiency related issues (a.o. Hood et al., 2000; Kao et al., 2008; Henderson et al.,2009). It is believed that feedback driven remediation based on indicators can further improve the efficiency of permanganate-based ISCO technique. Using the PHT3D model, which is a '3D, MODFLOW/MT3DMS-based reactive multicomponent transport model' (Prommer et al., 2001), this study will provide in modeling scenarios to increase insights in the use of indicators. Focus will be to find indicators amongst the mentioned field parameters that can be used to quantify the remediation progress made during the ISCO process.

Therefore, the aim of this research is to:

1. find indicators which increase insights in the efficiency of chemical oxidation during the remediation process, and
2. see if injection characteristic adjustments (such as rate, concentration, depth) can be based upon indicators found under (1).

The research questions that will be answered are the following:

Q$_1$: **Is pH an effective indicator for the progress made during the KMnO$_4$ based ISCO remediation of a DNAPL contaminant source?**

> Q$_{1A}$: How does this pH indicator work for different aquifer conditions?
> Or:
> How sensitive is this indicator to presence of different organic matter content, pyrite content and calcite content?

Q$_2$: **Which other indicators can be used to improve the determination of efficiency?**

Q$_3$: **Can certain general rules be applied, based on measurements of the indicators, to adjust injection characteristics in order to improve efficiency?**

1.3 Report outline

To answer the research questions, Chapter 2 first describes the main hydrological and geochemical processes for ISCO remediation at a PCE contaminated site. By declaring the governing equations the processes affecting the fate and transport of aqueous phase PCE are described first. Then the geochemical reactions that are triggered by injecting potassium permanganate in the subsurface are described, as well as the influence on the carbonate equilibrium. Goal of these paragraphs is to define possible indicators from the defined stoichiometric relations which can be used to indicate the efficiency of an ISCO remediation progress.

In the third chapter the model packages, the way in which they are coupled and the most important input files are described.

In the fourth chapter a batch model has been created to see how:

1) the defined indicators reflect on the different oxidation processes and

2) the interaction between different oxidation processes affect the indicators.

Flow is excluded to study only the oxidation reactions without flow induced mixing effects.

Once it is known how the different oxidation processes reflect on the defined indicators, it is investigated if they can be used in a more realistic field situation. To do so, a 2D flow model has been constructed. As there is no field data available for this study, this flow model is based on literature studies.

In the Discussion section (chapter 6), this study is reflected and results are related results obtained in other studies.

In the Conclusions and Recommendations section (Chapter 7) the main conclusions are summarized and recommendations for further research are made.

2. Background and principles

2.1 Introduction

In this chapter a detailed description is given of the main principles and the background of hydrological and geochemical processes that apply at a PCE contaminated site, subject of permanganate based chemical oxidation.
These are:

- Dissolution of non-aqueous phase PCE into the aqueous phase.
- Transport of aqueous phase PCE concentration by
  - Advection
  - Diffusion
  - Dispersion
- Retardation of aqueous phase PCE transport due to:
  - Sorption
- Decrease of (aqueous) contaminant concentration due to:
  - Degradation

These processes, which influence the fate and transport of (aqueous) PCE in the subsurface, are described first in §2.2, where it is emphasized here that the only degradation process included is oxidation by potassium permanganate. Biodegradation of PCE through reductive dechlorination is not taken into account within this study, as this process is not expected relevant under the highly oxidizing conditions during ISCO treatment.
Competition between the contaminant and organic material present in the soil matrix to react with the oxidant causes loss of oxidant. The second part of this chapter (§2.3 and §2.4) focuses on the implications of injecting potassium permanganate into the soil. The oxidation of non-target components (organic matter and pyrite) is described by their chemical reactions (§2.3). The influence of the oxidation reactions of both the target component (PCE) and the non-target components on the geochemistry is described in §2.4.

2.2 Hydrogeological processes

Solutes dissolved in groundwater are subject to a number of different hydrogeological processes through which they are either transported or removed from the groundwater. The processes described in this paragraph are declared by their governing equations. The equations in this chapter are based upon transport of solutes through saturated porous media (single-phase flow) (Fetter, 2009). In this case the dissolved solute of interest is the aqueous phase PCE, which dissolves into groundwater from the nonaqueous phase PCE.

The main transport process is advection. Advection is the process by which dissolved solutes are carried along by the flowing groundwater. Flowing groundwater is moving at rates that are both greater and less than the average linear velocity. This effect is known as hydrodynamic dispersion. When the flowing groundwater carries along dissolved solutes, dispersion causes mixing and spreading of the solutes.

Solutes dissolved in groundwater are also subject to other processes, such as sorption and chemical reactions. Dissolved solutes can adsorb onto the surfaces of the mineral grains or onto organic carbon present in the aquifer. As a result of this the solutes will move slower through the aquifer than the groundwater that transports them: this is called retardation.

By chemical reactions the composition of the groundwater can be changed. In this case of looking at in situ chemical oxidation of a PCE contaminated site this result in the oxidation of aqueous phase PCE thereby producing a.o. chloride.

Each of the abovementioned processes is now described into more detail by declaring their governing equation and the way the process is included in this modeling study.

2.2.1 Dissolution

Non-aqueous phase PCE is immobile (i.e. not transported by flowing groundwater) when present in the subsurface at or below residual saturations (Langevoort, 2009, p. 131; Mayer and Miller, 1996). Thus before PCE can be transported by or extracted from the groundwater, it must dissolve into it. Dissolution takes only place at the interface of the nonaqueous phase PCE and the groundwater.

The dissolution rate, or mass transfer rate, from non-aqueous phase PCE (PCE_{NAPL}) to aqueous phase PCE ($PCE_{(aq)}$) is a decisive parameter in this research, since it determines – in combination with the groundwater flow characteristics – the concentration of $PCE_{(aq)}$. Moreover, since potassium permanganate has negligible solubility in PCE_{NAPL} – precluding a direct chemical reaction between the oxidant and the DNAPL - the dissolution process determines how much of the contaminant becomes available to react with the oxidant. This is described by Heiderscheidt et al. (2008), who shows that for a tank-scale ISCO experiment the mass transfer from the DNAPL to the aqueous phase is an important limiting factor on ISCO efficiency.

The driving force of the dissolution process is the difference between the actual concentration in water and the maximum concentration that PCE can reach in water: the solubility limit.
The solubility limit of PCE is the concentration of the aqueous phase ($PCE_{(aq)}$) in equilibrium with the nonaqueous phase (PCE_{NAPL}) (Mayer and Hassanizadeh, 2005). The solubility limit value for PCE, as well as the intervention- and target value as set by the Dutch Government and other parameter values for PCE, are given in table 2.1.
$PCE_{(aq)}$ concentration will tend to equilibrium, i.e. the solubility concentration. The closer to the equilibrium situation the slower the dissolution will be. However, non-equilibrium exist when the rate of processes in the aqueous phase, such as advection or degradation/oxidation are potentially faster than the dissolution rate (Langevoort, 2009. pp.131).

Table 2.1   *Parameter values for PCE.*

PCE	Value	Unit	Source
• Formula	C_2Cl_4	-	-
• Solubility limit (at 25°C)	197.8	[mg / l]	Mayer and Hassanizadeh (2005)
• Density (at 25°C)	1622	[g / l]	Mayer and Hassanizadeh (2005)
• Molar Mass	165.83	[g / mole]	Mayer and Hassanizadeh (2005)
• Mass transfer coefficient	0.98	[day^{-1}]	Henderson et al. (2009)
	5.2	[day^{-1}]	Langevoort (2009)
• Intervention (MCL) value	0.04	[mg / l]	VROM (2009)
	$2.4\cdot10^{-7}$	[mole / l]	
• Target value	0.00001	[mg / l]	VROM (2009)
	$6\cdot10^{-11}$	[mole / l]	

When the aqueous concentration is low, the mass flux from the non-aqueous phase into the aqueous phase will be relatively high. When the aqueous concentration tends towards the solubility limit, the flux will decrease. The following first-order kinetic relation describes the rate of dissolution:

$$r_{diss}^{PCE} = -\kappa^{PCE}(C^{sat,PCE} - C_{aq}^{PCE})$$ (2.1)

Where:

r_{diss}^{PCE} = the dissolution rate from the pure phase PCE to PCE(aq) [mole l^{-1} T^{-1}]

κ^{PCE} = lumped mass transfer coefficient of PCE[1] [1/T]

$C^{sat,PCE}$ = the solubility of PCE in water [mole l^{-1}]

C_{aq}^{PCE} = the aqueous phase concentration of PCE [mole l^{-1}]

Two values have been obtained for the mass transfer coefficient of PCE: one value from Henderson et al. (2009) and one from Langevoort (2009) (table 2.1). The difference between the values of Langevoort (2009) and Henderson et al. (2009) could be due to the difference in scale of interest, respectively laboratory scale and field scale. Mayer and Miller (1996) prove that both the magnitude and configuration of a residual NAPL source zone have an impact on the mass transfer rate coefficient. Within this study a field-scale model is used, therefore the value of Henderson et al. (2009) is used predominantly. The value given by Henderson et al. (2009) is specified as a 'model calibration parameter', while Langevoort (2009) obtained the mass transfer coefficient through an empirical equation (adapted from Mayer and Miller, 1996), involving the dimensionless Sherwood number, *Sh* (Langevoort, 2009, pp. 132; Mayer and Miller, 1996):

$$Sh^{PCE} = \frac{\kappa^{PCE}d^2}{D_m^{PCE}} = \beta_0^{PCE}\,Re^{\beta_1^{PCE}}(S^{PCE})^{\beta_2^{PCE}}$$ (2.2)

Where:

κ^{PCE} = lumped mass transfer coefficient [1/T]
d = mean particle diameter [L]

---

[1] The lumped mass transfer coefficient κ^{PCE} actually substitutes the product of an average mass transfer coefficient, k^{PCE}, for the total specific interfacial area between the pure phase PCE and groundwater for an representative elementary volume (REV), a.

κ^{PCE} is used because for field situations it is not possible to make detailed estimates of the interfacial area (Langevoort, 2009 p.17).

D_m^{PCE} = molecular diffusion coefficient [L/T^2]

Re = Reynolds number $\left(= \dfrac{v \rho d}{\mu} \right)$

Where:

v = specific discharge [L T^{-1}]

ρ = density of fluid [M L^{-3}]

d = diameter of the tube, or in this case of flow through porous medium: representative grain diameter [L]

μ = dynamic viscosity of fluid [M L^{-1} T^{-1}]

S^{PCE} = Saturation of PCE in the NAPL (= 1 in this case, since only PCE)

β_0^{PCE}, β_1^{PCE} and β_2^{PCE} = empirical parameters

Kim and Gurol (2005) have also examined DNAPL dissolution rates. Their batch experiments show that the rate of dissolution of a DNAPL is proportional to the volume of the DNAPL. As the volume of the DNAPL decreases the dissolution rate decreases. Schnarr et al. (1998) prove that this is also valid at field scale. As in this study a field scale is simulated, this effect must be taken into account. To do so the formulation for the PCE$_{NAPL}$ dissolution rate includes a mechanism for rate decrease with decreasing PCE$_{NAPL}$ saturation: a ratio of PCE$_{NAPL}$ concentration over initial PCE$_{NAPL}$ concentration (eq. 2.3).

Another important effect concerning the dissolution from the PCE$_{NAPL}$ into the groundwater has to do with the distribution of the PCE$_{NAPL}$. As dissolution can only take place at the surface between the nonaqueous phase PCE and groundwater, the total surface area that is in contact with water is important. For example, dissolution from residual droplets will be faster compared to an equal volume distributed as one connected pool. This because the area in contact with water is larger when the total volume is spread out over small droplets. In this study it is assumed that PCE$_{NAPL}$ is present at residual saturation divided over spherical droplets. For a spherical shape it holds that if the volume decreases, the surface area decreases at lower pace. This has to do with the fact that the surface area decreases quadratic, while volume decreases with the third power of the radius. In other words, the smaller the diameter of the droplets, the more surface area it has relatively to its volume. By adding a power of 2/3 to the ratio, this area/volume effect is taken into account for. This yields:

$$ r_{diss}^{PCE} = -\kappa^{PCE} (C^{sat,PCE} - C_{aq}^{PCE}) \left(\frac{C_{t=t}^{PCE\,NAPL}}{C_{t=0}^{PCE\,NAPL}} \right)^{2/3} \qquad (2.3) $$

Where:

$C_{t=0}^{PCE\,NAPL}$ = initial concentration pure phase PCE [mole l$_{bulk}^{-1}$]

$C_{t=t}^{PCE\,NAPL}$ = concentration pure phase PCE at t=t [mole l$_{bulk}^{-1}$]

As in Henderson et al. (2009) the concentration of pure phase PCE$_{NAPL}$ and PCE$_{(aq)}$ are related by a 1:1 stoichiometric relation, indicating that for every dissolving mole PCE$_{NAPL}$ one mole of PCE$_{(aq)}$ is added to the groundwater:

$$ C_2 Cl_{4\,(DNAPL)} \rightarrow C_2 Cl_{4\,(aq)} \qquad (2.4) $$

2.2.2 Advection

Once dissolved to the aqueous phase, PCE is transported by flowing groundwater. Advection of solutes occurs as a result of the motion of their host fluid, i.e. groundwater. The amount of solute that is being transported (mass flux) is a function of its concentration in the groundwater and the velocity at which groundwater is flowing (Fetter, 2008 p.50). The quantity of groundwater flowing, which is called convection, will be described first.

Convection
The quantity of groundwater flowing is given by Darcy's Law, which states that the amount of water flowing through a certain cross sectional plane is proportional to the head loss and inversely proportional to the flow length. In the 1D form Darcy's Law can be expressed as:

$$Q_x = -K_x A \frac{dh}{dx}$$

(2.5)

Where:

Q_x = volumetric discharge in x-direction [l / T]

K_x = hydraulic conductivity in x-direction [L]

A = cross-sectional surface plane perpendicular to flow direction [L^2]

$\frac{dh}{dx}$ = hydraulic head gradient in x-direction [L/L]

Instead of the volumetric flow rate the specific discharge, or Darcy flux, is often used to indicate flow rates. This is the volumetric flow rate divided by the cross sectional area, A, giving:

$$q = \frac{Q}{A} = -K_x \frac{dh}{dx}$$

(2.6)

The actual velocity at which the water flows through the pores, referred to as effective velocity or pore velocity, is then the Darcy flux corrected for the void space in the matrix (porosity ϕ):

$$v_{eff} = \frac{q}{\phi}$$

(2.7)

It is implied in the above equations that the specific discharge is parallel to the direction of dh/dx and that the medium is isotropic (i.e. $K_x=K_y=K_z=K$). However due to anisotropy in the subsurface, this form of Darcy's Law is sometimes not sufficient to describe convection in a non-laboratory setting. In a more general form, specific discharge is a first order tensor, or vector, meaning that it is a quantity consisting of three components (q_x, q_y and q_z) which all have both a magnitude and a direction. It is expressed as **q**. Also, the hydraulic head is a vector comprising h_1, h_2 and h_3 and expresses as **h**. Hydraulic conductivity, **K**, is a second-order tensor, and can be described by nine components. Using the nabla symbol (∇) to denote Darcy's Law as del notation yields:

$$\mathbf{q} = \mathbf{K} \square \nabla \mathbf{h}$$

(2.8)

Advection
The governing equation to describe the movement of solutes as a result of the motion of their host fluid is given by the balance of mass for the solute (Hassanizadeh, 2007).
In a one-dimensional form this is:

$$\frac{\partial \phi C_{aq}^{PCE}}{\partial t} + \frac{\partial F}{\partial x} = r_{sources} - r_{sinks}$$

(2.9)

Where:

ϕ = porosity [-]

C_{aq}^{PCE} = the aqueous PCE concentration [ML^{-3}]

F = the solute mass flux [$ML^{-2}T^{-1}$]

$r_{sources}$ = rate of sources = dissolution rate r_{diss}^{PCE}

r_{sinks} = rate of sinks = adsorption rate r_{ads}^{PCE} and oxidation rate r_{ox}^{PCE}

In a three dimensional form this becomes:

$$\frac{\partial \phi C_{aq}^{PCE}}{\partial t} + \nabla \cdot F = r_{diss}^{PCE} - r_{ads}^{PCE} - r_{ox}^{PCE}$$ (2.10)

If there is only advective transport, the mass flux is given by:

$$F = C_{aq}^{PCE} q .$$ (2.11)

Implementing the mass flux F yields:

$$\frac{\partial \phi C}{\partial t} + \nabla \cdot (C_{aq}^{PCE} q) = r_{diss}^{PCE} - r_{ads}^{PCE} - r_{ox}^{PCE}$$ (2.12)

2.2.3 Hydrodynamic dispersion

As mentioned in the introduction of this paragraph, differences in flow velocities in the pores of the porous medium cause mixing of the solutes known as the process of mechanical dispersion. Hydrodynamic dispersion is the sum of mechanical dispersion and diffusion.

Diffusion
"A solute in water will move from an area of greater concentration toward an area of lower concentration" (Fetter, 2008 p45). This process is known as molecular diffusion, and can be described by Fick's first law, which states that the mass of fluid diffusing is proportional to the concentration gradient. Fick's first law adapted for porous media yields (Hassanizadeh, 2007):

$$F = -\phi D_{eff} \frac{\partial C_{aq}^{PCE}}{\partial x}$$ (2.13)

Where
D_{eff} = effective molecular diffusion coefficient [L^2/T], which is related to the molecular diffusion coefficient by tortuosity.

Because under most conditions of groundwater flow diffusion makes up a negligible part of the total hydrodynamic dispersion term (Fetter, 2008 p.57) it is neglected within this study.

Mechanical dispersion
Where diffusive spreading is a consequence of concentration differences, mechanical dispersion is caused by deviations of pore-scale and small scale flow velocity from the average flow velocity. These deviations are due to (fig. 2.1):
1. the fact that some pores are larger than others, which allows the fluid flowing through these pores to move faster,
2. the irregular shape of the grains in the matrix some of the fluid particles will travel along longer flow paths in the porous media than other particles while they travel the same linear distance, and
3. the fact that fluid will move faster in the center of the pores than along the edges.
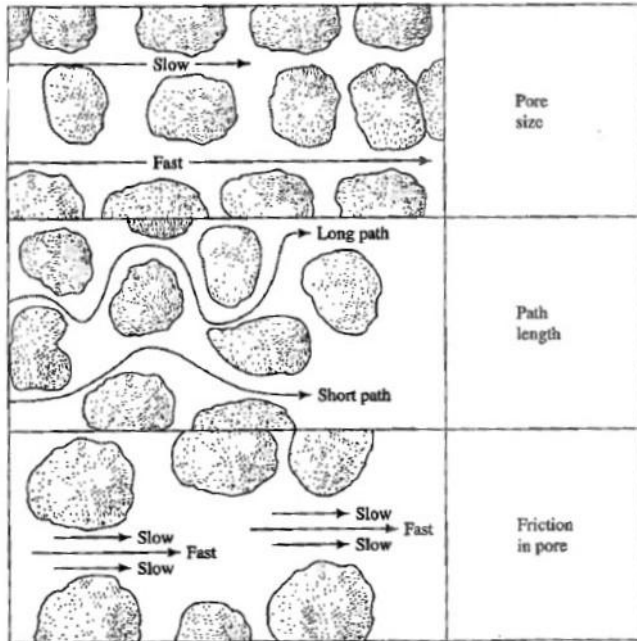
Figure 2.1   *Mechanical dispersion (source: Fetter, 2008)*

These phenomena together are referred to as mechanical dispersion and, like diffusion, cause mixing of the solute concentrations resulting in a dilution of the solute at the advance edge of flow (Fetter, 2008 p.53). The mixing that occurs along the direction of the flow path is called longitudinal dispersion. But the mixing will not restrict to the direction of the flow path, it also occurs normal to the flow path direction: transverse dispersion.

The amount of dispersion is a function of the average linear velocity and a property of the medium, called dispersivity α.

Hydrodynamic dispersion
Diffusion and mechanical dispersion are combined in the hydrodynamic dispersion coefficient, D. The governing equation to express hydrodynamic transport can again (like advective transport) be expressed in the mass balance (one-dimensional):

$$\frac{\partial \phi C_{aq}^{PCE}}{\partial t} + \frac{\partial F}{\partial x} = r_{diss}^{PCE} - r_{ads}^{PCE} - r_{ox}^{PCE} \tag{2.14}$$

Only now, the hydrodynamic dispersion mass flux is implemented in F:

$$F = C_{aq}^{PCE} q + J \tag{2.15}$$

Where J is the hydrodynamic dispersion mass flux derived from Fick's first Law:

$$J = -\phi D \frac{\partial C_{aq}^{PCE}}{\partial x} \tag{2.16}$$

The hydrodynamic dispersion coefficient D combines the effective molecular diffusion coefficient and mechanical dispersion:

$$D = D_{eff} + \alpha v \approx \alpha v \tag{2.17}$$

Filling in the combined advective and dispersive mass flux (eq. 2.15 and 2.16) in equation 2.12 gives the following one-dimensional advection-dispersion mass balance:

$$\frac{\partial \phi C_{aq}^{PCE}}{\partial t} + \frac{\partial}{\partial x}\left(C_{aq}^{PCE}q - \phi D \frac{\partial C_{aq}^{PCE}}{\partial x}\right) = r_{diss}^{PCE} - r_{ads}^{PCE} - r_{ox}^{PCE} \qquad (2.18)$$

In three-dimensional form, using Nabla notations, the total transport equation can be written as follows:

$$\frac{\partial \phi C}{\partial t} + \nabla \square (C_{aq}^{PCE}q) - \nabla \square (\phi D \square \nabla C_{aq}^{PCE}) = r_{diss}^{PCE} - r_{ads}^{PCE} - r_{ox}^{PCE} \qquad (2.19)$$

Note: the transformation from one dimensional form to three dimensional form is somewhat more complicated than presented here. For a detailed description the reader is referred to a standard work, such as Fetter (2008).
Now the two sink terms, being the adsorption rate and the oxidation rate, are further specified.

2.2.4 Sorption

Where the previous described processes transport and spread out the contamination through the aquifer, sorption retains solutes at their position. The main consequence of sorption processes is the (temporal) removal of the solute from the groundwater and consequently the retardation of the solute movement through the aquifer. There are several different sorption processes: adsorption, chemisorptions, absorption and ion exchange (Fetter, 2008. p.121). Adsorption is the process by which a solute clings to a solid surface of the soil matrix. The primary adsorptive surface is the fraction of organic solids in the soil or aquifer (Fetter 2008, p.135). A larger organic content of the soil results in more adsorption.

The amount of adsorbed mass is measured as mass fraction, s, which is the mass of adsorbed solute per unit mass of dry soil (Hassanizadeh, 2007). "When the adsorptive process is rapid compared with the flow velocity, the solute will reach an equilibrium condition with the sorbed phase. This process can be described by an equilibrium sorption isotherm (Fetter, 2008 p.122)":

$$s = K_d C_{aq}^{PCE} \qquad (2.20)$$

Where:
s = mass of adsorbed solute per unit mass of dry soil [-]
K_d = distribution coefficient [L^3/M], which is a soil characteristic parameter.
C_{aq}^{PCE} = concentration of aqueous phase PCE in equilibrium with the mass of solute sorbed onto the solid [M/L^3]

The distribution coefficient K_d is related to the amount of organic content in the soil by:
$$K_d = f_{oc} \cdot K_{oc} \qquad (2.21)$$

Where:
f_{oc} = mass fraction of organic carbon of the soil [M/M]
K_{oc} = Organic carbon partition coefficient, which is considered a constant for a given solute and given organic matter type for all soil types.

When K_d is known the retardation factor can be calculated:

$$R = 1 + \frac{(1-\phi)\rho_s}{\phi}K_d \qquad (2.22)$$

Where:

ρ_s = mass density of soil grains [M L^{-3}]

To implement the retardation factor in the advection-dispersion equation the time has to be scaled by R (Hassanizadeh, 2007):

$$R\frac{\partial \phi C}{\partial t} + \nabla \square (C_{aq}^{PCE} q) - \nabla \square (\phi D \square \nabla C_{aq}^{PCE}) = r_{diss}^{PCE} - r_{ads}^{PCE} - r_{ox}^{PCE} \qquad (2.23)$$

From this equation it is clear that adsorption has two effects:
1) Retard the movement of dissolved PCE, and
2) Decrease the availability of aqueous phase PCE, as the soil matrix takes up a certain amount.

However, despite these effects adsorption is neglected within this study. It is assumed that adsorptive effects do not influence oxidation processes as long as there is sufficiently PCE available: "The relevance of taking the adsorption of solutes into account depends on the presence residual NAPL. If relatively large amounts of residual NAPL is present, the amount adsorbed to soil particles is often insignificant" (Langevoort, 2009). As well, stated by Hønning (2007): "A low $K_{o.w.}$ value indicates that sorption of PCE is often limited in sandy aquifers". The $K_{o.w.}$ value (or Octanol - Water partition coefficient) is a measure of the hydrophobicity of an organic compound. The more hydrophobic a compound, the less soluble it is, therefore the more likely it will adsorb to soil particles.

Only at the end of the dissolution process, once all non-adsorbed PCE$_{NAPL}$ has been dissolved the adsorbed fraction would influence the aqueous concentration. As the focus of this research is the oxidation process of aqueous PCE, pyrite and organic matter, the interaction between these compounds and their reflection on potential indicators it is assumed that adsorption will not influence the conclusion.

One more argument to not incorporate the adsorption effect has to do with practical limitations raised by PHT3D. From equation 2.21 it is known that the K_d value depends on the organic matter content of the soil. In this study, the organic matter content is subject of chemical oxidation and thus it is not a constant value. This implies that the K_d value is dynamic, not constant. PHT3D only accounts for constant K_d values.

Equation 2.19 thus becomes:

$$\frac{\partial \phi C}{\partial t} + \nabla \square (C_{aq}^{PCE} q) - \nabla \square (\phi D \square \nabla C_{aq}^{PCE}) = r_{diss}^{PCE} - r_{ox}^{PCE} \qquad (2.24)$$

2.2.5 Oxidation by potassium permanganate

ISCO principle

In this study the oxidation of PCE$_{(aq)}$ by potassium permanganate is the only sink term in equation 2.23. In this research chemical oxidation is the main process. The main effect of chemical oxidation of PCE$_{(aq)}$ is to increase the dissolution 'driving force', i.e. the difference between the actual aqueous concentration and the maximum aqueous concentration (solubility limit). When aqueous phase PCE is oxidized the concentration gradient is maximized and thus the dissolution rate will be maximal. This is shown schematically in figure 2.2.
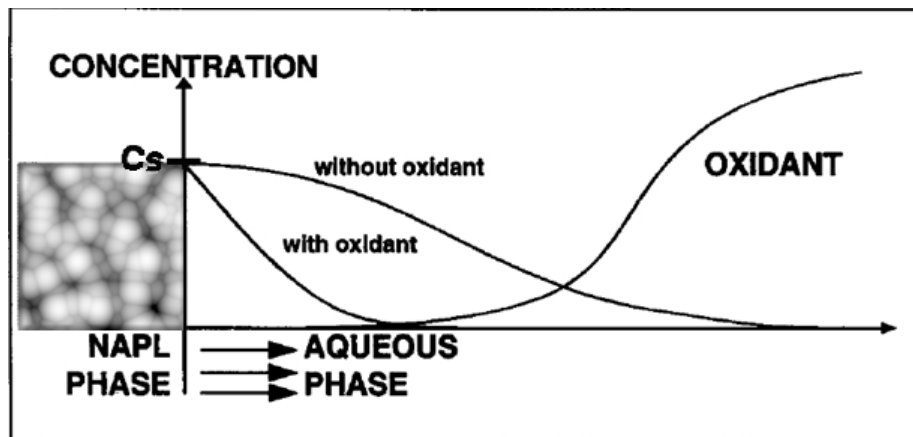
Figure 2.2   *Conceptual model describing mass removal by chemical oxidation.*
Cs = solubility limit of PCE. (source: Schnarr et al., 1998).

Stoichiometric reaction

In this study the molar concentrations of $PCE_{(aq)}$ and permanganate are related by the following stoichiometric relation (Heiderscheidt et al., 2008; Hood et al., 2000; Schnarr et al., 1998):

$$3C_2Cl_{4(aq)} + 4MnO_4^- + 4H_2O \rightarrow 6CO_{2(aq)} + 12Cl^- + 4MnO_{2(s)} + 8H^+ \qquad (2.25)$$
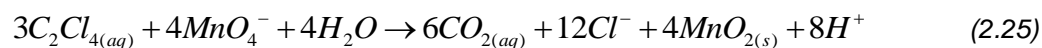
So for the oxidation of every mole $PCE_{(aq)}$ 4/3 mole permanganate is needed. Furthermore the stoichiometric relation shows the production of $CO_{2(aq)}$, Cl^-, manganese oxide (mineral) and H^+ as a result of PCE oxidation. Especially the production of H^+ (which cause a decrease of pH) and the production of Cl^- (which is unique for the oxidation of $PCE_{(aq)}$) play an important role in this research.

Permeability loss due to the production and accumulation of manganese oxide has been reported in several studies, while other studies show no significant reduction in permeability (Heiderscheidt et al., 2008; Henderson et al., 2009). Within this study permeability is kept constant, and thus no permeability loss by manganese oxide accumulation has been taken into account.

Rate expression

Huang et al. (2002) have studied the kinetics, reaction pathways and product distribution of oxidation of $PCE_{(aq)}$ by potassium permanganate. Their experimental results have demonstrated that the reaction is first order in both $PCE_{(aq)}$ and $KMnO_4$ and appears to be independent of pH (within the range of pH 3 – 10). The $PCE_{(aq)}$ degradation rates can be accelerated by increasing reaction temperature and oxidant concentration.

Huang et al. (2002) also state that the oxidation of $PCE_{(aq)}$ by permanganate proceed in a similar way as the reaction of $TCE_{(aq)}$ and permanganate. Contrary to the experiments conducted by Huang et al. (2002) in a field situation as modeled in this study, neither the potassium permanganate concentration nor the $PCE_{(aq)}$ concentrations are constant. In this study the oxidation of PCE thus depends on two first order reactants. Therefore, the oxidation of PCE is included as second order reaction in similar fashion as Henderson et al. (2009) implemented the oxidation of $TCE_{(aq)}$. i.e. a second order kinetic reaction with an overall reaction rate proportional to MnO_4^- and PCE concentrations (Henderson et al., 2009; Hood et al., 2000):

$$r_{ox}^{PCE} = -k_{ox}^{PCE}[PCE_{(aq)}][MnO_4^-] \qquad (2.26)$$

Where:

k_{ox}^{PCE} = Second order oxidation rate constant [mole^{-1} l day^{-1}]

$[PCE_{(aq)}]$ = aqueous phase concentration of PCE [mole l^{-1}]

$[MnO_4^-]$ = concentration of permanganate [mole l^{-1}]

Values for the second order oxidation rate constant, k_{ox}^{PCE}, found in literature are considerable consistent (table 2.2).

Table 2.2 *Reaction rate constants TCE and PCE with permanganate.*

Contaminant	Type rate constant	Oxidation rate constant contaminant – MnO₄⁻	Unit	Source
TCE	2nd order	56.200	Mole^{-1} l^2 H$_2$O l^{-1} bulk day^{-1}	Henderson et al. (2009)
TCE	2nd order	57.888	Mole^{-1} l day^{-1}	Yan & Schwartz (1999)
TCE	2nd order	55.296 – 79.488	Mole^{-1} l day^{-1}	Kao et al. (2008)
PCE	Pseudo 1st order	3,9	day^{-1}	Yan & Schwartz (1999)
PCE	Pseudo 1st order	6,9	day^{-1}	Huang et al. (2002)
PCE	2nd order	3.888	Mole^{-1} l day^{-1}	Yan & Schwartz (1998)
PCE	2nd order	3.528	Mole^{-1} l day^{-1}	Hood et al. (2000)
PCE	2nd order	3.024	Mole^{-1} l day^{-1}	Huang et al. (2002)

The final equation describing the change of mass over time, including all the described and included processes yields:

$$\frac{\partial \phi C}{\partial t} + \nabla \cdot (C_{aq}^{PCE} q) - \nabla \cdot (\phi D \nabla C_{aq}^{PCE}) =$$

$$\left(\kappa^{PCE} (C^{sat,PCE} - C_{aq}^{PCE}) \frac{(C_{t=t}^{PCE\,NAPL})^{2/3}}{(C_{t=0}^{PCE\,NAPL})^{2/3}} \right) - \left(k_{ox}^{PCE} [PCE_{(aq)}][MnO_4^-] \right) \qquad (2.27)$$

So far focus has been the fate and transport of (aqueous phase) PCE. The way dissolution and oxidation are defined in this modeling study as well as transport processes have been described by the governing equations, resulting in the final equation 2.27.

However, when studying the efficiency of in situ chemical oxidation of PCE in a field situation, as is simulated within this study, competition for the oxidant between target and non-target components play a major role (as already mentioned in §1.1 and §2.1).

The oxidation of non-target components such as organic matter and pyrite has major implications on the mineral and groundwater composition. And, as well an opposed effect on the pH compared to PCE oxidation (i.e. an pH increase due to H$^+$ consumption). In the next paragraph focus is the oxidation of non target compounds which are commonly present in soil matrices. As well the effect of the different oxidation reaction on the soil and groundwater geochemistry is described in more detail.

2.3 Geochemical processes

"Natural oxidant demand that is present in aquifer sediments competes for the injected oxidant as it consumes permanganate" (Henderson et al., 2009). The natural oxidant demand is referred to as NOD. It is generally expressed in grams MnO_4^- consumed per kilogram dry soil (Hønning, 2007). The competition between NOD and the contaminant leads to serious loss of injected oxidant, which is – as described in Chapter 1 – one of the reasons to start the UPSOIL project. The NOD can be several orders of magnitude larger than the demand by PCE contamination. And as a result of that, both the rate and extent of NOD are important factors when evaluating the effectiveness and efficiency of in situ chemical oxidation projects (Urynowicz et al., 2008). Xu and Thomson (2008) mention in their study about the influence of NOD that "the natural oxidant demand, which is most commonly present in aquifer systems that may contribute to permanganate consumption, consist of organic matter and reduced minerals containing Fe^{2+} e.g. pyrite and siderite" (Xu and Thomson, 2008). In this study sedimentary organic matter (SOM) and pyrite are included as NOD. Pyrite is included in this research as it is commonly present as a reactive mineral within the Dutch subsurface (e.g. Hartog et al., 2002). Siderite ($FeCO_3$) less frequently acts as a reactive reductant in Dutch subsurface. Reactions with dissolved species (such as dissolved Fe^{2+}) in native groundwater are not considered as their contribution to overall permanganate consumption is expected to be negligible compared to the reactions with the sedimentary species (Hartog et al., 2002).

Because of competition for permanganate, the presence of reactive sedimentary reductants reduces the rate of PCE oxidation. In the first part of this paragraph the oxidation of sedimentary organic matter (§2.3.1) and pyrite (§2.3.2) by permanganate are described by their stoichiometric relations and oxidation reactions. The impact on the soil geochemistry, i.e. the groundwater and mineral composition as well as the pH, of all oxidation reactions ($PCE_{(aq)}$, SOM and pyrite) is described in (§2.3.3).

2.3.1 Sedimentary organic matter

SOM generally consist of original plant tissue (and its partially decomposed equivalents) and humus, which is the more reactive part of SOM (Hønning, 2007). Humus, usually the biggest part of SOM, is not a specific compound and does not have one typical structural markup. Within this research the elemental composition of sedimentary organic matter is defined as CH_2O, as in Henderson et al. (2009).

The content of SOM depends on the sediment genesis and depth. Topsoils generally have SOM content around 5% by weight. Aquifer sediments typically have a lower SOM content. In figure 2.3 the NOD for different laboratory studies are shown by the permanganate consumption by organic matter per kilogram soil. Obviously, the permanganate consumption does not only depend on the amount of NOD present in the soil, but also on its reactivity and the reaction stoichiometry through which it oxidizes by permanganate.

Type of Study	Geology	MnO$_4^-$ (g/l) [a]	NOD observations [a]	References
Batch	Sand	0.2 - 2	1.6 – 4.3 g/kg	Greenburg et al., 2004
Batch	Sand	3.7	0.2 g/kg	Mumford et al., 2004
Batch	Sand	0.2 - 37	0.06 – 9.8 g/kg	Crimi and Siegrist, 2005
Batch	Sand	3.7	1.2 g/k	Mumford et al., 2005
Batch	Sand	0.75 - 15	0.3 – 53 g/kg	Xu and Thomson, 2006
Batch	Sand	5 - 20	0.5 – 2 g/kg	I, Hønning et al., 2007a
Batch	Sandy till	0.05 - 20	1 – 8 g/kg	I, Hønning et al., 2007a
Batch	Clayey till	0.05 - 20	5 – 20 g/kg	I, Hønning et al., 2007a
Column	Silty clay	0.4 - 4	2.1 – 8.1 g/kg	Struse et al., 2002
Column	Sand	1.6 - 3.4	0.1-0.6 g/kg	Mumford et al., 2005
Column	Sand	0.75 - 15	0.2 – 27.5 g/kg	Xu and Thomson, 2006

[a] The oxidant concentrations are reported as g KMnO$_4$/l in most studies, but have been converted to g MnO$_4^-$/l for the purpose of comparison with the investigations in this thesis.

Figure 2.3   *Examples of laboratory studies investigating natural oxidation demand (NOD) (source: adapted from Hønning, 2007)*

Stoichiometric reaction

The stoichiometric relation between permanganate and soil organic matter is defined as:

$$CH_2O + 12H^+ + 12MnO_4^- \rightarrow 12MnO_{2(s)} + 9CO_{2(aq)} \qquad (2.28)$$
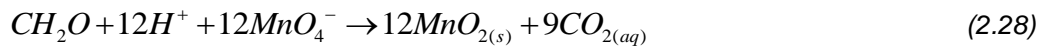
From this relation it follows that the oxidation of organic matter consumes H$^+$, which results in an increase of pH (when no other processes are taken into account). Like with the oxidation of PCE$_{(aq)}$ CO$_2$ is formed. The production of CO$_2$, in a closed system resulting in an increase in CO$_2$ pressure, has a strong impact on the geochemistry of the subsurface. This is further discussed in §2.3.3.

Rate expression

Amongst others, Xu and Thomson (2006) have shown that the oxidation of natural oxidant demand for a given permanganate concentration doesn't go by an instantaneous linear reaction. Instead, the oxidation of organic matter can be described by 'an independent first-order kinetic model' (Urynowicz et al., 2008). The oxidation of organic matter initially goes rapid but is followed by a much slower depletion rate.

In this study the oxidation rate expression is defined by a kinetic reaction which causes rapid oxidation at first, and as the organic matter content decreases the oxidation rate decreases too. Henderson et al. (2009) take account for a rate decrease with decreasing SOM saturation by including a surface/volume ratio within the formulation of SOM oxidation (see Appendix A). As organic matter is not present in a typical mineral structure, such as residual PCE is in droplets and pyrite is as cubes, the surface/volume ratio is not included in this study.

Within this research the oxidation rate of SOM is both dependent on the concentration of permanganate, as well as on the concentration of SOM (eq. 2.29). Because of this dependence on SOM presence, a rate decrease with decreasing SOM saturation is included.

$$r_{ox}^{SOM} = -k_{ox}^{SOM}[CH_2O][MnO_4^-] \qquad (2.29)$$

Where:

r_{ox}^{SOM} = oxidation rate soil organic matter by permanganate [$mole \ l^{-1} \ day^{-1}$]

k_{ox}^{SOM} = oxidation rate constant [$mole^{-1} \ l \ day^{-1}$]

$[CH_2O]$ = concentration of soil organic matter $\left[mole\, l^{-1} \right]$

$[MnO_4^-]$ = concentration of permanganate $\left[mole\, l^{-1} \right]$

The oxidation rate constant, which has been adapted from Henderson et al. (2009), is shown in table 2.3 (see as well Appendix A).

2.3.2 Pyrite

In addition to Henderson et al. (2009) pyrite is included in this study. Pyrite, or iron disulfide (FeS_2), is commonly present in Dutch subsurface (Hartog et al., 2002).

Stoichiometric reaction
Although limited information is available on the reaction kinetics by oxidants other than oxygen, the oxidation of pyrite by permanganate is included in this research using the following relation:

$$FeS_{2(s)} + H^+ + 5MnO_4^- \rightarrow 5MnO_{2(s)} + 2SO_4^{2-} + FeOOH_{(s)} \qquad (2.30)$$

The oxidation of pyrite by potassium permanganate consumes H^+. The reaction results in the precipitation of manganese dioxide (like with the oxidation of PCE and SOM). As well in the precipitation of an iron(III)-oxide-hydroxide species, $FeOOH$, which is known as the mineral goethite.

Rate expression
The oxidation reaction of pyrite by oxygen has been found to be first order with respect to the surface area (Appelo and Postma, 1994, p.268). This is also found by Chirita (2001), in an experimental study to the kinetics of aqueous pyrite oxidation by potassium dichromate: "A direct relationship between the oxidation rate and the initial particle surface area was found."
Therefore, the rate expression includes a conversion from the volumetric concentration to the surface area of a cubic:

$$r_{ox}^{pyrite} = -k_{ox}^{pyrite} [MnO_4^-] \left(6 \left([FeS_2]_{t=0} \right)^{2/3} \right) \frac{\left([FeS_2]_{t=t} \right)^{2/3}}{\left([FeS_2]_{t=0} \right)^{2/3}} \qquad (2.31)$$

$$r_{ox}^{pyrite} = -k_{ox}^{pyrite} [MnO_4^-] \, 6 \left([FeS_2]_{t=t} \right)^{2/3} \qquad (2.32)$$

Where:

r_{ox}^{pyrite} = oxidation rate pyrite by permanganate $\left[mole\ l_{bulk}^{-1}\ day^{-1} \right]$

k_{ox}^{pyrite} = oxidation rate constant for pyrite $\left[mole^{-2/3}\ dm^2\ day^{-1} \right]$

$6 \left([FeS_2]_{t=t} \right)^{2/3}$ = Concentration of pyrite converted to reactive surface [mole dm^{-2}]

In table 2.3 different oxidation rate constants for soil organic matter as well as for pyrite are given. These values have been found in different literature studies, which are also mentioned in table 2.3. For both organic matter as well as for pyrite information on oxidation rate constants for the oxidation reaction with potassium permanganate turned out to be scarce. The value for soil organic matter adapted from Henderson et al. (2009) is implemented in that study as a 'model calibration parameter', and – as far as one can know from the paper - not based on measurements/experiments. Although a value is obtained from laboratory test conducted at Deltares, the value of Henderson et al.(2009) is prevailed in this study since the derived parameter is for field-scale as is the model developed in this study.

The encountered oxidation rate constants of the reaction with pyrite are all surface controlled reactions. However, that is the only similarity as the oxidation rate constants differ up to eight orders of magnitude. When looking at the oxidants used, it can be seen that no rates have been found which are based on the oxidation reaction of pyrite by potassium permanganate. The value given by Chandra and Gerson (2010) has not been used, as it is assumed that the oxidation of pyrite by potassium permanganate expires faster than the oxidation of pyrite by oxygen. Both values given by Matta et al. (2007) have been used. They are preferred above the values given by Chirita (2003) from a conservative point of view. When the low values given by Chirita (2003) are used, the oxidation of pyrite by potassium permanganate will hardly influence the efficiency of an ISCO remediation process.

Table 2.3   *Oxidation rate constants for organic matter and pyrite from literature*

Mineral	Oxidant	Type rate constant	Oxidation rate constant	Unit	Source
SOM	MnO_4^-	Model calibration parameter	4.32	[day^{-1}]	Henderson et al. (2009)
SOM (various types	MnO_4^-	1st order	0.15	[day^{-1}]	Laboratory tests Deltares.
Pyrite	O_2	1st order, surface controlled reaction	0.0227	[Mole dm^{-2} day^{-1}]	Chandra and Gerson, 2010
Pyrite	H_2O_2 (Fenton's Reagent)	1st order, surface controlled reaction	108.3	[Mole dm^{-2} day^{-1}]	Matta et al.(2007)[b]
Pyrite	H_2O_2 (Fenton's Reagent)	1st order, surface controlled reaction	0.128	[Mole dm^{-2} day^{-1}]	Matta et al.(2007)[c]
(aqueous) Pyrite	$K_2Cr_2O_7$ Potassium dichromate	1st order, surface controlled reaction	9.86 10^{-6}	[Mole dm^{-2} day^{-1}]	Chirita, P. (2003)[d]
(aqueous) Pyrite	$K_2Cr_2O_7$ Potassium dichromate	1st order, surface controlled reaction	6.85 10^{-5}	[Mole dm^{-2} day^{-1}]	Chirita, P. (2003)[e]

[a] Results from laboratory test carried out at Deltares as part of the UPSOIL project. Organic matter included: Forrest peat, Reed peat, Oakwood, Protamylasse, Antracite and cellulose.
[b] at pH = 3
[c] at pH = 6,8
[d] at pH = 2.8
[e] at pH = 0.97

From the oxidation reactions it can be seen that H$^+$ production and consumption and CO_2 production are involved. These components affect a very important, groundwater composition controlling equilibrium: carbonate equilibrium.

2.3.3   Carbonates, carbon dioxide and pH

Carbonate reactions involve one of the most common minerals on the face of the Earth: calcite. Aquifers made of carbonates, such as limestones and dolomites, are only present in a small part of the shallow subsurface of the Netherlands. However, also sandy aquifers may contain abundant carbonate minerals as accessory minerals or cement around the more inert grains (Appelo and Postma, 1994. pp. 86).

Carbonate minerals have a dominant effect on groundwater chemistry due to their high reactivity and the buffering effect on pH. Dependent on several factors, such as groundwater pH, temperature and CO_2 pressure (p[CO_2]) calcite either dissolve or, from water in equilibrium with calcite, it precipitates. If water is in equilibrium with calcite the following is valid for the mentioned factors (assuming that thresholds are exceeded):

pH increases → calcite precipitates;
p[CO_2] increases → calcite dissolves;
Temperature increases → calcite precipitates.

The first two of the above mentioned factors play a role within this study because pH and CO_2 are included by the oxidation reactions studied within this research. Therefore it is important to understand their effects and interaction on groundwater composition. For example, when looking at the oxidation reaction of organic matter (eq. 2.28) it can be seen that H^+ is consumed and $CO_{2(aq)}$ is produced. An increase in pH will lead to calcite precipitation, but the increase of p[CO_2] has the opposite effect: calcite dissolution. Which of these effects prevails, and how the interaction between calcite dissolution and precipitation relates to changes in p[CO_2] and pH, is now described.

Calcite dissolution / precipitation
The following chemical relation gives the dissolution of calcite:

$$CaCO_3 \Leftrightarrow Ca^{2+} + CO_3^{2-} \tag{2.33}$$

The carbonate-ion CO_3^{2-} can adopt a proton (H^+), for example available due to PCE oxidation, to form bicarbonate (HCO_3^-):

$$HCO_3^- \Leftrightarrow H^+ + CO_3^{2-} \tag{2.34}$$

And, adopting a second proton to form carbonic acid (H_2CO_3):

$$H_2CO_3^* \Leftrightarrow H^+ + HCO_3^- \tag{2.35}$$

The concentrations or relative proportions of the carbonate-ion and carbonic acid are influenced by the pH (H^+ availability) of the groundwater. If more protons are available, pH is lower and carbonic acid will be the dominant specie. In figure 2.4 this is shown schematically by plotting pH against the percentage HCO_3^-, the intermediate carbon specie, in the total dissolved carbon species.
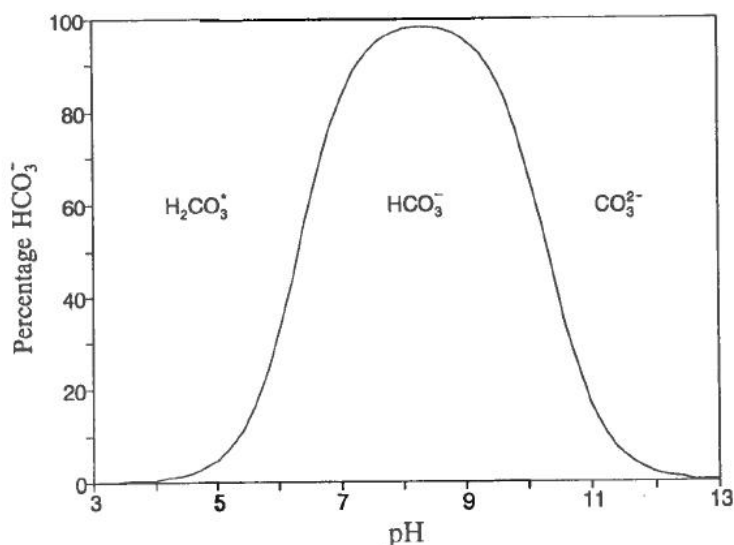
Figure 2.4   *Bicarbonate percentage as part of total dissolved carbon species as function of pH (source: Appelo and Postma, 1994).*

PCE oxidation
When PCE is being oxidized H^+ - a strong acid - is produced and subsequently pH will decrease. However, as long as the mineral calcite is available the decreasing pH (and increasing $p[CO_2]$) cause dissolution of calcite (once a certain threshold value is passed). As calcite dissolves carbonate-ions are produced (eq. 2.33). Carbonate ions can adapt two protons to form carbonic acid, a weak acid. Because the released H^+ is captured in carbonic acid, a weaker acid, the pH does not decrease as much compared to a situation in which no calcite is available for dissolution. Thus, the pH decrease is buffered due to calcite dissolution.

From the oxidation reaction with potassium permanganate (2.24) it also follows that CO_2 is produced. CO_2 associates to some extent with water molecules to form carbonic acid (Appelo and Postma, 1994):

$$CO_{2(g)} + H_2O \Leftrightarrow H_2CO_3^* \tag{2.36}$$

Where
$$H_2CO_3^* = CO_{2\,(aq)} + H_2CO_3 \tag{2.37}$$

The production of aqueous CO_2 is another pH lowering effect of the oxidation of PCE. But as can be seen in the reaction above, protons are 'captured' to form carbonic acid. This means that the stronger acid H^+ is again converted to the weaker acid H_2CO_3. The production of aqueous CO_2 tempers the pH lowering.
In water under higher $p[CO_2]$ more calcite can dissolve. Water can be supersaturated with respect to calcite. This means that a larger amount of carbonate-ions can be present in the water, which in turn results in a larger ability to buffer pH decreases.

Organic matter oxidation
As opposed to the oxidation of PCE the oxidation of organic matter consumes protons (eq. 2.28) resulting in an increase of groundwater pH. For each mole organic matter, twelve protons are consumed and twelve moles of permanganate are used. The oxidation reaction of organic matter indicates that besides the proton consumption also CO_2 is produced. Thus two opposing effects on the pH result from the oxidation of organic matter. But since H^+ is a strong acid, and CO_2 only partly dissociates to H_2CO_3, a weak acid, the first effect will have a stronger influence on the pH. Hence it is expected that the pH will increase as a result of organic matter oxidation.

Pyrite oxidation
The oxidation of pyrite does not involve CO_2, but only the consumption of protons. From stoichiometry it follows that for each mole pyrite being oxidized, one proton is consumed and five moles of MnO_4^- are used (eq. 2.30). Compared to the oxidation of organic matter there are less protons consumed per mole permanganate in the oxidation of pyrite. However, since there are no buffering processes involved in the oxidation of pyrite it is expected that the oxidation of pyrite results to the strongest effect on pH.

2.4 Indicator selection

The goal of this chapter is to define the involved processes which have to be taken into account when conducting a modeling study. In this paragraph an overview is given of the previously described oxidation and dissolution reactions (table 2.4). In appendix A also an overview of the oxidation reactions as included in Henderson et al. (2009) is shown. Before describing the used model packages this paragraph summarizes the stoichiometric relations and, for each component, indicates the expected effect on different components. The effects on the components described in the tables hold for only the concerned process.

Goal of this paragraph is to select different potential indicators for the progress of an in situ chemical oxidation of a PCE contaminated site.

Table 2.4   *overview (oxidation) processes and stoichiometric relations*

Process	Stoichiometric relations
Dissolution of nonaqueous PCE into the aqueous phase	$C_2Cl_{4(DNAPL)} \rightarrow C_2Cl_{4(aq)}$
Oxidation of aqueous phase PCE by permanganate	$3C_2Cl_{4(aq)} + 4MnO_4^- + 4H_2O$ $\rightarrow 6CO_{2(aq)} + 12Cl^- + 4MnO_{2(s)} + 8H^+$
Oxidation of soil organic matter by permanganate	$CH_2O + 12H^+ + 12MnO_4^-$ $\rightarrow 12MnO_{2(s)} + 9CO_2$
Oxidation of pyrite by permanganate	$FeS_2 + H^+ + 5MnO_4$ $\rightarrow 5MnO_{2(s)} + 2SO_4^{2-} + FeOOH_{(s)}$

Table 2.5   *Oxidation of PCE(aq) by potassium permanganate*

Involved components		Effect
PCE_{aq}	↓	First concentration will tend towards solubility limit. Once permanganate is available it will decrease stoichiometrically.
Cl^-	↑	Only produced from the oxidation of PCE(aq). Conservative with respect to other components in groundwater.
Ca^{2+}	↑	Directly related to the calcite dissolution/precipitation and thus to the pH and p[CO2] development. Due to the oxidation reaction of PCE(aq) pH will decrease and p[CO2] will increase: consequently CaCO3(s) will dissolve, thereby increasing [Calcium]. Once all calcite has been dissolved, concentration will remain constant.
CO_2 species	↑	CO2 increases stoichiometrically. Because CO2 partly dissociates to carbonic acid it has a pH lowering effect. But it depends on pH which of the CO2 species is dominant (fig. 2.3).
pH	↓	pH will decrease mainly due to production of H+. Depends on presence calcite and [CO2 species] whether or not the pH decrease is tempered.
PCE_{NAPL}	↓	As long as no permanganate is available PCE_NAPL will slowly decrease due to dissolution. Once permanganate start oxidizing PCE(aq) the driving force behind PCE_NAPL dissolution is maximized (fig. 2.2) and dissolution speeds up.
$MnO_{2(s)}$	↑	Will increase stoichiometrically. Either precipitates in the sediment or as (mobile) colloids in the groundwater.
$CaCO_3$	↓	Will dissolve due to decrease in pH.

Table 2.6   *Oxidation of organic matter by potassium permanganate*

Involved components		Effect
CH_2O	↓	Decreases stoichiometrically
Ca^{2+}	↓	Directly related to the calcite dissolution/precipitation and thus to the pH and p[CO_2] development. Due to the oxidation reaction of SOM pH and p[CO_2] will increase. Two opposite effects. Because H⁺ is a stronger acid pH will go up and the produced carbonic acid shifts towards the carbonate ion. Consequently $CaCO_{3(s)}$ will precipitate, thereby decreasing [Calcium].
CO_2 species	↑	CO_2 increases stoichiometrically. Because CO_2 partly dissociates to carbonic acid it has a pH lowering effect. But it depends on pH which of the CO_2 species is dominant (fig. 2.3). Because of the precipitation of calcite, carbonate ion is 'captured'. This can cause a decrease in CO_2 concentration.
pH	↑	There are two opposite effects on the pH: 1) consumption of H+ → increase of pH 2) production of CO_2 → decrease of pH Because H+ is a stronger acid, and CO_2 only partly dissociates to H_2CO_3, which is a weak acid. The first effect is 'stronger', thus it is expected that pH will increase.
$MnO_{2(s)}$	↑	Increases stoichiometrically. Either precipitates in the sediment or as (mobile) colloids in the groundwater.
$CaCO_3$	↑	Precipitates due to increase in pH and increased availability of carbonate ion; so increases.

Table 2.7   *Oxidation of pyrite by potassium permanganate*

Involved components		Result
$FeS_{2(s)}$	↓	Decreases stoichiometrically
Ca^{2+}	↓	Directly related to the calcite dissolution/precipitation and thus to the pH and p[CO_2] development. Due to the oxidation reaction of pyrite pH will increase and consequently $CaCO_{3(s)}$ will precipitate, decreasing [Calcium]. No buffering effects are included in this oxidation reaction
CO_2	↓	Although not involved in the stoichiometric reaction, the concentration of the CO_2 species may decrease. This due to the precipitation of calcite, which 'captures' carbonate ions from groundwater.
SO_4^{2-}	↑	Increases stoichiometrically.
pH	↑	Increases due to uptake of H⁺
$MnO_{2(s)}$	↑	Increases stoichiometrically. Either precipitates in the sediment or as (mobile) colloids in the groundwater.
$CaCO_3$	↑	Precipitates due to increase in pH; so increases.

Based on the tables above, as well as the described processes in this chapter, the following expectations can be denoted:
- If concentration of chloride increases, $PCE_{(aq)}$ is oxidized by permanganate;
- If concentration of sulfate increases, pyrite is oxidized by permanganate;
- Oxidation of target and non-target compounds has opposed effects on the pH due to H^+ production and consumption, respectively.
- Pyrite has the strongest effect on pH. This because the other two oxidation processes are affected by buffering processes (CO_2 production and calcite dissolution);
- The resulting pH of the different oxidation processes affects the calcium and CO_2 species concentration through calcite dissolution / precipitation.
- The mass transfer rate of PCE_{NAPL} to $PCE_{(aq)}$ is the limiting factor in the oxidation of PCE. This is based on the fact that the oxidation rate constant is three orders of magnitude bigger than the dissolution rate constant.

In table 2.8 an overview is given of the expected indicators based on this chapter.

Table 2.8   *Indicator overview*

Process	Indicator	Strong / weak indicator[2]
$PCE_{(aq)}$ oxidation	Chloride concentration	Strong
	pH	Strong
	Calcium concentration	Weak
	Carbon species concentration	Weak
SOM oxidation	pH	Weak
	Calcium concentration	Weak
	Carbon species concentration	Weak
Pyrite oxidation	SO_4^{2-}	Strong
	pH	Weak
	Calcium concentration	Weak
	Carbon species concentration	Weak

The effects of the different oxidation processes on the components are now described separately for each process. Resulting in the expectation that the components in table 2.8 can be used as indicators for the progress of an ISCO remediation process. In the next chapter the model which has been used is described. Then, in chapter 4 a 'batch experiment' is simulated to see how the different oxidation processes, when happening at the same time, reflect on the indicators.

---

[2] An indicator is defined strong if it is unique for an oxidation reaction. pH changes are not unique for one particular oxidation reaction, but still it is defined a strong indicator, as the 'direction of pH development' is unique for the oxidation of the target or non-target compounds. So it is a strong indicator concerning the oxidation of $PCE_{(aq)}$ (as only the oxidation of PCE decreases pH) but a weak indicator for the oxidation of SOM and pyrite (as both processes are expected to increase pH, so no distinction can be made).
Calcium is classified as weak indicator, as it does not directly result from the oxidation processes, but from the precipitation/dissolution of calcite. This in turn depends on both pH and CO_2 pressure. It is expected however, that if the calcium concentration increases, this indicates that $PCE_{(aq)}$ is being oxidized.

3. Model Description

3.1 Introduction

Now that the goal of this study (Ch.1) and the different processes involved (Ch.2) are described, this chapter describes model that has been used to simulate the involved processes.

To simulate the fate and transport of (aqueous) PCE in saturated porous media, as well as chemical oxidation processes related to ISCO remediation processes a combination of two models has been used (figure 3.1):

- MODFLOW (version 2005**)** to model the groundwater flow, and
- PHT3D (version 2.10) to model the reactive transport within saturated porous media. PHT3D incorporates:
    - MT3DMS (version 5.3): which simulates three-dimensional advective-dispersive multi-species transport (Prommer and Post, 2010), and
    - PHREEQC-2 (Release 2.17) which models the mass transfer from the nonaqueous phase to the aqueous phase, chemical (oxidation) reactions and chemical equilibria.
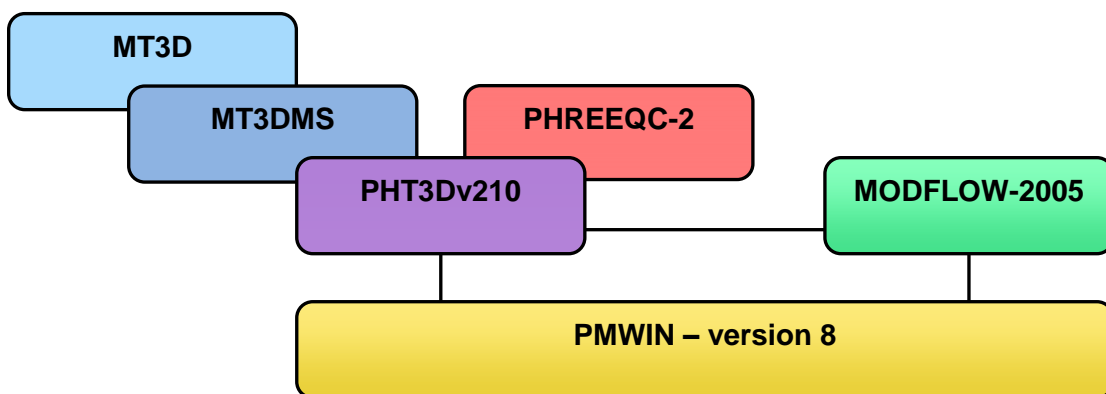
Figure 3.1   *Model package overview*

To create the input files the graphical-user-interface PMWIN (version 8) has been used. The GUI has primarily been used to create the model discretization and to synchronize time step size between both models (MODFLOW and PHT3D). Once input files were created by PMWIN, they were manually adjusted to run different scenarios

In paragraph 3.2 of this chapter a brief description is given for each of the abovementioned model packages. The interdependence between the different model packages, as well as the functioning, is best described by the input files. This is done in paragraph 3.3. An extensive overview of the input models and how they can be adjusted is included in Appendix B. To conclude this chapter the relation between the model packages and the different in- and output files is visualized in paragraph 3.4.

3.2 Model packages

3.2.1 MODFLOW

MODFLOW is a modular three-dimensional finite difference groundwater model, which has been created and published by the United States Geological Survey (USGS) (Chiang, 2007). It is originally designed to simulate saturated three dimensional groundwater flow through porous media. The original version (MODFLOW-88) did not include solving equations other than the groundwater flow equation. In the more recent version, which has been used in this study (MODFLOW-2005), also other processes, such as 'Parameter estimation', 'Observation processes' and 'Sensitivity processes' have been implemented in the code. However, within this research only the groundwater flow equation is called for.

3.2.2 PHT3D

PHT3D is a three dimensional reactive multi-component transport code for saturated porous media (Prommer and Post, 2010). It is a coupling of the MT3DMS model and PHREEQC-2.
The manual describes the PHT3D as follows: "A modular 3D multi-species transport model for simulation of advection, dispersion and chemical reactions of contaminants in groundwater systems".
MT3DMS contributes the 'multi-species transport model' part. MT3DMS is a further development of MT3D. MT3D "could be used to simulate changes in concentration of single species miscible contaminants in groundwater" (Chiang, 2007). MT3DMS adds the possibility to simulate multiple species (MS). So for multiple species dissolved in groundwater the different transport processes (advection, dispersion, diffusion) as well as sorption and basic chemical reactions can be simulated.
PHREEQC-2 provides for the 'chemical reactions of contaminants in groundwater systems'.

3.2.3 PHREEQC-2

PHREEQC-2 is a model for 'a wide variety of low-temperature aqueous geochemical calculations' (Parkhurst and Appelo, 1999). It is based on 'equilibrium chemistry of aqueous solutions interacting with minerals, gases, solid solutions, exchangers, and sorption surfaces, but also includes the capability to model kinetic reactions with rate equations that are completely user-specified in the form of Basic statements' (Parkhurst and Appelo, 1999). The latter mentioned has been applied in this study. Through modifications of the original extensible PHREEQC-2 database the kinetic oxidation reactions, as described in Chapter 2, have been implemented in the database file (to see the Basic statements see Appendix C).

3.3 Input files

The interdependence between the different packages can best be described by the main 'coupling file', which is the "name file": *"model name".pht3dnam.* This file is a simple list of the files that PHT3D calls for. This is similar to the functioning of MT3DMS, only two additional files are needed for PHT3D compared to a MT3DMS simulation: the pht3d_ph.dat file and the pht3d_datab.dat file, which is the PHREEQC-2 database file.
An example of a name file is shown in figure 3.2.


```
1  List   7    pht3d.out
2  FTL    66   mt3d.flo
3  BTN    31   pht3dbtn.dat
4  ADV    32   pht3dadv.dat
5  DSP    33   pht3ddsp.dat
6  SSM    34   pht3dssm.dat
7  GCG    35   pht3dgcg.dat
8  PHC    36   pht3drct.dat
9  PHC    64   pht3d_ph.dat
```

Figure 3.2   *Example of a PHT3D name file*

3.3.1   MODFLOW

In- and output files that are created by PMWIN/MODFLOW are given in table 3.1. Of the specified files only the MT3D.FLO file is called for by PHT3D (fig. 3.2). The .FLO file is used to read off groundwater fluxes. This MT3D.FLO file is the link between MODFLOW and PHT3D: it is created by MODFLOW (output) and used as input file for PHT3D. As in this study hydrological flow characteristics are mainly kept constant, the input files are – once created by MODFLOW – not adjusted. A short description is given in table 3.1.

Table 3.1   *MODFLOW files*

File name	File type	Description / Content
discret.dat	ASCII	Discretization file. Domain, cell and time discretization.
bas6.dat	ASCII	Basic Package file. Boundary and initial head conditions
bcf6.dat	ASCII	Block-Centered Flow Package file. Layer type, Conductivity, Specific Storage.
budget.dat	Binary	Cell-by-Cell flow terms.
ddown.dat	Binary	Drawdown, the difference between the starting heads and the calculated hydraulic heads.
heads.dat	Binary	Hydraulic head file.
output.dat	ASCII	Detailed run record and simulation report.
MT3D.FLO	Binary	The flow transport link file between MODFLOW and PHT3D.

3.3.2 PHT3D

Considering the *.pht3dnam* file (fig. 3.2), all but the MT3D.FLO and pht3d_ph.dat file are in- or output files created by PHT3D. In table 3.2 again an overview of the different files and their content, as described in the manuals, is given. Once these files are created through PMWIN they have been adjusted manually to carry out different modeling scenarios. To be able to manually adjust the files an overview is created to indicate which parameters are defined where in the files. This overview is added to this report as appendix (Appendix B). The descriptions given there are based upon the PHREEQC-2-, MT3DMS- and PHT3D manuals (Parkhurst & Appelo, 1999; Prommer & Post, 2010; Zheng & Wang, 1999).

Table 3.2   *PHT3D input files*

File name	File type	Description	Content (Zheng & Wang, 1999)
Pht3dbtn.dat	ASCII	Basic Transport Package	"Definition of the problem, specification of the boundary and initial conditions, determination of the step size, preparation of mass balance information, and printout of the simulation results."
Pht3dadv.dat	ASCII	Advection Package	Defines the method with which advective transport is simulated.
Pht3ddsp.dat	ASCII	Dispersion Package	"Defines the parameter matrix of the dispersion term for the matrix solver."
Pht3dssm.dat	ASCII	Sink & Source Mixing Package	"Defines the parameter matrix of all sink/source terms for the matrix solver."
Pht3dgcg.dat	ASCII	Generalized Conjugate Gradient Solver Package	"Solves the matrix equations resulting from the implicit solution of the transport equation."
Pht3drct.dat	ASCII	Chemical reactions Package	"Solves the concentration change due to reaction explicitly or formulates the coefficient matrix of the reaction term for the matrix solver."
Pht3d.out	ASCII	Output file	Run record and simulation report.

3.3.3 PHREEQC-2

The last file mentioned in the Name file (fig. 3.2) is a PHREEQC-2 file: pht3d_ph.dat. In addition to the mentioned files in figure 3.2, one more PHREEQC-2 file is called for: the database file (table 3.3).

Table 3.3   *input files PHREEQC-2*

File name	File type	Description	Content (Prommer and Post, 2010)
Pht3d_ph.dat	ASCII	PHREEQC-2 reaction file	"File that carries information about the number, names and types of chemicals included in a PHT3D simulation, reaction rate constants (and other reaction parameters)"
Pht3d_datab.dat	ASCII	PHREEQC-2 database file	File in which both equilibrium and kinetic reactions are defined. As well all reaction parameters and constants must be included in this file.

The database file is shortly discussed by the data blocks of which it is put up.

The PHT3D database file is analogous to the original PHREEQC-2 database file. The database file consists of the following data blocks 'Solution_Master_Species', 'Solution_Species', 'Phases', 'Exchange_Master_Species', 'Exchange_Species' and 'Rates' (Parkhurst and Appelo, 1999). Except for the 'exchange (master) species' data block, in which cation/anion exchange is defined, all data blocks have been used in this study.

In the 'Solution_Master_Species' data block all included components are defined. The element names, alkalinity contribution, chemical formula as well as the element gram formula weight are defined in this data block.

In the 'Solution_Species' data block the chemical reaction, the log K value and the activity coefficient for all aqueous species are defined.

In the 'Phases' data block the same is defined as in the 'Solution_Species', only now for the included minerals and gas phases. Also temperature dependence of log K can be defined here for the gas and mineral reactions. As no gas phase and temperature change is included these definitions have not been adjusted.

In the 'Rates' data block the rate expressions for kinetic reactions are defined through numbered BASIC statements. The kinetic rate expressions which are defined in Chapter 2 are written as such BASIC statements, and included in this report in Appendix D.

Except the implemented BASIC statements the default PHREEQC-2 database has been used.

In the pht3d_ph.dat file the different 'species' are defined as 'mobile equilibrium', 'mobile kinetic', 'immobile kinetic' or 'mineral equilibrium' (Appendix C). In table 3.4 the components that are included in this study are defined.

Table 3.4   *Overview included components / species within this study*

Category	Components/ species
Mobile equilibrium components (10)	pH ; pe ; MnO_4^- ; Cl^- ; K^+ ; Ca [a]; $C(4)$ [b] ; $S(6)$ [c] ; Na^+ ; Br^-
Mobile kinetic components (1)	PCE$_{(aq)}$
Immobile kinetic components (4)	Dummy[3] PCE$_{NAPL}$; Dummy PCE$_{(aq)}$; Dummy Som ; Dummy Pyrite
Mineral equilibrium (5)	PCE$_{N\,APL}$; Calcite ($CaCO_3$); Organic matter (CH_2O) ; Pyrite (FeS_2) ; Pyrolusite $\left(FeOOH_{(s)} \right)$

[a] $Ca\quad = Ca^{2+} + CaHCO_3^+ + CaCO_3 + CaSO_4 + CaH^+$

[b] $C(4)\ = CO_3^{2-} + CaCO_3 + CaHCO_3^+ + CO_{2(aq)} + HCO_3^-$

[c] $S(6)\ = SO_4^{2-} + CaSO_4 + KSO_4^- + HSO_4^-$

---
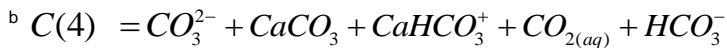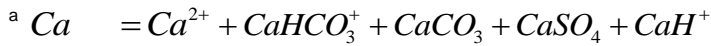
[3] The immobile components that are included in kinetic defined reactions in the database (see Appendix C) have to be defined as 'dummy variable'. This is due to a limitation of PHT3D: a component cannot be used in the kinetic reaction of another component. As can be seen in Appendix C, initially none of the components are used in the kinetic reaction of another component. However, to be able to create and model scenarios in which kinetic reactions are defined differently, the kinetic components are defined as 'dummies'.

3.4 Model setup

Figure 3.3 shows the relations between the different model packages and the input files. In bold the input files which have been used predominantly in this study are indicated.

Figure 3.3   *Overview relations between model packages and input files.*

4. Batch model

4.1 Introduction

At the end of Chapter 2 it is concluded that, based on stoichiometric and geochemical relations, Cl^-, SO_4^{2-}, pH, Ca, CO_2 are expected to be able to indicate the progress and efficiency of an ISCO remediation with permanganate of a PCE contaminated site.

A no flow PHT3D model has been created to test if these components are indeed effective indicators, and to meet the first aim and answer the first 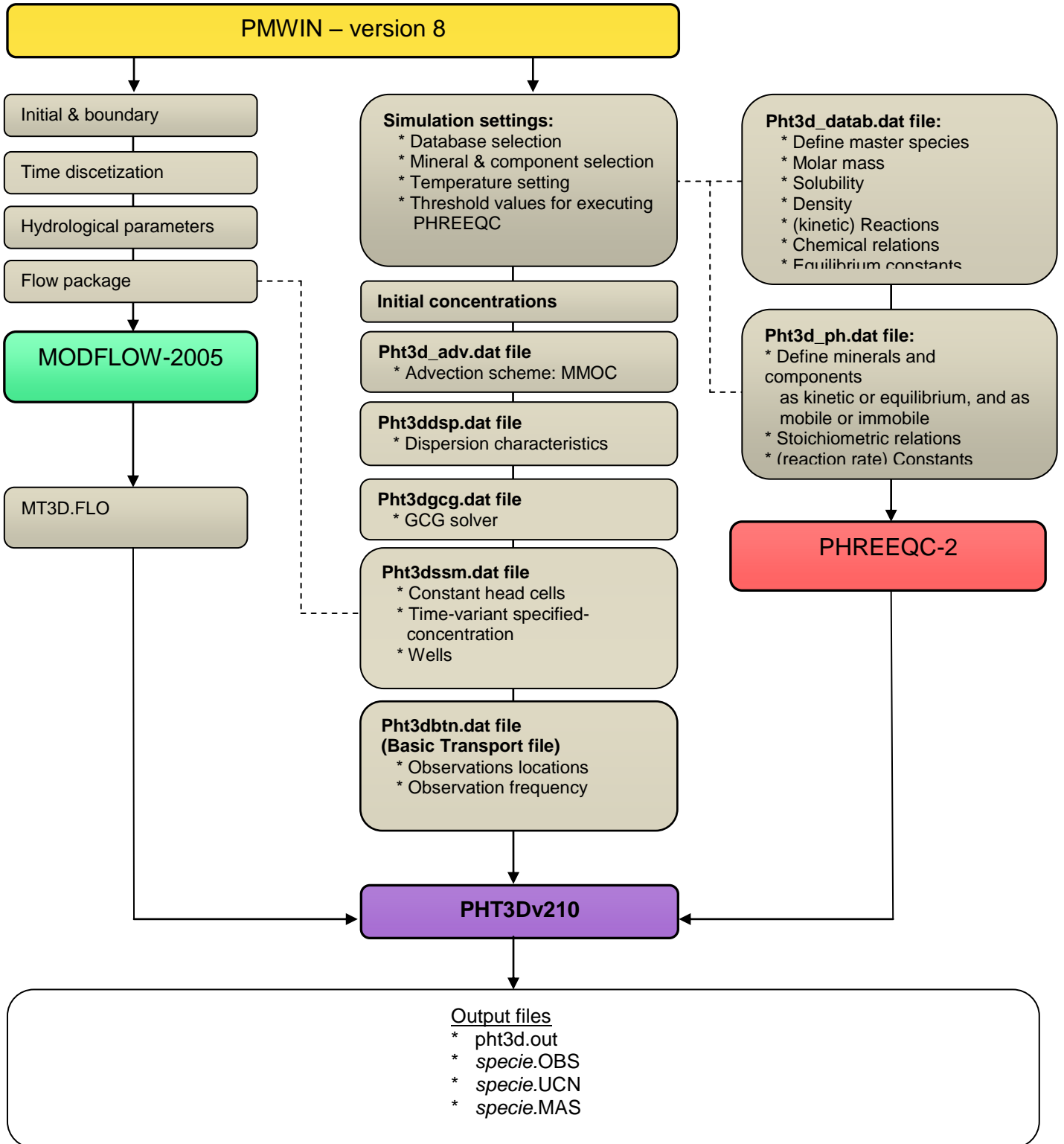research questions (table 4.1). The flow effects are excluded such that the interaction (or competition) between the different oxidation processes and their reflection on the potential indicators can be fully understood. In addition, the effect of different soil composition (i.e. different NOD) on pH and the other potential indicators could be investigated more explicitly by excluding flow effects.

The model can be considered a batch experiment as it is exactly known what is present in one cell, and, no exchange take place between cells. When time and permanganate are sufficiently available all chemical reactions will follow the stoichiometric relation as it is defined in the database. Because of this fact, one can calculate – using stoichiometric relations – how much moles of a certain component would be produced if all available permanganate reacts with one reductant. For example, if 100% of the added permanganate reacts with PCE, it can be calculated how much moles of chloride are produced. In a similar fashion the amount of moles sulfate produced from the reaction with pyrite can be determined. However, when insufficient permanganate is added for all reactions to complete (i.e. to deplete all reductants) the effect of competition for permanganate can be observed. By comparing the actual amount of moles chloride and sulfate to the maximum amount which could have been produced if 100% of the permanganate reacts with PCE or pyrite, respectively, it can be determined what part of permanganate reacted with the target component $PCE_{(aq)}$.

As mentioned in Chapter 1, competition results in serious oxidant losses. It is thus interesting to see how this competition affects the indicators mentioned and, when later used in a flow model if these indicators can give quantitative information about the efficiency of the ISCO process.

First the setup and input values of the model are described now.

Table 4.1 *Overview research goal and questions*

Goal 1	Find indicators which increase insights in the efficiency of chemical oxidation during the remediation process.
Goal 2	See if injection characteristic adjustments (such as rate, concentration, depth) can be based upon indicators found under (1).
Question 1	Is pH an effective indicator for the progress made during the $KMnO_4$ based ISCO remediation of a DNAPL contaminant source?
a)	How does the pH indicator work for different aquifer conditions (such as different SOM, pyrite and calcite content)?
Question 2	Which other indicators can be used to improve the determination of efficiency?
Question 3	Can certain general rules be applied, based on measurements of the indicators, to adjust injection characteristics in order to improve efficiency?

4.2 Setup & Input

The volume of the cell of the batch model is 0.2[m³] or 200[liter]. In this cell both soil and groundwater are present. No gas phase is included. The cell is not in contact with atmosphere, such that produced carbon dioxide doesn't escape, i.e. closed conditions. This is conform a DNAPL contaminated site which is well below the groundwater level. Since there is no flow in the batch model, the hydrological parameters such as conductivity, dispersivity etc. are not relevant and thus solely matrix and groundwater composition are described here. As this research is not based on a real site, the described characteristics are based on Henderson et al. (2009).

Soil matrix
In table 4.2 the characteristics of the soil matrix are given. In the first column the input values are given. In the description the same values are given using the more standard units, the density and molar mass (which are used to calculate the mass fractions) are given as well. The input concentrations for mineral phases are defined as $mole/l_{bulk}$. The input values for the aqueous phases need to be in mole per liter pore water ($mole/l_{water}$) (Prommer and Post, 2010). The values used by Henderson et al. (2009) are given as reference values.
The soil matrix of the aquifer is composed of medium to coarse grained sand, in which no clay is present. In addition to Henderson et al. (2009) pyrite is present in the soil matrix.
When the NOD value, which has been calculated based on molar masses, dry weighted mass of the sediment and stoichiometric relations, is compared to the values shown in the reference table (figure 2.3) it can be seen that the value is initially set rather high.

Table 4.2 *Soil matrix characteristics*

Soil matrix characteristics and mineral phases	Input	[unit]	Description	Values Henderson et al. (2009)
Porosity	0.3	-		0.35
ρ_b	1700	kg/m³	Bulk density soil matrix (Mass of oven dry soil matrix.)	1700 kg/m³
Organic matter	0.01	$mole/l_{bulk}$	0.07% Vol. fraction	0.02 – 0.07% mass fraction
Density	*1380*	g/l		
Molar mass	*30.026*	$g/mole$		
Pyrite	0.01	$mole/l_{bulk}$	490 ppm	0 ppm
Density	*5010*	g/l		
Molar mass	*119.98*	$g/mole$		
Total Natural Oxidant Demand (NOD)	11,2	$g\,MnO_4^- / \text{dry weighted sediment}$		-
Calcite	0.01	$mole/l_{bulk}$	0.12% Vol. fraction	0.2 – 0.5 Weight %
Density	*2710*	g/l		
Molar mass	*100.1*	$g/mole$		
PCE$_{NAPL}$	0.09	$mole/l_{bulk}$	3% saturation	8 % saturation
Initial mass in cell	-	-	3 [kg]	4470 [kg]
Distribution			Residual	Pool

Groundwater composition

In table 4.3 the groundwater composition is given. From this table it can be seen that permanganate is already included in the groundwater. Where in the 2D Flow model, as well as in reality, permanganate is added by injection, in this batch model it is initially present in the cell. So, as the model starts, oxidation reactions immediately start. It is implemented in this 'non-realistic' way because injecting the permanganate with a pulse injection will cause flow and dispersion, which will change the 'batch content'. By implementing it as 'initial concentration' for each cell it is known exactly what the concentrations are at t=0.

Table 4.3   *Groundwater composition*

Aqueous components	Input	[unit]	Description	Pre-injection groundwater chemistry values Henderson et al. (2009)
PCE_{aq}	0	$mole / l_{water}$		-
MnO_4^-	$2.5 \cdot 10^{-2}$	$mole / l_{water}$	10% saturation in solution	$1 \cdot 10^{-15}$
K^+	$2.5867 \cdot 10^{-2}$	$mole / l_{water}$		$8 \cdot 10^{-5}$
Cl^-	$1.0 \cdot 10^{-3}$	$mole / l_{water}$		$5.2 \cdot 10^{-3}$
Ca	$1.646 \cdot 10^{-3}$	$mole / l_{water}$		$1.3 \cdot 10^{-3}$
$CO_2 \; species$	$3.622 \cdot 10^{-3}$	$mole / l_{water}$		$2.4 \cdot 10^{-3}$
$SO_4^{2-} \; species$	$1.05 \cdot 10^{-5}$	$mole / l_{water}$		-
pH	7.3	Standard unit		6.0
Temperature	25	^0C	Default value for PHREEQC-2	Not specified

In table 4.3 it can be seen that potassium and permanganate are included as individual components in the model. Note the somewhat unusual and exact concentration of K$^+$. This implies that it is an actual measurement, which it is not. This value is chosen such that all aqueous solutions together are charge balanced. This is important since 'more robust model results are obtained if all aqueous solutions that are applied in the simulations are fully charge balanced' (Prommer and Post, 2010). Since potassium is a conservative component in this model it can be used to charge balance the total aqueous solution without further consequences.

When performing an ISCO remediation project, the injected solution usually contains about 40 g/l permanganate. In this batch model however a permanganate saturation of 10% of this value is added, i.e. 4 gram / liter. This to prevent for depletion of one of the reductants. As we are interested in the competition for permanganate and the effect on the concentrations of the potential indicators, the depletion of one of the reductants will disturb the observation. To clarify: if for example permanganate has a "preference" to react with organic matter, all permanganate will first react with organic matter. When all available organic matter reacted, permanganate will start to react with the other reductants. When the final concentrations of the potential indicators are then studied, solely based on the measured concentrations this preference for permanganate to react with organic matter does not appear.

A second reason to use a 10% saturated permanganate solution is of practical nature. The time it takes for the reactions to fulfill, thus for all permanganate to react, is shorter. Since several model runs have been conducted, this saved time.

Concerning the temperature of the groundwater ($25\,^0C$): this is not realistic. In the Netherlands groundwater temperature usually fluctuates around 12 ^0C, depending on the season and depth. Closer to the surface the temperature will tend towards the surface

temperature. $25\,^{0}C$ is the default temperature included in PHREEQC and although temperature is expected to influence some key parameters, such as the solubility of PCE, it is assumed not a relevant parameter in this study. Also, from Knaus et al. (2000) it is known that for the temperature range $0 - 50\,^{0}C$ the solubility of PCE is constant. Temperature dependent kinetic expressions for the permanganate oxidation reactions with pyrite and organic matter are not available. Therefore the effect of temperature was not included in the model. The effect of temperature on the oxidation of various reductants is studied separately within the UPSOIL project.

4.3   Methods & Results

Indicators
To see how the different oxidation processes affect the potential indicators different runs have been conducted in which the different oxidation processes are included.
As only a 10% permanganate saturated solution is added, the time until all included permanganate reacted was short. When the model finished, from the potential indicators' observation files the concentration could be taken. So for each potential indicator the concentration after the different oxidation reactions (and different combination) is known. By plotting the concentrations against the change in pH, a clear overview of the potential indicators could be given. This is shown in figure 4.1 on the next page.
As all axes in figure 4.1 are plotted on the same log-scale, it can be seen which oxidation reactions cause the largest change in the concentrations for each potential indicator. For each graph in figure 4.1 the results are now briefly discussed.

pH versus Ca
Though calcium is not involved in the stoichiometry of the different oxidation reactions, it can be seen in the graph that the concentration is highly affected by the different oxidation reactions. This is a direct result of the change in pH. As explained in §2.3.3 changes in pH result in the dissolution or precipitation of calcite (also depending on temperature and P_{CO_2}).

This again affects the concentration of calcium. When pH decreases, due to oxidation of PCE, calcite dissolves and the concentration of Ca^{2+} increases. The opposite holds for the oxidation reactions of the non-target compounds. A difference in the effect on pH between the oxidation of pyrite and organic matter can be seen. As expected the oxidation of pyrite shows the largest effect on pH. The oxidation of organic matter results in a lower increase of pH. This has to do with the production of CO_2, resulting in an increase of carbonic acid (as described in §2.3.3).
Since all effects 'head in different directions' and because the differences in calcium concentrations are large, pH and Ca^{2+} are assumed useful indicators. However, it is important to realize that due to the low amount of permanganate added the calcite is not totally dissolved and thus water is continuously in equilibrium with calcite. When more permanganate was added and all calcite got dissolved during PCE oxidation the concentration of Ca^{2+} remained the same while the pH decreases up to a pH of 2.

pH versus CO2
The second graph shows the CO_2 against the pH. It is clear that the effect of the different oxidation reactions on the concentration of CO_2 is small compared to the effect on calcium concentration. The maximum change in concentration is one order of magnitude, caused by the oxidation of PCE.
The oxidation of pyrite results in a small decrease. This is due to the increase of the pH, which results in a lower share of carbonic acid in the carbonate species (figure 2.3). As CO_2 consist partly of H_2CO_3 the concentration of CO_2 decreases slightly.

pH versus chloride
The concentration of chloride is only affected by the reaction of PCE with permanganate. It is neither affected by one of the other oxidation processes, nor by (buffering) geochemical processes like for example CO_2 is. Therefore it is assumed a strong and useful indicator for the oxidation process of PCE. Main disadvantage of using chloride concentration as indicator for PCE oxidation is the fact that chloride is naturally present in groundwater. This is discussed in section 6.3.

pH versus sulfate
Where chloride is unique for the oxidation reaction of PCE, sulfate is unique for the reaction of permanganate with pyrite. The effect on the concentration is large: almost 3 orders of magnitude. Sulfate is thus a strong indicator for the oxidation of pyrite.
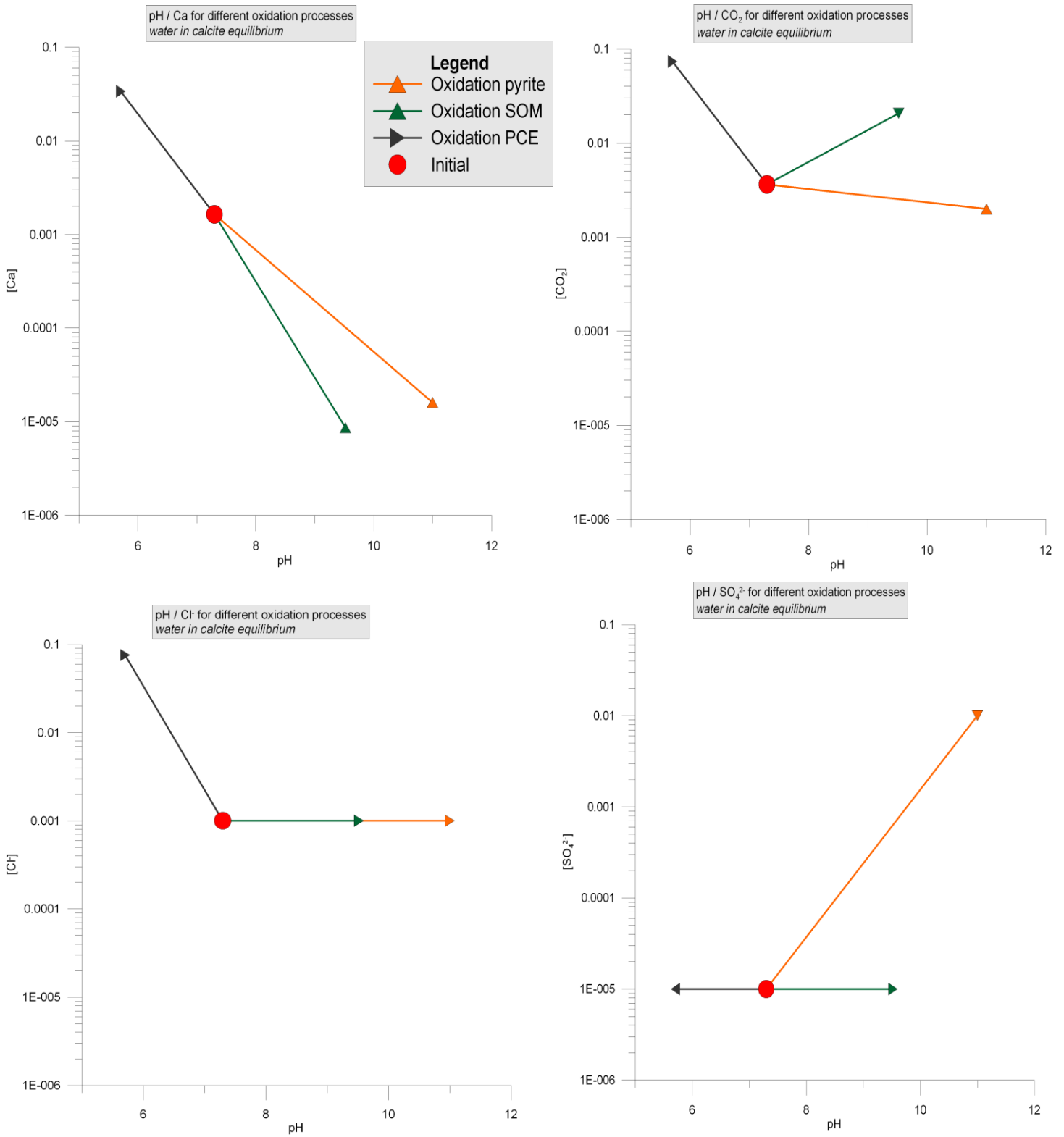
Figure 4.1 *Potential indicators for different oxidation processes – separately*

Now the same batch model is used to include different oxidation processes at the same time, which results in figure 4.2 (shown on the next page). Goal is to get a better insight in the interdependent relations between the different oxidation processes.

First thing that strikes from this figure is the dominancy of the oxidation reaction of pyrite on the indicators. Secondly it can be seen that all but the chloride graph show a nod in the graph at pH =9. This has to do with a shift in dominancy within the carbon species: from the bicarbonate specie to the carbonate ion specie (figure 2.3). The bicarbonate specie has a pH buffering effect, as it can adapt one proton. The carbonate ion does not have this ability; therefore the increase in pH speeds up once the carbonate ion becomes the dominant carbon specie.

From the green lines, indicating the oxidation of PCE and organic matter, it can be seen that first the oxidation of organic matter has a predominant effect on pH. Although PCE already oxidizes, as in the chloride graph it can be seen that the concentration increases, the pH increases at first. Then, at a certain moment more protons are being produced than can be buffered by carbonate species. This results in a reversal: pH starts to decrease.

From figure 4.1 and 4.2 it can be concluded that:
- When [Ca] is plotted against pH a distinction can be made between the different oxidation processes. Especially between target and non-target oxidation, as they 'move in different directions'. Therefore, for this batch model, plotting pH versus [Ca] gives a clear indication about which oxidation process dominates. This holds as long as the water remains in equilibrium with calcite.
- The same holds for CO_2 versus pH, although differences in concentrations are less distinct.
- The oxidation of pyrite causes the highest increase in pH of the two non-target compounds. As well, pyrite is the strongest reductant of the three components. This is especially clear from figure 4.2.
- Chloride and sulfate are unique of the oxidation reactions of PCE and pyrite, respectively.
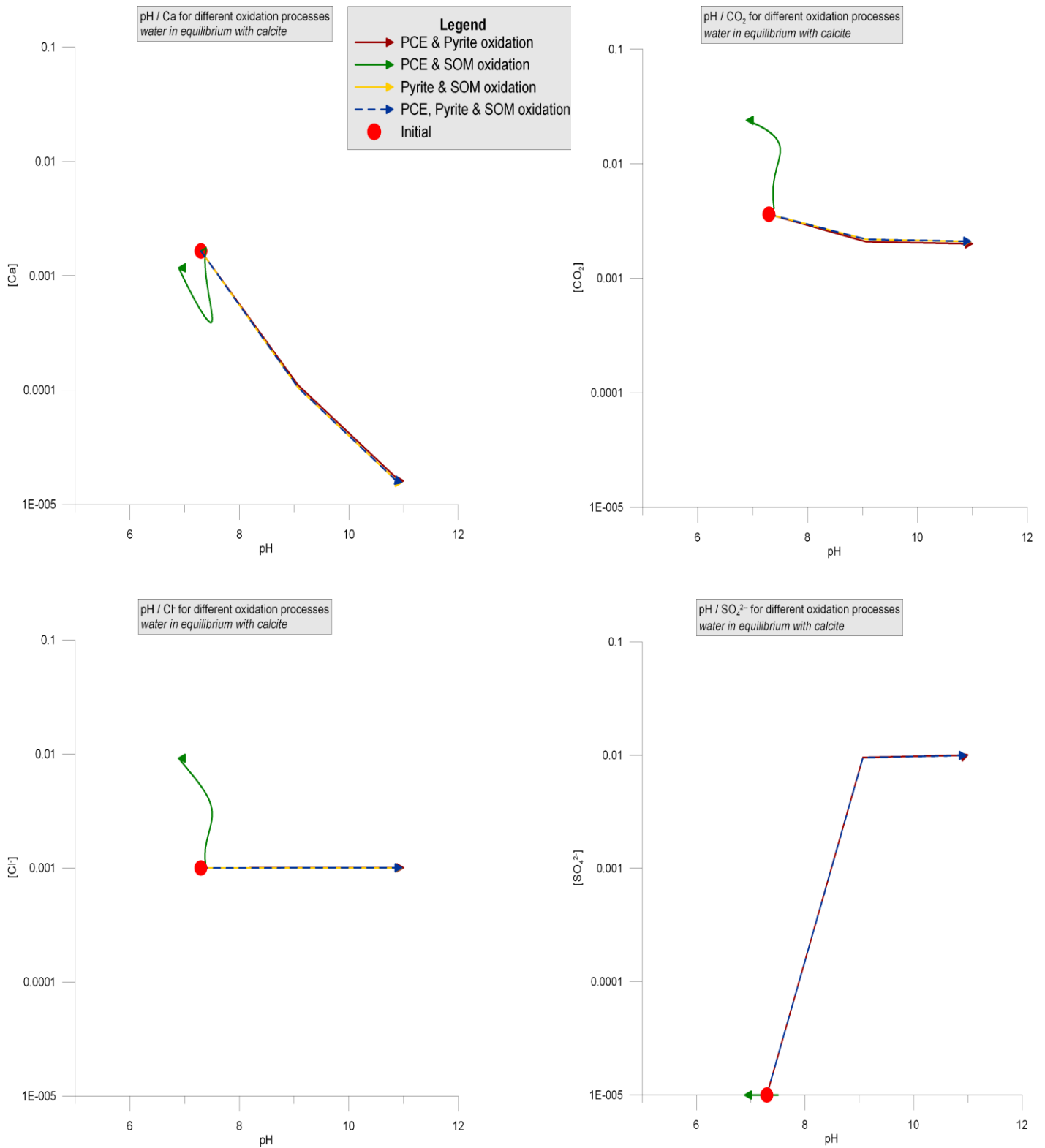
Figure 4.2   *Potential indicators for different oxidation processes – combined*

Scenarios

In the graphs discussed so far only a small amount of permanganate is available. Though it can be deducted from the results that most of the permanganate is used to react with pyrite, it is not known exactly how much permanganate is 'used' by each of the reductants. In other words, the efficiency[4] of the available permanganate cannot be read off these graphs. Using the chloride concentrations the efficiency can be determined exactly in this batch model. As well, the amount of permanganate reacting with pyrite can be determined from the sulfate concentrations. To see the effect of different efficiencies on the pH and [Ca] indicators, several scenarios have been conducted (table 4.4).

Both chloride and sulfate are used to determine the permanganate efficiency. The efficiency could be adjusted by 'simulating' different aquifer conditions: a lower presence of pyrite results in a larger share of the injected permanganate available for organic matter and PCE oxidation. In table 4.4 the soil matrix composition for the different runs is shown. It can be seen in this table that the Reference input value contains the highest pyrite content. This has been chosen such from a conservative point of view. The same is valid for the organic matter content, although two runs have been conducted with a higher organic matter content. The NOD values are given in the last column of table 4.4 (for reference values of different studies see figure 2.3).

Table 4.4   *Input mineral phases Batch model scenarios – all processes*

Run	$[PCE_{NAPL}]$ (mole / l_{bulk})	[PCE] *Vol. fraction*	[SOM] (mole / l_{bulk})	SOM *Vol. fraction*	[Pyrite] (mole / l_{bulk})	[Pyrite] (ppm)	NOD (g MnO4- / kg dry weighted sediment)
Ref.	0,09	3%	0,01	0,07%	0,01	494,0	11,1
1	0,09	3%	-	-	-	-	-
2	0,09	3%	0,001	0,01%	0,0001	4,9	0,8
3	0,09	3%	0,0015	0,01%	0,0005	24,7	1,3
4	0,09	3%	0,0025	0,02%	0,0005	24,7	2,1
5	0,09	3%	0,0025	0,02%	0,00075	37,1	2,2
6	0,09	3%	0,006	0,04%	0,0008	39,5	4,9
7	0,09	3%	0,005	0,04%	0,001	49,4	4,2
8	0,09	3%	0,006	0,04%	0,001	49,4	5,0
9	0,09	3%	0,007	0,05%	0,001	49,4	5,8
10	0,09	3%	0,0075	0,05%	0,0015	74,1	6,3
11	0,09	3%	0,005	0,04%	0,01	494,0	7,2
12	0,09	3%	0,016	0,12%	0,001	49,4	12,8
13	0,09	3%	0,009	0,07%	0,0017	84,0	7,6
14	0,09	3%	0,015	0,11%	0,001872	92,5	12,3
15	0,09	3%	0,0075	0,05%	0,002	98,8	6,5

In a similar fashion a series of runs has been conducted without organic matter as well as a series without pyrite presence. For all runs the resulting pH and [Ca] are plotted, resulting in figure 4.3. Of the different indicator graphs shown in figure 4.1 the pH versus [Ca] is used. This because the [Ca] is affected by all oxidation processes differently and [Ca] yields larger concentration differences than the concentration of [CO$_2$]. The concentrations of chloride and sulfate are used to calculate the efficiency for each run. In figure 4.3 the efficiencies for all runs are also shown, as labels along the line. The efficiency is calculated by dividing the total produced moles chloride by the maximum moles of chloride produced if all available permanganate reacts with PCE. The same holds for pyrite, using the total moles of sulfate. As in all cases the amount of permanganate got depleted, it is known that remaining permanganate reacts with organic matter.

---

[4] To recall: efficiency is defined as the amount of the (injected) permanganate that reacts with the target component: $PCE_{(aq)}$.
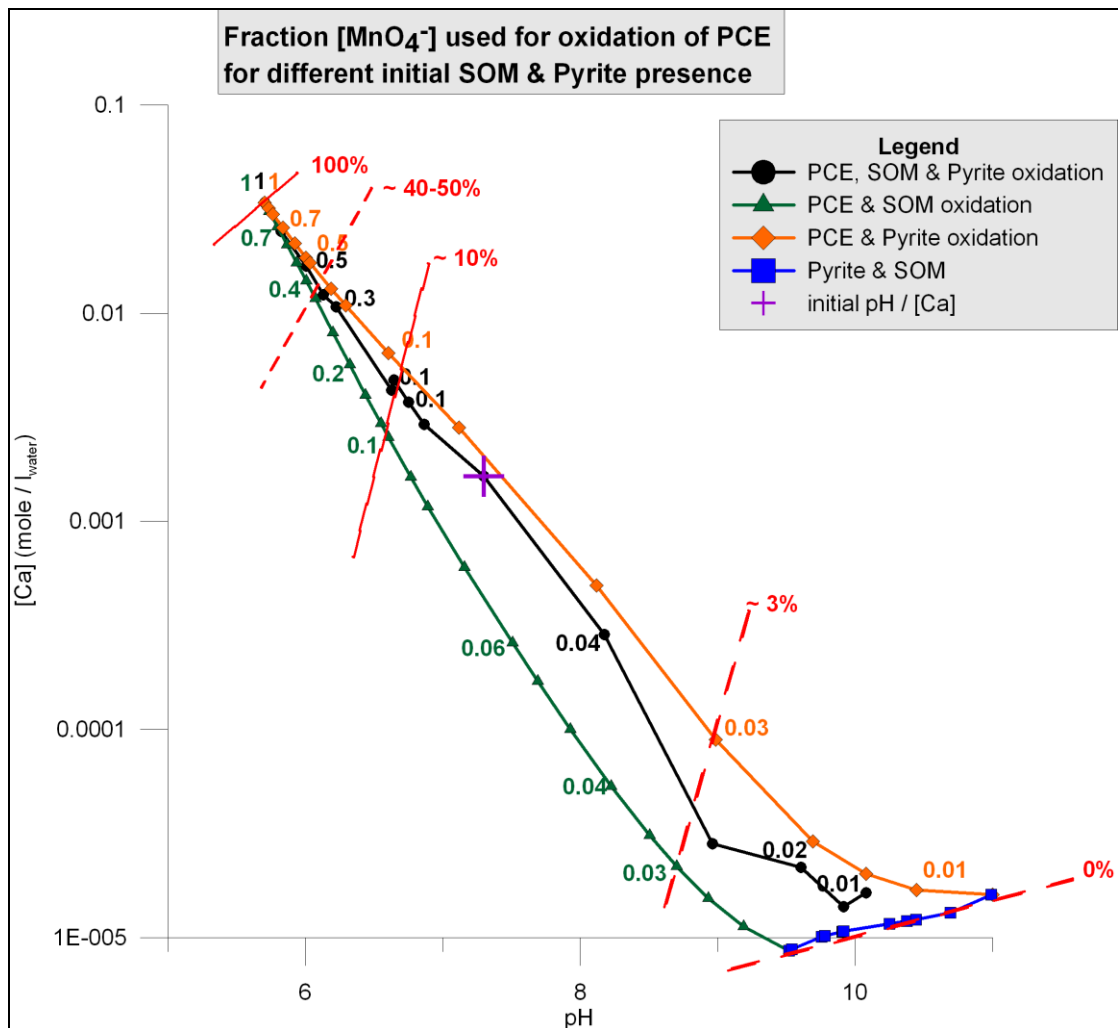
Figure 4.3   *Efficiencies for different aquifer conditions.*

The labels '1' indicate 100% efficiency, meaning that PCE is the only reductant present in the soil matrix and all added permanganate reacts with PCE. The oxidation of SOM & PCE can be seen as the 'lower boundary' and the oxidation of Pyrite and PCE the 'upper boundary'. If all processes are included (black line) the line varies in between these two. If more pyrite is present, the black line moves towards the orange line, if more organic matter is present towards the green line. The red dotted lines included in figure 4.3 cluster the corresponding efficiencies.

Figure 4.3 is plotted on log-scale. In figure 4.4 the same data is plotted on a linear scale, and instead of pH and [Ca] the changes in [H$^+$] and in [Ca] are plotted.

These figures show that for a specific initial situation, based on calcium and pH measurements a type curve can be produced. This type curve can be used to determine the efficiency of the ISCO remediation process, based on chloride and sulfate measurements.

It is emphasized again that in this specific situation the water is continuously in equilibrium with calcite. Even if 100% of the permanganate reacts with PCE calcite doesn't dissolve completely. If due to PCE oxidation calcite does deplete, the calcium concentration remains at a certain maximum concentration (since there is no flow).

In the batch model no mixing takes place, neither due to flow nor due to distribution through a domain. In reality this does play a role. When measuring at a certain location in the field it is possible that first the effects of upstream oxidation of pyrite and organic matter are measured, and then the effects of the oxidation of PCE. How flow affects the ability to use the different indicators is subject of the next chapter.

Further on in this research figure 4.3 is used to see if, for the same initial situation, it can be used to determine the efficiency of the ISCO remediation process in a more realistic flow situation.
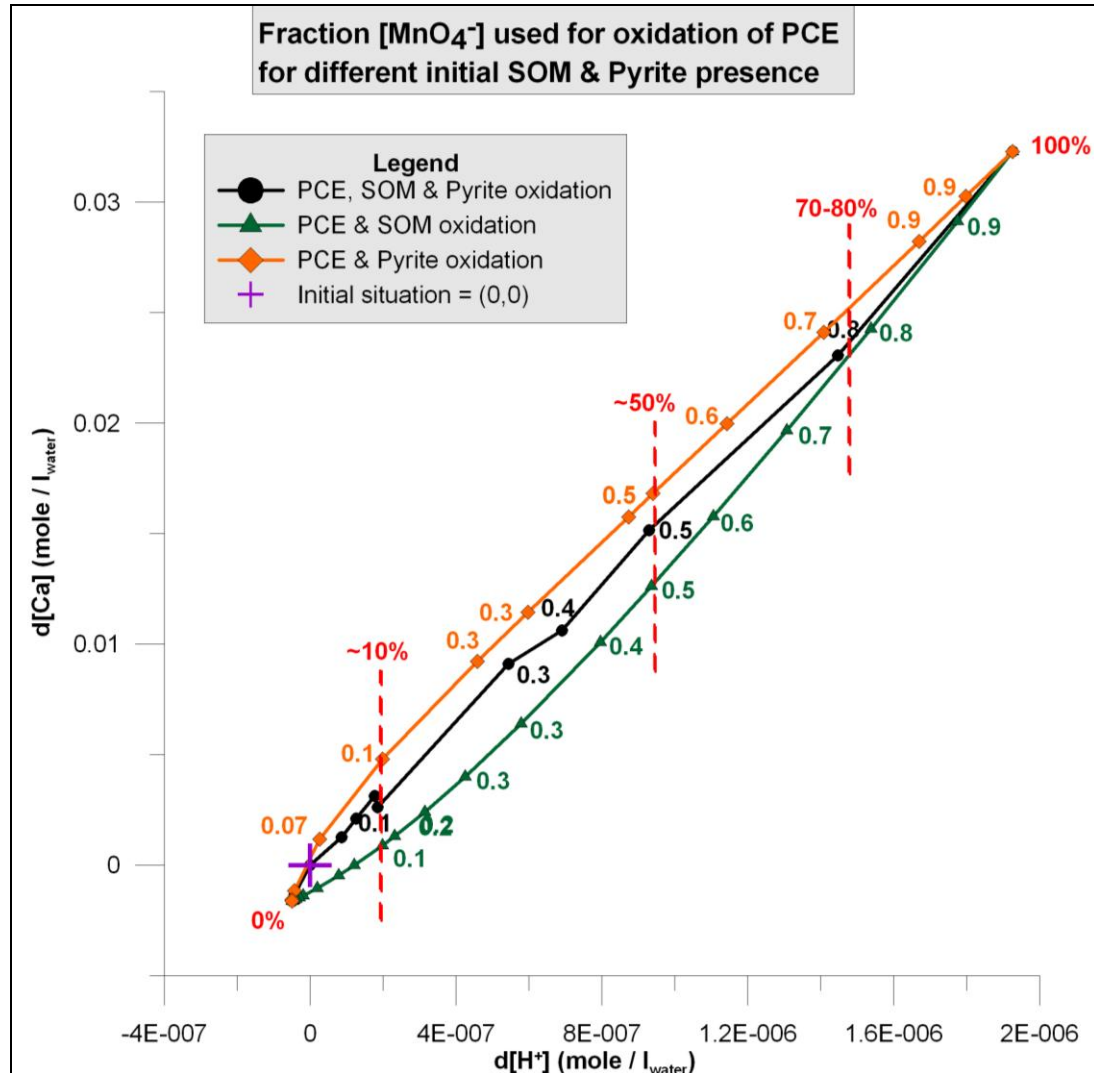
Figure 4.4   *Efficiencies for different aquifer conditions – linear axes*

4.4 Sub conclusion

In this chapter the behavior of the different selected indicators during the different oxidation processes is investigated. First the effect of the different oxidation processes on each of the indicators is looked at separately. From this it can be confirmed that chloride and sulfate are strong indicators for the oxidation of $PCE_{(aq)}$ and pyrite, respectively. It must be realized though that these are components are naturally present in groundwater. All natural waters contain chloride and sulfate ions. This is further discussed in §6.3.

The 'direction in which pH goes' is a strong indicator whether target or non-target compounds are being oxidized. The same holds for the calcium concentration. The CO_2 species concentration show less distinct results, as for both $PCE_{(aq)}$ and organic matter oxidation the CO_2 concentration increases.

When the different oxidation processes are included at the same time, such that competition between the different compounds arises, it is obvious that pyrite is the strongest reductant.

From figure 4.3 it can be seen that for a given initial situation a type curve can be created in which efficiencies are presented, based on the different selected indicators. For a given situation the indicators prove to be useful.

This chapter focused on the response of the selected indicators on the different oxidation processes within a controlled situation. Next chapter focuses on the response of the selected indicators to different field situation using a more realistic, 2D field scale model.

5. 2D flow model

5.1 Introduction

In this chapter the 2D flow model is described. Where previous chapter focused on the behavior of the different indicators in response to different oxidation processes this chapter focuses more on the applicability of this indicators in a field situation. As no field data from a real ISCO remediation project is available the model has been constructed based on the field situation which is described in Henderson et al. (2009).

The 2D flow model is used to further answer the first research question, and as well the second research question. Different remediation techniques are simulated to see their effect on the efficiency. The results obtained by the different remediation techniques are compared to a reference scenario. Final goal is to see if 'field measurements' of the indicators can been used according to certain 'rules of thumb' to adjust the injection of permanganate, while remediation is in progress. The 'rules of thumb' are based upon insights acquired through the modeling results presented in this and previous chapter. Focus of this chapter is therefore, besides the response of the indicators in a 'field situation', to answer research question 3.

The main goals and questions of this study are recalled in table 5.1.

Table 5.1   *Overview research goal and questions*

Goal 1	Find indicators which increase insights in the efficiency of chemical oxidation during the remediation process.
Goal 2	See if injection characteristic adjustments (such as rate, concentration, depth) can be based upon indicators found under (1).
Question 1	Is pH an effective indicator for the progress made during the $KMnO_4$ based ISCO remediation of a DNAPL contaminant source?
a)	How does the pH indicator work for different aquifer conditions (such as different SOM, pyrite and calcite content)?
Question 2	Which other indicators can be used to improve the determination of efficiency?
Question 3	Can certain general rules be applied, based on measurements of the indicators, to adjust injection characteristics in order to improve efficiency?

5.2 Setup & Input

5.2.1 Domain size parameters

The domain size of the 2D flow model is given in table 5.2, and visualized in figure 5.1.

Table 5.2   *Domain size flow model*

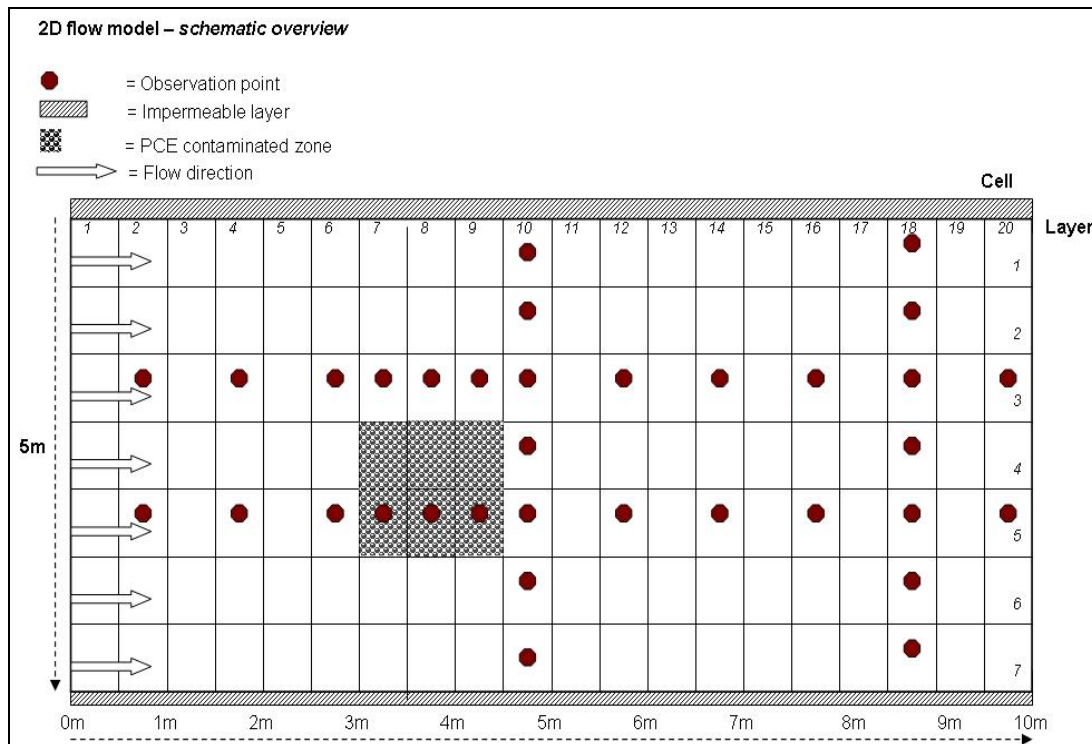| Domain	Size	Discretization
Length	10 meter	20 columns
Width	1 meter	1 row
Depth	5 meter	7 layers
Volume cell	$0.357[m^3]$: 357[liter]	

Figure 5.1   *Model mesh, source zone and observation point distribution*

5.2.2 Hydrogeological parameters

The aquifer is confined at the top and bottom by impermeable layers (figure 5.1). The aquifer is bounded by an impermeable layer on top allowing no atmospheric interaction or recharge. In between the two impermeable layers, in the middle of the aquifer, the source zone is situated. In the source zone PCE is present at residual saturations.

The aquifer is homogeneous, i.e. the porosity, as well as horizontal and vertical conductivity are constant through the domain as well as in time. In this study no permeability changes due to precipitation and/or dissolution of minerals is included. So the permeability of each layer is assumed to be homogeneous and isotropic. Permeability loss in the source zone is neglected. In table 5.3 hydrogeological values are summarized.

In figure 5.1 the flow direction is shown too. The flow velocity is initially set 90[m/year] (pore velocity) by creating head differences between the two constant head boundaries at both ends of the domain. Longitudinal dispersion is small, 1[cm] and transverse horizontal as well as transverse vertical dispersion is set 10% of the longitudinal dispersion. Because of the relatively small transverse dispersion, vertical movement of the water is negligible. Molecular diffusion is neglected in the model.

An overview of the hydrogeological characteristics is given in table 5.3. The soil matrix values are equal to the values given in table 4.2. Only difference is the total amount of PCE_{NAPL} present in the domain: 32[kg].

Table 5.3 *Hydrogeological parameter values*

Hydrogeological parameters	Input	[unit]	Description	Values Henderson et al. (2009)
Porosity	0.3	[-]		0.35
Hor. hydraulic conductivity	10	[m/day]		43 [m/day]
Vert. hydraulic conductivity	1	[m/day]		n.a.
Longitudinal dispersion	0,01	[m]		0,05 [m]
Transverse dispersion	0,001	[m]	10% longitudinal	0,005[m]
Molecular diffusion coefficient	0	[m^2/day]		$5,5*10^{-5}$ [m^2/day]
ρ_b	1700	[kg/m^3]	Bulk density soil matrix (Mass of oven dry soil matrix.)	1700 [kg/m^3]
ρ_s	2430	[kg/m^3]	Dry weighted mass sediment	

Groundwater composition

In table 5.4 the groundwater composition is given, as well as the composition of the injected water (or the oxidant solution). The oxidant solution has the same composition as the groundwater, only potassium and permanganate are added. Commonly during remediation projects nearby groundwater is used to inject the oxidant.

The injection of permanganate does not occur through a pulse injection, but by assigning a constant concentration to a constant head boundary. Although less realistic, as the conventional ISCO method is to inject the oxidant solution through pulse injection, the observations are better interpretable when excluding the 'turbulence' of a pulse injection.

Table 5.4   *Groundwater composition and oxidant solution.*

Aqueous components	Groundwater chemistry $mole/l_{water}$	Oxidant solution $mole/l_{water}$	Groundwater chemistry Henderson et al. (2009) $mole/l_{water}$	Oxidant solution Henderson et al. (2009) $mole/l_{water}$
PCE_{aq}	0 [a]	0	-	
MnO_4^-	0	$2.5\cdot10^{-1}$	$1\cdot10^{-15}$	$2.7\cdot10^{-1}$
K^+	0.000999	0.250999	$8\cdot10^{-5}$	$2.7\cdot10^{-1}$
Cl^-	$1.0\cdot10^{-3}$	$1.0\cdot10^{-3}$	$5.2\cdot10^{-3}$	$7.3\cdot10^{-4}$
Ca	$1.646\cdot10^{-3}$	$1.646\cdot10^{-3}$	$1.3\cdot10^{-3}$	$3.8\cdot10^{-4}$
$CO_2\ species$	$3.622\cdot10^{-3}$	$3.622\cdot10^{-3}$	$2.4\cdot10^{-3}$	$6.7\cdot10^{-4}$
$SO_4^{2-}\ species$	$1.05\cdot10^{-5}$	$1.05\cdot10^{-5}$	-	-
pH	7.3	7.3	6.0	6.9
Temperature	25 ºC	25 ºC	Not specified	Not specified

5.2.3 Model parameters

The modeling parameters that are discussed in this section comprise the time discretization and the advection and solver schemes.

Time discretization
The total time modeled in each run is 850 days, which is based on the time it takes in the reference model situation to completely oxidize the source zone. In PHT3D there are two options available to determine the time step length. The first option includes that the user defines the time step length, but "depending on the advection scheme selected, the transport simulator MT3DMS may sub-divide the user-defined time step length into several transport steps that fulfill the stability factor and accuracy criteria for physical transport (i.e. the Courant number) (Post and Prommer, 2010)." The second option includes that no time steps are defined, but they are determined automatically by the model based on the stability factor and accuracy criteria. The first option is used in this study. The number of time steps defined is 1700, such that one time step includes ½ day. Time steps and stress periods are equally defined in both the flow model (MODFLOW) and the transport model (PHT3D) to prevent for inconsistencies.

Advection scheme
The advection scheme is of major importance for transport modeling, as it tells how the model has to solve the advection-dispersion-reaction equation. Therefore some background information is given, mainly based on the MT3DMS manual, written by Zheng and Wang (1999). For an extensive description of advection solving schemes the reader is referred to this manual.
Numerically solving the advection-dispersion equation causes difficulties because in the transport equation (see eq. 2.26) a first derivative term (advection) and a second derivative term (dispersion) co-exist. And although "numerous techniques have been developed within and outside the groundwater modeling community in the last three decades, there is still not a single technique that can yield completely satisfactory solutions under general hydrogeological conditions" (Zheng and Wang, 1999).
There are three major 'families' of techniques to numerically solve the advection-dispersion-reaction equation: Eulerian, Lagrangian and combined Eulerian - Lagrangian methods.
The Eulerian approach is based on solving the transport equation using a fixed grid method, such as finite-difference or finite-element method. The Lagrangian approach solves the transport equation in a deforming grid through particle tracking.

The Eulerian approach has the advantages of a fixed grid, through which the dispersion-reaction-term can be solved effectively. However, if a problem is advection dominated (which is often the case in field situation) the Eulerian method may be 'susceptible to excessive numerical dispersion or artificial oscillation' (Zheng and Wang, 1999). To overcome such problems a fine grid and small time steps are needed, which lead to extra computational load. The Lagrangian approach provides more efficient solutions for advection-dominated problems, while almost no numerical dispersion results. However, without a fixed grid, numerical instabilities and computational difficulties can result. Especially if the media is nonuniform and bounded by complex boundaries and/or multiple sinks and sources are present in the domain. Moreover, particle tracking is based on velocity interpolation and this interpolation can lead to local mass balance errors.

The combined Eulerian – Lagrangian approach clearly tries to combine the advantages of both approaches. This by solving the dispersion-reaction term using the Eulerian approach, while for the advection term a Lagrangian method (particle tracking) is used.

In PHT3D 5 the user can choose between five different advection solution schemes:
- Particle tracking based Eulerian – Lagrangian methods
  - Methods of Characteristics (MOC)
  - Modified Method of Characteristics (MMOC)
  - Hybrid MOC/MMOC (HMOC)
- Standard Finite Difference Method
- Third-order total-variation-diminishing (TVD) method (ULTIMATE)

Basically based on trial-and error the MMOC scheme has been used within this study. The criteria on which it the different advection schemes have been compared are run time needed for running the same model and the presence of inexplicable oscillations in the given results. The MMOC solution scheme proved to be most suited for this study.

The TVD scheme is "arguably the best compromise between the standard finite-difference method and the particle tracking based Lagrangian or mixed Eulerian-Lagrangian methods" (Zheng and Wang, 1999). It minimizes both numerical dispersion and artificial oscillation. However, it caused minor uncertainties in the mass balance. And one of the limitations of PHT3D is that pH is calculated based on the ion-balance. Relative small-scale errors in the mass balance consequently result in major errors on pH calculation.

5.3 Scenarios

The first model that is created has been described by the input values given along this report (input files Chapter 3; soil matrix characteristics: table 4.2; domain: table 5.2; hydrogeological characteristics: table 5.3 and groundwater composition: table 5.4). This is the reference model, and it is the model with which the different scenarios are compared.

Different scenarios have been created from the Reference model to see the influence of three different types of variations:

1) Different field specific characteristics.
2) Different chemical / oxidation rate characteristics.
3) Different remediation techniques.

In the subparagraph for all scenarios of the different categories an overview is given in which the parameters that have been adjusted are indicated. The domain is the same for all scenarios. The differences with respect to the Reference model are highlighted in bold.

5.3.1 Site characteristic scenario's

Table 5.5   *Site characteristic model scenarios*

Scenario	[PCE] (Vol fraction)	[SOM] (Vol fraction)	[Pyrite] (ppm)	[Calcite] (Vol fraction)	Distr. PCE$_{NAPL}$ (layers x cells)
Reference	3%	0,07%	494	0.12%	2 x 3
No PCE presence	**0%**	0,07%	494	0.12%	2 x 3
No SOM presence	3%	**0%**	494	0.12%	2 x 3
No pyrite presence	3%	0,07%	**0**	0.12%	2 x 3
No pyrite & no SOM presence	3%	**0%**	**0%**	0.12%	2 x 3
No Calcite	3%	0,07%	494	**0%**	2 x 3
Lower [PCE$_{NAPL}$]	**1%**	0,07%	494	0.12%	2 x 3
Higher [PCE$_{NAPL}$]	**5%**	0,07%	494	0.12%	2 x 3
PCE distribution 1	3%	0,07%	494	0.12%	**3 x 2**
PCE distribution 2	3%	0,07%	494	0.12%	**1 x 6**

5.3.2 Reaction rate scenario's

Table 5.6   *Reaction rate scenario's (for references of values see Chapter 2)*

Scenario	k_{ox}^{PCE} [mole^{-1} l day^{-1}]	κ^{PCE} [day^{-1}]	k_{ox}^{SOM} [mole^{-1} l day^{-1}]	r_{ox}^{pyrite} [mole dm^{-2} day^{-1}]
Reference	5620	0.98	4.32	108
Low oxidation rate pyrite	5620	0.98	4.32	**0.128**
High dissolution rate PCE	5620	**5.2**	4.32	108
Low oxidation rate pyrite & high dissolution rate PCE	5620	**5.2**	4.32	**0.128**
Instantaneous[5]	**10000**	**10000**	**10000**	**10000**

5.3.3 Remediation plan scenario's

Table 5.7   *Remediation technique scenarios*

Scenario	Permanganate injection [kg/day]	Layers in which injected	Oxidant solution concentration [mole l^{-1}]	Flow velocity [m/year]
Reference	11.2	7	0.25 (= 40 g l^{-1})	91.25
Lower [KMnO$_4$]	1.12	7	**0.025 (= 4 g l^{-1})**	91.25
Segmented injection	3.2	**2**	0.25	91.25
Slow Flow	2.23	7	0.25	**18.75**

---

[5] In the instantaneous model the oxidation reaction kinetics have been adjusted. For every reductant the oxidant demand is determined from the stoichiometric relation.

5.4   Results

The model results are presented through two dimensional graphs. Since many different components are included, graphs are the most effective way to present the model results. The graphs represent observed values from the end of the domain. The observations are either of one specific layer (1 cell) or of one column (= 7 cells). In reality, the values for a specific layer can be obtained using a measurement device which can be placed at depth in a well. This concerns concentration measurements. However, the level of contamination is usually indicated by the magnitude of the contamination flux. Although determining the flux in field situations comes with upscaling difficulties – as it is always based on point measurements – in this modeling study the flux can be determined exactly by using the model data over the whole depth of the domain.

First the results of the Reference model are discussed. Goal is to describe the interaction between governing processes and their reflection on the concentration of the components. All included species, the aqueous components as well as the minerals, are discussed through a concentration / time plot (minerals) and a breakthrough curve (aqueous components). In both plots the pH is shown too. In addition, for the Reference model a pH overview of the domain is included.

Secondly, the results of the scenarios of the different categories are discussed. The results of all scenarios contribute to an increased insight in the use of indicators during an ISCO remediation process. Especially the scenarios from the first category contribute to an increased insight in the behavior of the selected indicators under different field conditions. While the scenarios from the third category focus on the effect of different remediation strategies on the ISCO remediation efficiency.
The focus of the second category is to see the significance of the chosen oxidation rates on the model outcomes. The oxidations and dissolution rates are based upon different literature studies, so these scenarios provide for a sensitivity analysis of the results with respect to the chosen oxidation/dissolution rates. As well, by performing a model run in which all kinetically based oxidation reactions are set very high to model instantaneous reactions, the influence of the defined kinetics can be seen. The results of these scenarios focus on both the indicators, as well as on remediation efficiency.
Although the categories have different focuses for all three categories the results presented are the same:
1)   pH, Ca and CO_2 species;
2) MnO_4^- efficiency based on chloride concentrations;
3)   mass PCE_{NAPL} in the domain, and
4)   mass flux $PCE_{(aq)}$ out of the domain.

The efficiency of the scenarios could be determined in similar fashion as is done for the 'Batch model': it is known how much permanganate is added to the domain and through the amount of moles chloride produced it is known how much of the injected permanganate reacted with $PCE_{(aq)}$. This has been calculated for all modeled scenarios, and is plotted against time. Because concentrations are measured at the end of the domain, while the oxidation of $PCE_{(aq)}$ occurs mainly near the source zone, a time lag is included in the efficiency calculations.

5.4.1   Reference model results

The results of the Reference model are shown in figure 5.2 and figure 5.3. These figures show the concentrations of the 5th layer, in which residual PCE_{NAPL} is situated, at the end of the domain (cell 18). The observations are presented of this location in the flow path behind the source zone, because concentration differences are most evident there. As the vertical movements of the water are negligible the $PCE_{(aq)}$ plume concentrates in the flow paths behind the source zone (see figure 5.5).

The concentrations of the immobile and the mobile phases are shown separately for clarity reasons. The pH is included in both graphs, indicated by the red line. Note that in figure 5.2 concentrations are plotted on a linear scale, while in figure 5.3 concentrations are plotted on a log-scale. The aqueous components are plotted on the log scale, because the concentrations differ some orders of magnitude.

Mineral phases (fig. 5.2)

Mineral phases are not easy to measure in field situations, since minerals form in the soil matrix and are immobile. They are therefore not useful as indicator. Their dissolution and precipitation does affect the groundwater composition. Therefore the mineral phases are discussed here as it is important to know when the different oxidation process begin and end in order being able to understand the aqueous phase concentrations which are discussed hereafter.

PCE_{NAPL}

First, it is noted that the concentration of PCE_{NAPL} is measured at a different location in the domain (figure 5.2).

The concentration decreases from t=0[days] onwards, as PCE_{NAPL} dissolves into the aqueous phase. The start of the oxidation of $PCE_{(aq)}$ is indicated by the node at t≈50 [days]. The dissolution increases due to oxidation of the aqueous phase, which increases the driving force of the dissolution process: the difference in maximum aqueous concentration (solubility limit) and the aqueous concentration (fig. 2.2). As PCE_{NAPL} saturation diminishes, the dissolution rate decreases. PCE_{NAPL} is totally depleted after 810 days. Although $PCE_{(aq)}$ has the 'fastest' oxidation rate constant of the three components (see Chapter 2 and Appendix A), figure 5.2 shows that the oxidation of $PCE_{(aq)}$ is limited by the dissolution from the nonaqueous phase into the aqueous phase.

It is important to realize that in field situations PCE_{NAPL} is often not completely depleted. The remaining PCE_{NAPL} is known for its rebound effect, which is infamous especially during pump & treat remediation projects. If remediation stops before remaining PCE_{NAPL} is totally removed, PCE re-enters the aqueous phase as soon the remediation stops. The two graphs (fig. 5.2 and 5.3) indicate that observations could lead to the decision to stop remediation after 100 days, based on the diminished $PCE_{(aq)}$ flux and the breakthrough of permanganate. However, since there is still PCE_{NAPL} available, this would result in a rebound effect.

Oxidation of pyrite

In the 18th cell of the 5th layer, permanganate breaks through at t=107days. The fast oxidation of pyrite starts at t=101days in the 18th cell and after t≈108 days pyrite is completely depleted. This indicates that permanganate becomes available for the other reductants, only when pyrite is almost oxidized. So as long as there is sufficient pyrite available for oxidation, all permanganate is consumed by the oxidation reaction with pyrite and consequently permanganate does not break through. This is in line with the observations described in chapter 4.
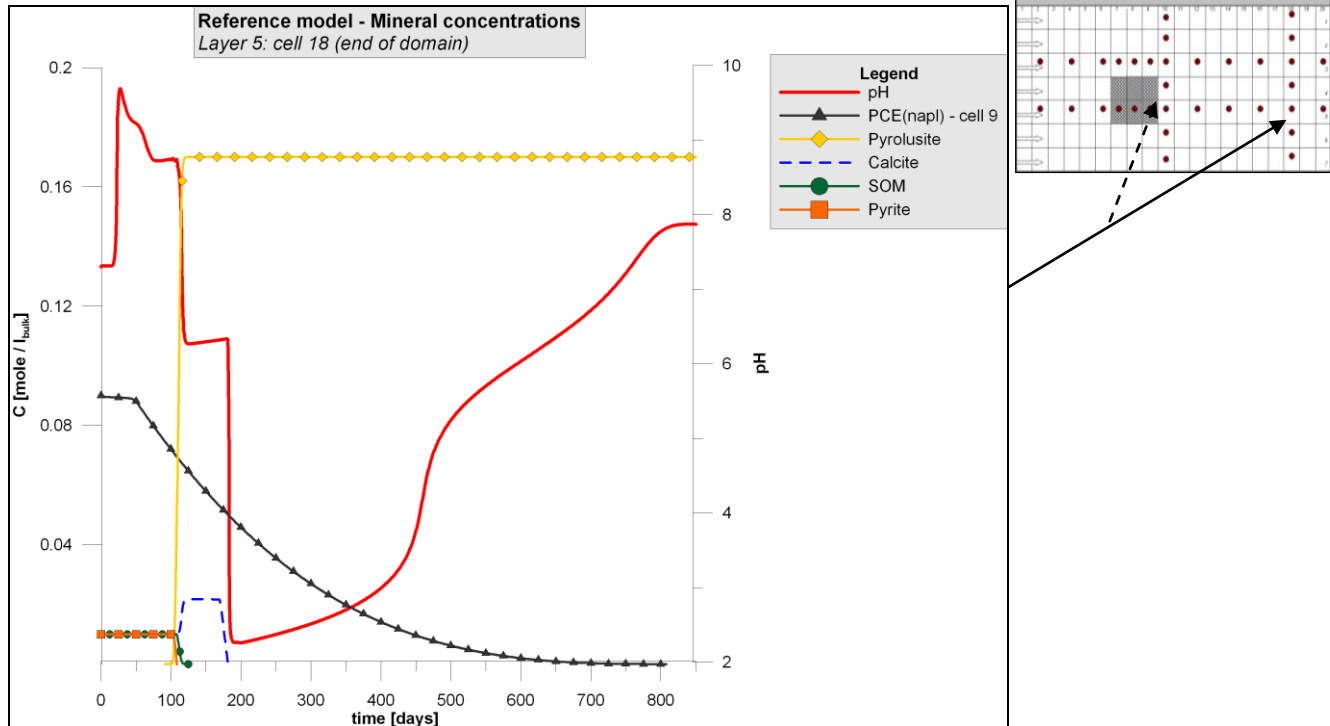
Figure 5.2   *Mineral concentrations and the pH. Note: the concentration of PCE$_{NAPL}$ is from within the contaminated source zone (cell9).*
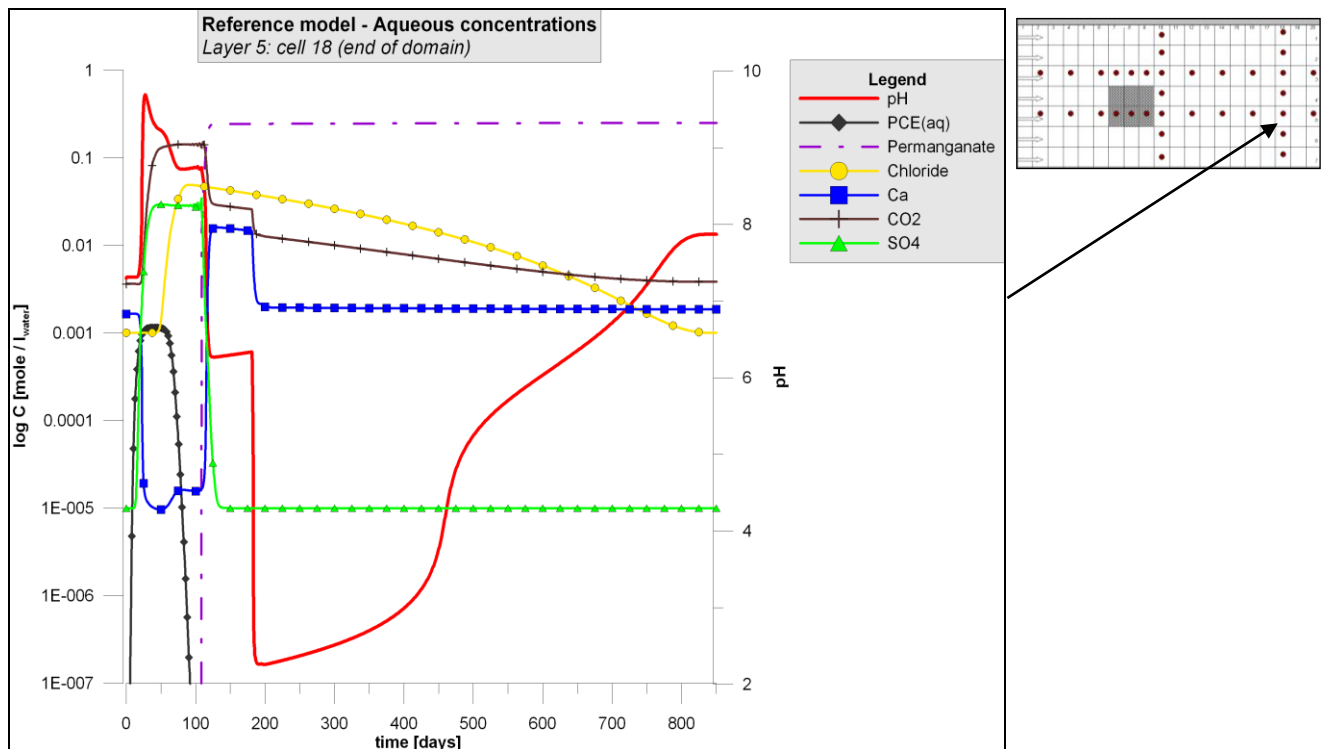

Figure 5.3   *Results Reference model. Aqueous phase concentrations.*

Oxidation of SOM
The oxidation of organic matter is slower than the oxidation of pyrite: The oxidation of SOM starts once pyrite is depleted, at t=108days, and is depleted after t=131days. Once organic matter is totally oxidized no oxidation processes take place at this location in the domain. So all changes in concentrations are caused by the upstream oxidation of $PCE_{(aq)}$ (near the source zone).

Pyrolusite
The mineral pyrolusite ($MnO_{2(s)}$) is a reaction product of all three oxidation reactions. However, at this location in the domain the precipitation of this mineral is mainly the result of the oxidation of pyrite. After t=124[days] pyrolusite is at its maximum and constant concentration of 0,17[mole / l_{bulk}]. A pyrolusite dissolution due to low pH conditions is not included in this model.
The precipitation of pyrolusite is linked to loss of permeability of the aquifer in several studies (see Henderson et al., 2009). In this study the loss of permeability is not taken into account.

pH
As the first oxidation of mineral phases in the 18th cell take place after 100 days, the high pH peak before t=100[days] must originates from the oxidation of pyrite upstream. In figure 5.4 the development of pH in time for the whole domain is shown. This figure illustrates that pH decrease by PCE oxidation is largely offset by the pH increase due to NOD oxidation. The pH only drops significantly due to the PCE oxidation after NOD is completely depleted in the source zone.
When organic matter starts to oxidize (increase of [CO_2 species] – figure 5.3), pH starts to decrease until pH remains stable at ~8,7. This indicates that the oxidation of organic matter 'tempers' the pH increase. In other words, if only pyrite oxidation takes place higher pH values are obtained. When pyrite is depleted (sharp decrease in SO_4^{2-} at t=109) the pH tumbles to a new 'stable' value of ~6,3. Due to ongoing organic matter oxidation (until t=131days) and calcite equilibrium the pH even slightly increases, as it tends towards initial value. Once organic matter is depleted and all calcite has been dissolved pH decreases sharply under the influence of only $PCE_{(aq)}$ oxidation. Then, as PCE_{NAPL} saturation decreases and thus less $PCE_{(aq)}$ enters the water, the pH starts to increase towards initial value. The big curvature, visible around t=400[days], is described into more detail later on, in combination with the concentration of the CO_2 species.
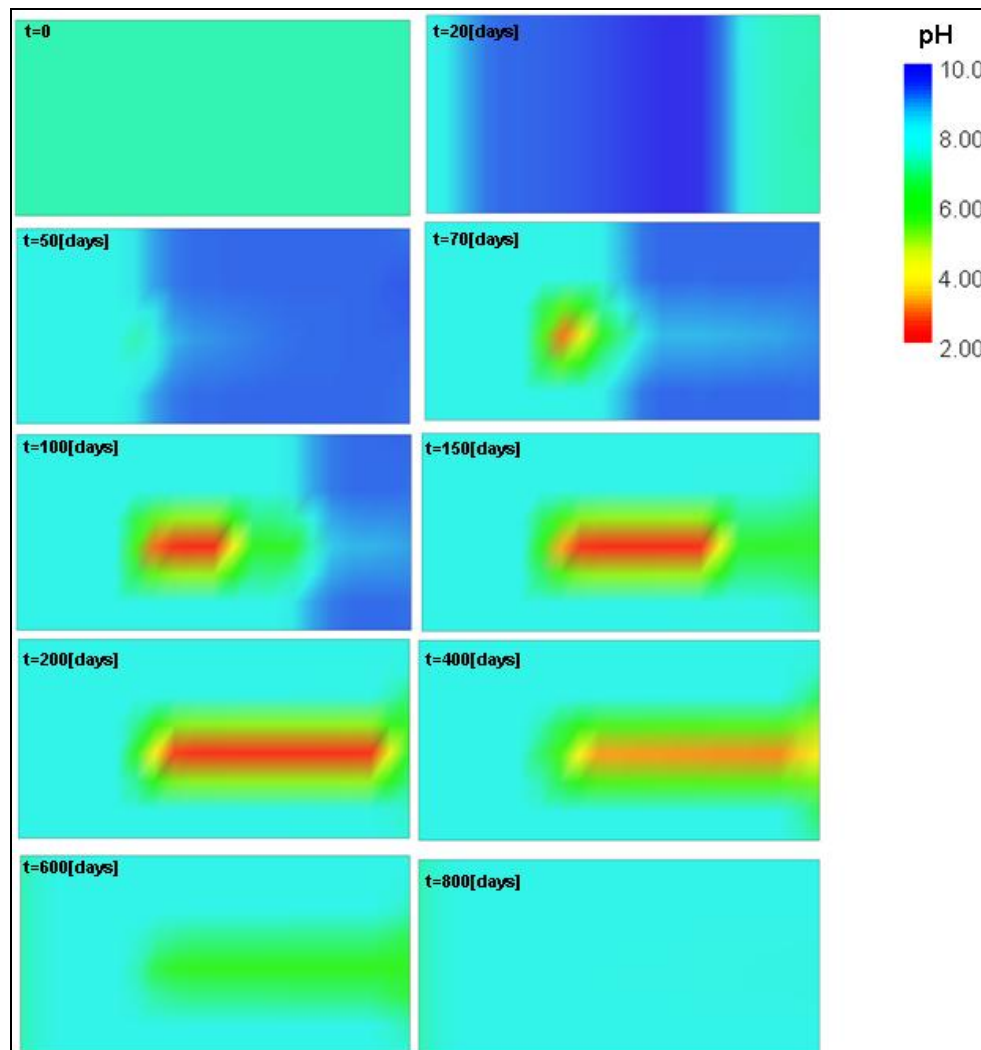
Figure 5.4   *pH in domain (the angular shape is due to the relatively coarse grid of the model).*

Calcite

Whether calcite precipitates or dissolves is outcome of the delicate carbonate equilibrium, in which pH and $p[CO_2]$ play an important role (see §2.3.3). To recall: an increase in pH leads to precipitation of calcite, and an increase in $p[CO_2]$ to dissolution (assuming other parameters are constant and thresholds are exceeded).

Although not visible in figure 5.2 the concentration of calcite increases very slowly from t=0 until t=107[days]. When oxidation of organic matter starts, the calcite concentration increases at higher pace. During the first 107 days almost no calcite precipitates in the 18th cell, although groundwater with a higher pH (up to almost 10) flows through the cell. Once organic matter begins to oxidize calcite precipitation starts to accelerate. This has to do with the CO_2 production. CO_2 partly dissociates to carbonic acid, H_2CO_3. In figure 5.5 (which is a combination of figure 2.3 and the model results) it can be seen that under higher pH conditions carbonic acid forms CO_3^{2-}, because the carbonate-ion is the dominant carbon specie under higher pH values. The carbonate-ion reacts with calcium to precipitate as calcite, $CaCO_{3(s)}$. However, the main cause of calcite precipitation in the 18th cell between t=100 – 200[days] follows from figure 5.6. This figure indicates a strong increase in calcite concentration just after the source zone when the oxidation of $PCE_{(aq)}$ starts. The oxidation of $PCE_{(aq)}$ causes a decrease in pH resulting in the dissolution of calcite in the source zone. Calcium is thus released into the groundwater (also clearly reflected in figure 5.3 around t=100days]). In combination with the increased CO_2 concentration the calcium precipitates as calcite.

The precipitation of calcite reflects in the concentration of the CO_2 species: a sharp decrease can be seen in figure 5.3 at t=115. At t=128[days] the concentration of calcite is at its maximum, just before organic matter is totally depleted (at t=131[days]). Then calcite slowly starts to dissolve. This dissolution has to do with the ongoing $PCE_{(aq)}$ oxidation (figure 5.4 and 5.6). From t=169days on calcite concentrations decreases fast towards 0: at t=181 all calcite is depleted. Exactly at this moment (t=181) a sharp pH decrease is measured (fig. 5.2 and 5.3). This is because the buffering capacity of calcite disappeared.
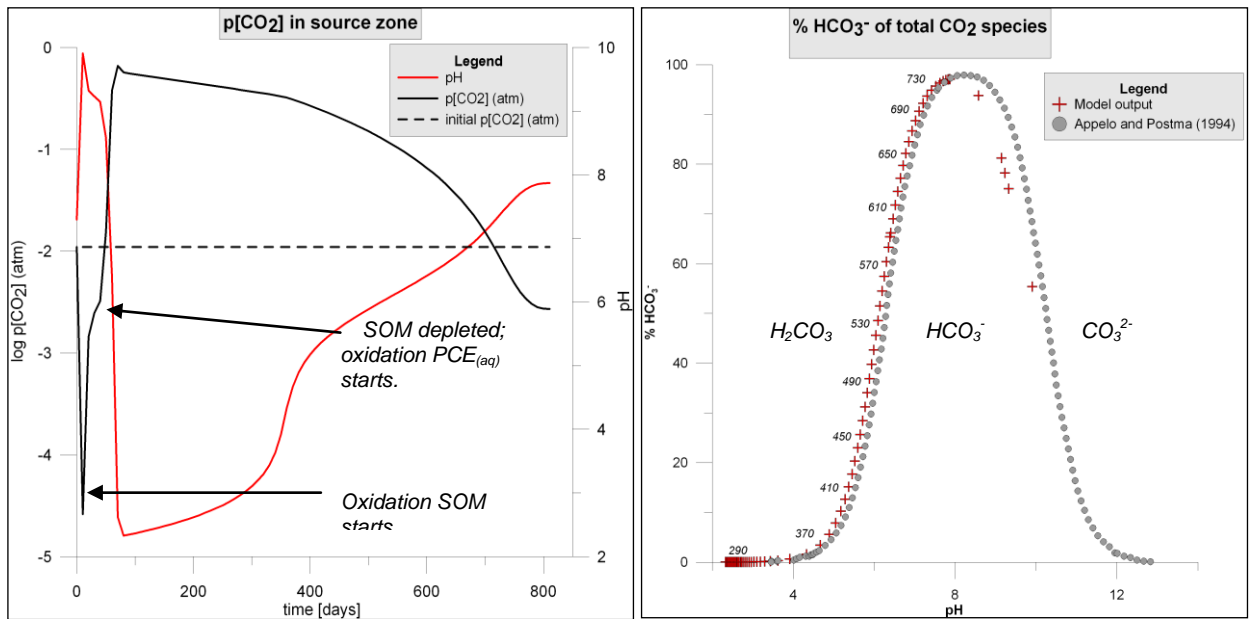
Figure 5.5 $p[CO_2]^6$ in source zone (left) and concentration of the bicarbonate in the total CO_2 species (right). Next to the curve time labels are shown. Note that these are measurements from within the source zone, not from the end of the domain. The data is obtained by using the Postfix option of PHREEQC-2.
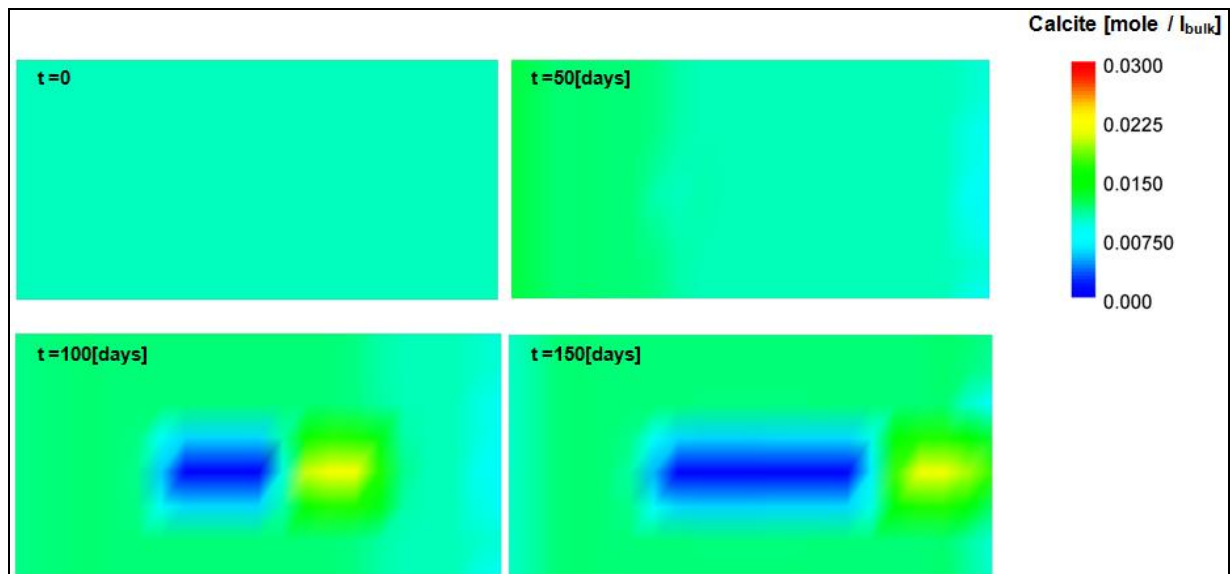
Figure 5.6   *Calcite concentrations through domain.*

---

[6] The p[CO$_2$] is calculated from Appelo and Postma (1994): $\left[HCO_3^- \right] = \dfrac{10^{-7.8} \cdot P_{CO_2}}{\left[H^+ \right]}$

Mobile phases (fig. 5.3)

$PCE_{(aq)}$ & Chloride
After 6 days the aqueous PCE concentration breaks through the intervention value (MCL = $2.4*10^{-7}$ mole/liter, table 2.1). The concentration increases towards the solubility limit and reaches a concentration of ~95% solubility limit at t=42 days. In figure 5.7 the $PCE_{(aq)}$ plume after 40 days is shown, to indicate that the distribution of $PCE_{(aq)}$ limits to the layers in which the source zone is situated.
After the peak at t=42[days] $PCE_{(aq)}$ concentration decreases as the oxidation of $PCE_{(aq)}$ starts. The start of $PCE_{(aq)}$ oxidation is clearly marked by the increase of chloride concentration. Below MCL concentrations are reached at t=90 days. So, within 42 days permanganate breaks through at the source zone, where it 'cuts of new supply', such that the $PCE_{(aq)}$ concentration at the observation point starts to decrease.
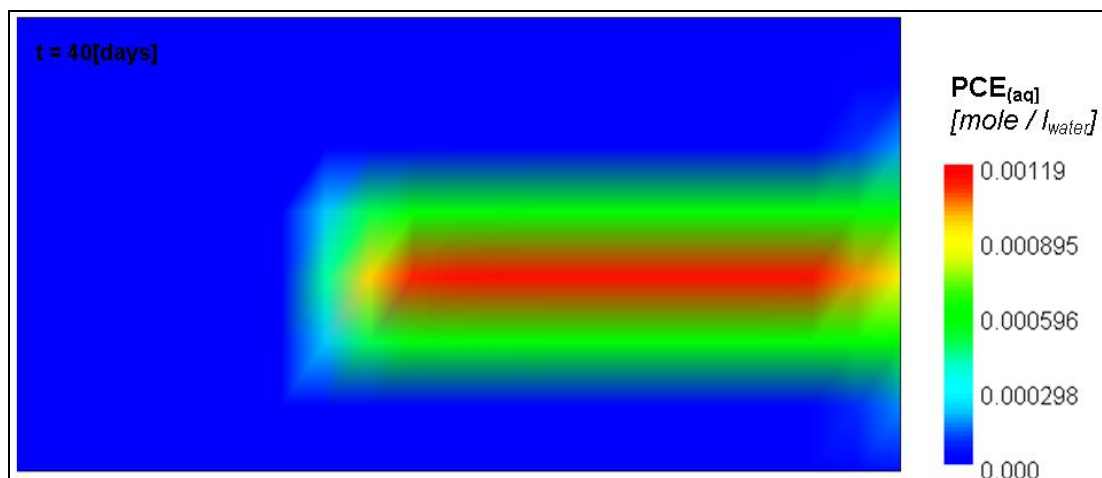
Figure 5.7   *$PCE_{(aq)}$ plume in domain.*

Permanganate
It takes until t=107[days] until permanganate breaks through at this observation point. This indicates that it takes 107 days for all pyrite and organic matter to oxidize. The breakthrough of permanganate at the observation point coincides with the depletion of pyrite in that cell. Figure 5.3 is plotted on log scale, which conceals that it takes until t=810 until the concentration of permanganate equals the injection concentration. From this it follows that the oxidation of $PCE_{(aq)}$ only uses a very small part of the injected permanganate concentration. This implies that a breakthrough of permanganate doesn't mean that there is no $PCE_{(aq)}$ oxidation going on.

SO_4^{2-}
The sulfate concentration can be directly linked to the oxidation of pyrite. It increases as soon as the first pyrite oxidation takes place in the domain.

pH, calcium and CO_2 species
These three components are strongly related to each other through carbonate equilibrium, as described above. This is reflected in figure 5.3: all major changes coincide in time.
Of these three components the calcium concentration is the least complex, as it just follows the precipitation and dissolution of calcite in the domain. It must be realized that the calcium concentration represents the calcite development from all upstream cells. This is the reason that the calcium concentration does not follow the calcite development shown in figure 5.2. After 100 days the first calcite starts to dissolve, upstream in the source zone, where the first $PCE_{(aq)}$ oxidation takes place (fig. 5.6). From then on downstream of the source zone calcite dissolves, adding calcium to the groundwater. This explains the strong increase in calcium concentration resulting in calcite precipitation in the observation cell. At t=181, once all calcite

up to and including the observation cell has been dissolved, calcium concentration drops towards initial concentration.

The CO_2 species concentration first shows a large increase, starting around t=25[days]. This links to the breakthrough of the first oxidation of organic matter upstream in the domain. At t=85 the concentration CO_2 species is at its maximum, when also the oxidation of $PCE_{(aq)}$ contributes to the CO_2 concentration. Then a first sudden drop in concentration is visible, which occurs at t=115. This is due to the following reasons:

- Calcite precipitates ('capturing' carbonate-ions);
- Depletion of organic matter upstream in the domain;
- And the available $PCE_{(aq)}$ is depleted, meaning that oxidation is now limited by dissolution.

Because directly after calcite has precipitated, it starts to dissolve and therefore the level of CO_2 concentration remains slightly higher than the next drop: calcite dissolution is an extra CO_2 source next to $PCE_{(aq)}$ oxidation. After t=180, when calcite is totally dissolved, this source diminishes which causes the second drop.

The pH development has already been described above, except for the curvature in the graph (t = 300 - 400[days]). Because only $PCE_{(aq)}$ is oxidizing and all other mineral phases are diminished, this curvature must associate with the carbonate equilibrium: the CO_2 species. Using the 'postfix' function, which is a PHREEQC-2 add on package which can be implemented in PHT3D, the type of CO_2 species could be further specified (figure 5.8).
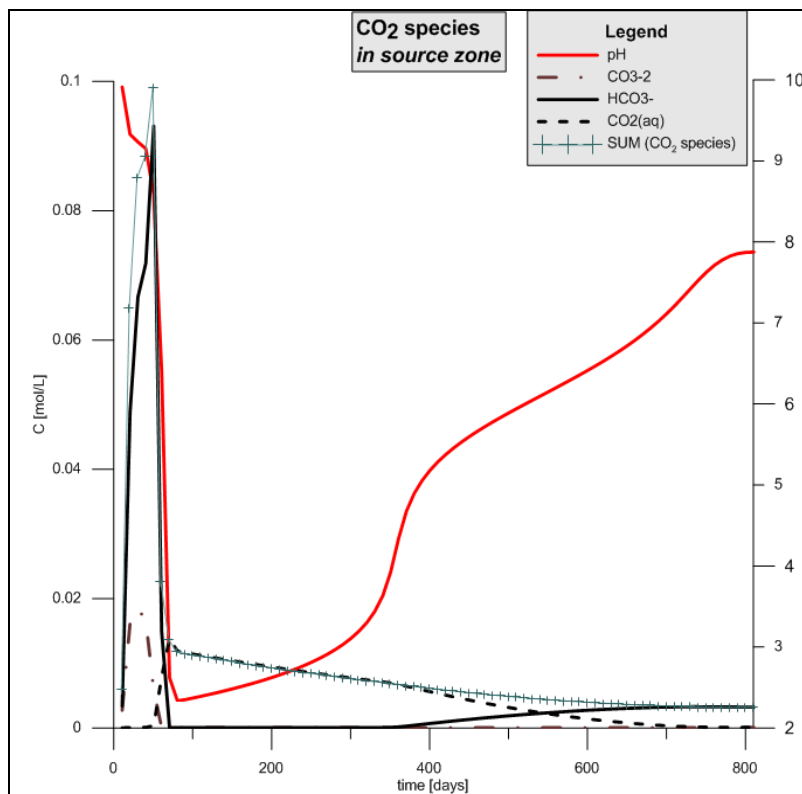
Figure 5.8   *CO_2 species in relation with pH development.*

During the oxidation of $PCE_{(aq)}$ H^+ and CO_2 are produced, causing a decrease in pH and an increase in $p[CO_2]$ (figure 5.5). The produced CO_2 adapts two protons to form carbonic acid, which is the dominant CO_2 specie under low pH conditions (fig. 5.8, at t≈100[days]). Because the saturation of PCE_{NAPL} decreases due to ongoing oxidation the production of protons and CO_2 decreases: pH goes slightly up, tending towards initial value. The sum of the CO_2 species decreases (fig. 5.8). From figure 5.5 it is known that around 370 days the dominancy within the CO_2 species shift from H_2CO_3 to HCO_3^-. During these transition phases the

buffering capacity decreases, which results in fluctuations of the pH (Bethke, 2008, p. 219). This is shown in figure 5.9.
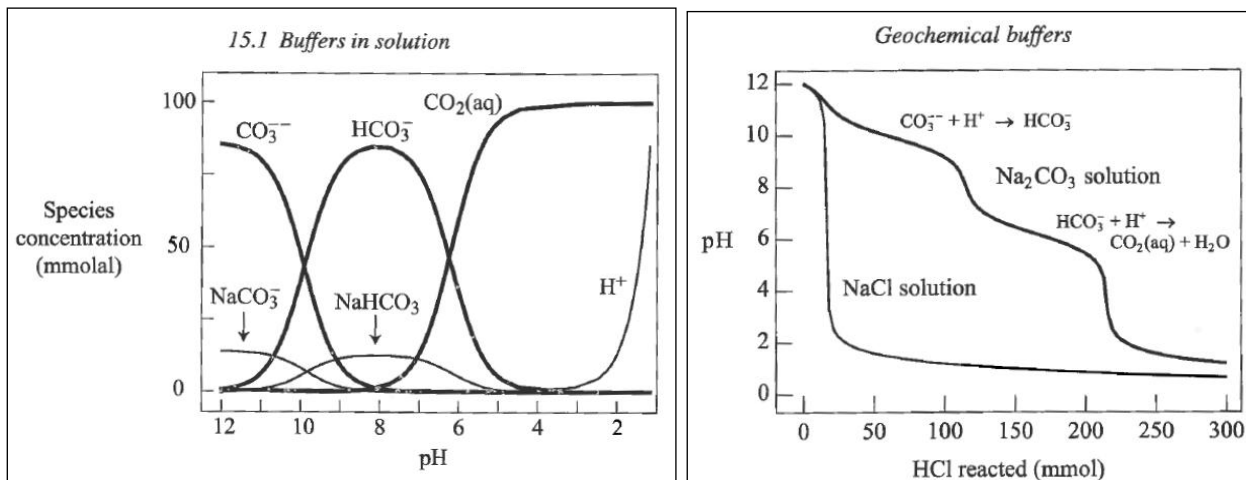
Figure 5.9   *Shift in dormancy of different CO_2 species. During transition moment buffering capacity decreases (left figure) resulting in pH fluctuations (right figure). (source: both figures adapted from Bethke, 2008)*

Consideration
The results discussed in this section show that using the concentration of the CO_2 species to indicate which oxidation process prevails is difficult. By which it is meant that from measuring only this indicator alone, it is not possible to draw solid conclusions. This is because the concentrations are influenced by upstream processes and come with a certain delay. Moreover, both the oxidation of target and non-target compounds result in an increase of CO_2 concentration. The concentration of calcium actually is only indicative if calcite is present. Once all calcite is dissolved, the initial calcium concentration is measured (as calcium is not produced by one of the oxidation reactions). This could provoke to conclude that no oxidation is going on.
Chloride and sulfate are strong indicators.
From the direction in which pH 'moves' it can be deduced which of the oxidation processes prevails. For pH the following rule of thumb applies: if $pH < pH_{initial}$ oxidation of $PCE_{(aq)}$ is ongoing.

Now that the concentration development for all components is discussed into detail the focus shifts toward describing the remediation efficiency of all modeled scenarios as well as the reflection on the indicators.

5.4.2 Field characteristic scenario's

On the next page the results of the different scenarios are presented (fig. 5.10). The graphs on the left side show the pH, calcium concentration and CO_2 species concentration. The graphs on the right side show the total mass PCE_{NAPL} in the domain, the mass flux $PCE_{(aq)}$ out of the domain and the remediation efficiency. The concentrations are measured in the 5th layer at the end of the domain. The fluxes are based on the average concentration at 9m from the inlet point, over the whole depth over the domain.

For the different scenarios is it discussed to what extent the presented indicators show similar results as the calculated efficiency. In other words: can the remediation efficiency as well be deduced from the indicator graphs?

Two general notes concerning the subparagraphs in which the scenario results are discussed:

1) It is denoted that not all scenario results are discussed for the shown graphs. Main focus is to link the efficiency with the indicators. Graphs that are relevant to this goal are discussed.

2) the scales of the axes of the plotted figures differ.

And, in addition, a note concerning the remediation efficiency:

Two types of efficiencies are considered in this study: peak (or maximum) efficiency and overall efficiency. Peak efficiency is based on the chloride flux. Since the background concentration is known, the increase in chloride concentration and thus, from stoichiometric relations, the amount of PCE oxidized could be determined.

The overall efficiency is based on the permanganate concentrations. It is known how much permanganate is injected over the total period. And from the measurements at the end of the domain it is known how much permanganate flowed out of the domain. Consequently it could be determined how much of the injected permanganate was included in oxidation reactions. The amount of permanganate which is still present in the domain is taken account for (it is determined from the scenario in which no organic matter and pyrite is present). From the chloride and sulfate measurements the part of the used permanganate for PCE and pyrite oxidation, respectively, could be determined.

In the figure 5.10 – 5.12 the peak efficiency is shown. In Appendix E bar charts are presented in which overall efficiency is given for the 'field characteristic ' and 'remediation' scenarios.

The peak efficiency is calculated and presented per day (fig. 5.10 – 5.12). As it is the goal to see to what extent the indicator concentrations correspond to the efficiency, the peak efficiency is discussed more extensively in this chapter.

Remediation efficiency

The efficiency graph shows that the efficiency of the bulk of the graphs has a maximum of ~1%. Two curves do show a different efficiency: If PCE_{NAPL} saturation is higher, a higher efficiency is obtained. If PCE_{NAPL} saturation is lower, a lower efficiency is obtained. This is what one would expect, as the amount of permanganate added is constant for all plotted scenarios here. More PCE_{NAPL} available results in more $PCE_{(aq)}$ entering the groundwater and thus more oxidation can take place.

Second observation concerning the efficiency of the remediation is that from this graph it cannot be concluded that the efficiency is influenced by the amount of NOD present in the domain. This can be explained by the fact that the efficiency graph is solely based on the chloride flux. The total amount of PCE_{NAPL} in the domain is the same for all scenarios (but for the 'higher PCE_{NAPL} saturation'- and the 'lower PCE_{NAPL} saturation' scenarios, which can be seen in the 'mass in domain' graph). Therefore, the total chloride flux which can be produced is unaffected. As far as it concerns the efficiency calculation, no distinction is made whether permanganate flows out of the domain unaffected or reacts with NOD. As a consequence only the time it takes until oxidation of $PCE_{(aq)}$ starts is influenced by the amount of NOD present, which reflects in the 'efficiency graph' by the moment that peak efficiency is reached. If no NOD is present (purple solid line) the peak efficiency is reached within 50 days. In the reference scenario this is around 90 days.

To be able to see the influence of the NOD present in the domain a further specification of the use of the injected permanganate is given in Appendix E. From the bar charts presented there it follows that ~9% of the total injected permanganate is used for oxidation reactions. Only if

organic matter is absent, significantly less permanganate is used. From these graphs it can also be seen that organic matter is the reductant with the largest oxidant demand (~70% of used permanganate is used in the oxidation reaction of organic matter). Permanganate used in the oxidation of $PCE_{(aq)}$ fluctuates around 3% of the total used permanganate. Oxidation of pyrite consumes around 27% of the total used permanganate.

Mass PCE_{NAPL} in domain
Looking at the graph in which the total mass PCE_{NAPL} in the domain is presented it can be seen that the higher PCE saturation does not significantly influence the time needed to totally 'clean up' the site. This again confirms that it is the dissolution rate that limits the oxidation of PCE. A higher PCE content implies more $PCE_{NAPL} \Leftrightarrow$ groundwater interfacial contact, which results in more $PCE_{(aq)}$ availability for oxidation. The higher the content is, the faster the mass depletion rate.

Mass flux
When looking at the $PCE_{(aq)}$ mass fluxes of the different scenarios little differences can be seen between the higher saturation scenario and the reference scenario. This is because the mass flux of the reference scenario already reaches 95% of the solubility limit, implying that
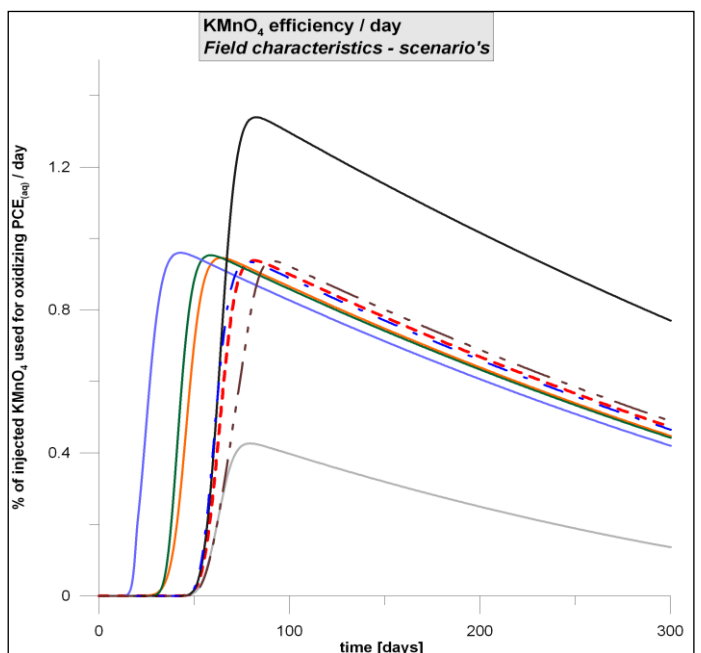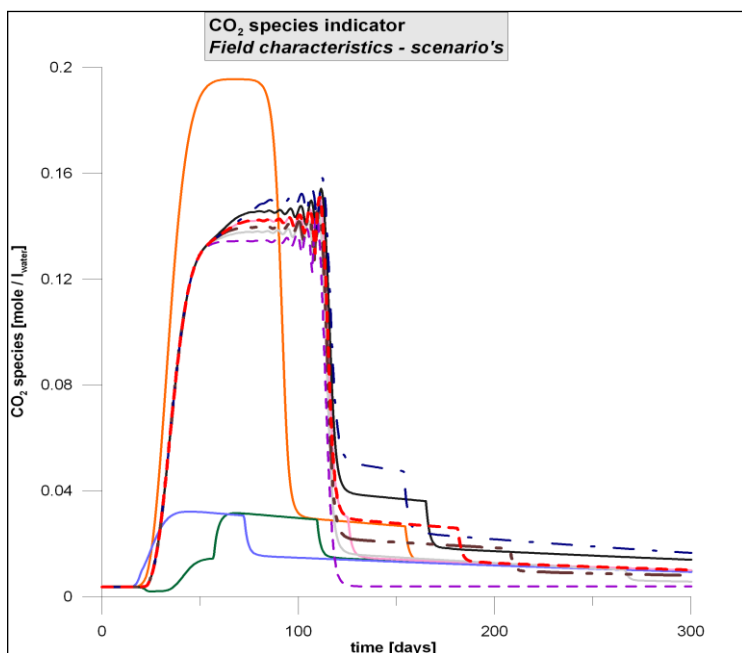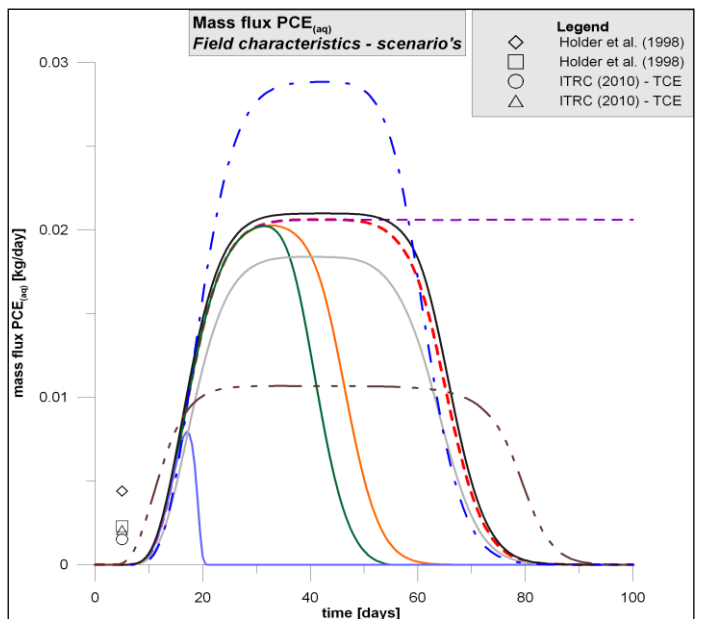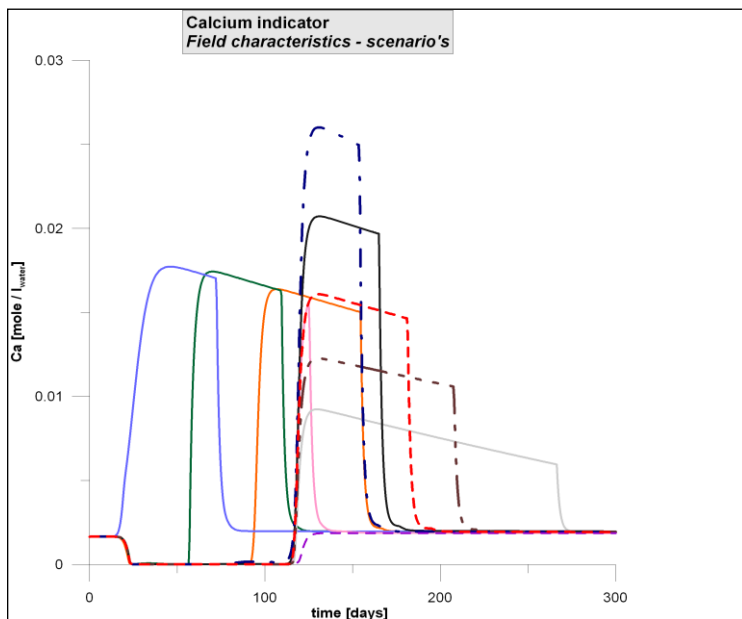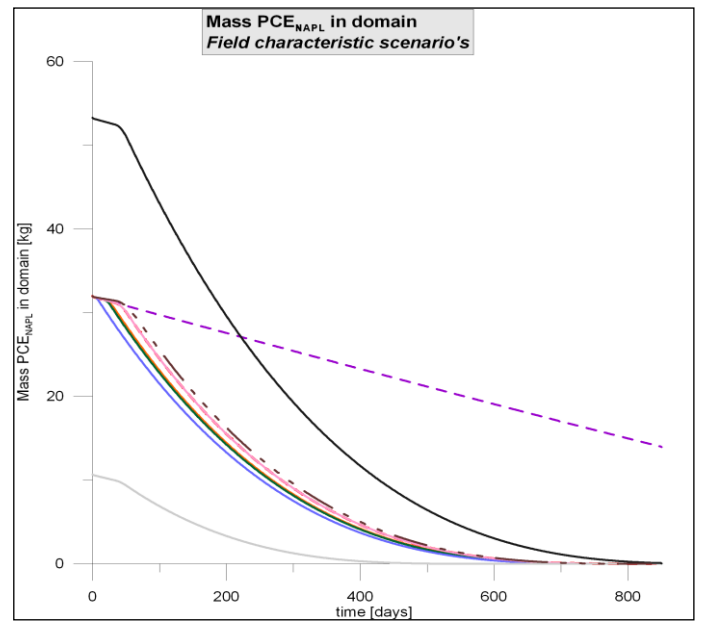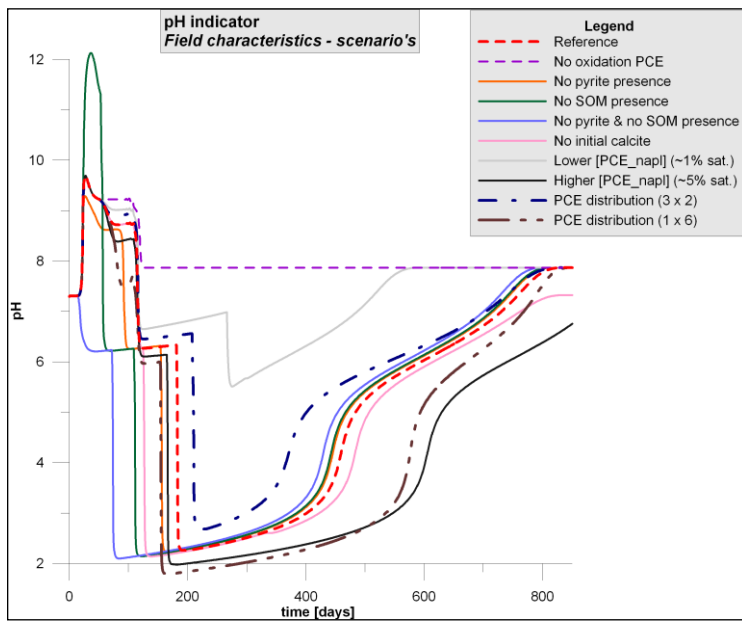
Figure 5.10 *Field characteristic scenarios*

only a 5% increase remains for the higher saturation scenario. This also explains why the lower saturation scenario differs much more from the reference scenario.

The distribution of the source zone does influence the mass flux, which is due to the fact that the flux is calculated over the whole depth of the domain. It is obvious that when three out of seven layers contribute, the flux is higher.

The $PCE_{(aq)}$ mass flux is smallest when no pyrite and organic matter is included, because injected permanganate oxidizes $PCE_{(aq)}$ right away.

Compared to the reference mass flux values (obtained from literature and converted to an equal cross section as this model), the modeled fluxes are considerably large: between 10 and 30 grams / day. This corresponds to a 'magnitude 6' plume, based on the 'plume magnitude classification system' as compiled by Newell et al. (2011). This classification system is based on a 40-plume database, and ranges from 'Magnitude 1' (<0.001 gram/day) to 'Magnitude 10' (>100.000 gram/day). Of the 40-plume database, the major category was the 'Magnitude 6' category (12 out of 40 plumes). The $PCE_{(aq)}$ mass flux from this study is thus assumed realistic.

Indicator - pH

Higher PCE_{NAPL} saturation: Because more $PCE_{(aq)}$ oxidizes, one would expect a lower pH. This is indeed reflected in the pH graphs: the higher PCE_{NAPL} saturation results in (slightly) lower pH values compared to the reference model. As well, the pH remains low for a longer period. However, when comparing the efficiency graph with the pH graph it can be seen that when efficiency is highest (varies between 50 and 100 days for the different scenarios) the pH is not at its lowest. This is due to the buffering effects. Efficiency is highest just after the depletion of SOM, when most PCE_{NAPL} is still available for oxidation. At that moment calcite is still available, and its dissolution causes buffering of the pH. Thus: the efficiency cannot be directly deduced from the pH.

Despite the fact that calcite dissolution prevents for a direct pH: PCE oxidation link, the pH graph does indicate that pH decreases to pH<$pH_{initial}$ values. In table 5.8 data from the observation files presents the time lag between the moment at which pH goes below initial pH and the time at which remediation is most efficient.

Table 5.8   *Maximum efficiency and pH for site characteristic model scenarios*

Scenario	Maximum efficiency reached at [days]	pH < $pH_{initial}$ [days]	Difference [days]
Reference	81	116	35
No SOM presence	59	58	1
No pyrite presence	65	93	28
No pyrite & no SOM presence	43	15	28
No Calcite	81	116	35
Lower [PCE_{NAPL}]	79	117	38
Higher [PCE]	83	115	32
PCE distribution 1	79	117	38
PCE distribution 2	92	113	21

From this table it follows that for all different field situation modeled, pH can be an effective indicator for the moment at which efficiency is highest. Especially when pH buffering function (caused by the oxidation of organic matter) lacks, the moment that pH goes below initial pH gives a strong indication that PCE is being oxidized.

No SOM present: The pH graph of this scenario clearly demonstrates the buffering effect due to the oxidation of organic matter. When no organic matter is present, the oxidation of pyrite causes pH to increase >12. When organic matter is being oxidized the produced CO_2 (weak acid) causes the pH to stay <10.

Indicator - calcium

In the calcium concentration curves the higher efficiency (as well as the lower) is reflected: the peaks correspond to the efficiency curves. This can be explained by the fact that once $PCE_{(aq)}$ oxidation starts, calcite starts to dissolve which results in an increase of calcium

concentration. So the calcium concentration does directly reflect the shift from non-target compounds oxidation to target compound oxidation, but only as long as there is calcite present.

Indicator – 'CO$_2$ species'
Two observations are made at first sight. First the strong increase in CO$_2$ concentration for the 'no pyrite scenario'. As no pyrite is present, all available permanganate first oxidizes organic matter. The oxidation of organic matter produces CO$_2$ and as the oxidation now happens in a shorter time period, the curve is higher. The area under the curves is equal to the other scenarios.
Second observation is the oscillations right before the concentration drop. These oscillations are caused by the fact that at that point in time the involved scenarios encounter two opposed effects (considering CO$_2$ concentration): dissolving calcite and the depletion of organic matter. The first causes the 'CO$_2$ species' concentration to increase, as carbonate ions are released. Due to the second reason the 'CO$_2$ species' production stops. The oscillations are the results of model instabilities in calculating the CO$_2$ concentration during these opposed effect.

From these graphs, it can be concluded that the pH does indicate which scenario proves to be more efficient, but differences are small and as well the moment in time at which highest efficiency is achieved does not correspond to the moment at which pH is lowest. For this modeled situation the moment at which pH drops below the initial pH showed to indicate the moment at which maximum remediation efficiency is reached with a time lag of utmost 38 days. The magnitude of this time lag depends on the distance to the source zone at which the observations are made.

5.4.3 Chemical / rate scenarios

On the next page again the indicator graphs are plotted on the left side, the efficiency related graphs on the right side (fig. 5.11).
The chemical / rate scenarios are mainly performed to see the influence of the rate constants and the defined kinetics on the results.

Remediation efficiency
As expected higher efficiencies are obtained by the scenarios in which the mass transfer rate constant for PCE is increased.
The instantaneous oxidation rate scenario shows that the 'upper limit' of the efficiency (for the situation in which pyrite and organic matter are present, and permanganate is injected continuously over the whole depth of the domain) is ~10%. This efficiency is a result of the target efficiency (2 out of 7 rows contain DNAPL) and the competition for permanganate in the source zone where PCE is present with SOM and pyrite.

Mass flux
Instantaneous reactions: In the instantaneous scenario the defined rates are not the limiting factor, but the availability of permanganate is. From the injection point on, in all encountered cells all reductants are totally depleted. Only when no pyrite, organic matter or PCE$_{(aq)}$ remains permanganate will enter the next cell. In the reference scenario, due to the slow dissolution of PCE, permanganate continues to the next cell once pyrite and (in less amount) organic matter are depleted. Even though there might still be PCE$_{NAPL}$ present in that cell. Therefore permanganate can 'travel' to the end of the domain and oxidize all encountered dissolved PCE. This explains why more mass leaves the domain as dissolved PCE in the 'instantaneous scenario' when compared to the reference scenario.

Mass in domain
Due to the high dissolution rate of PCE$_{NAPL}$ the source zone is free of PCE$_{NAPL}$ within 200 days, while in the 'reference model scenario' this takes more than 800 days.

Indicator - pH
Instantaneous reactions: The pH curve of the instantaneous scenario reflects the sequence of the model domain: first an increase in pH due to oxidation of the NOD upstream of the source

zone. Then a decrease in pH when oxidation of the source zone occurs. The decrease is less distinct than the decrease in the reference scenario, because at the same time oxidation of pyrite and organic matter present at the level of the source zone takes place. Then again an increase in pH, when the area downstream of the source zone is oxidized. The high efficiency obtained in this scenario does not reflect in the pH graph: pH decreases less compared to the 'reference scenario'. From the 'instantaneous scenario' it can be concluded that if all reductants oxidize simultaneously (in the same cell all three species are depleted at the exact same time), the oxidation of $PCE_{(aq)}$ has a dominant effect on the pH.

Lower oxidation rate pyrite: The low oxidation rate of pyrite in the corresponding scenario is reflected in the pH by the absence of the high peak at the beginning. It is read off the observation files that the depletion of pyrite in the first cell takes 18 days instead of 7 days (reference). The consumption of protons due to pyrite oxidation is thus spread out over a larger period. And because the oxidation of organic matter occurs simultaneously, the pH increase is partly buffered by the oxidation of organic matter.

Higher dissolution rate PCE: The pH curves of the scenarios which involve a high dissolution rate of PCE_{NAPL} show a nod around t=100 days. This has to do with the fact that oxidation of $PCE_{(aq)}$ and SOM occur simultaneously. Organic matter is totally depleted from the domain after 137 days then followed by calcite dissolution and precipitation, as can be seen in the calcium graph.

In table 5.9 the pH < $pH_{initial}$ indication point is again given. When the dissolution rate of PCE is set higher, the pH goes to a value below the initial PCE just before the highest efficiency is reached.

Table 5.9   *Maximum efficiency and pH for chemical-rate model scenarios*

Scenario	Maximum efficiency reached at [days]	pH < $pH_{initial}$ [days]	Difference [days]
Reference	81	116	35
Higher dissolution rate PCE	78	64	-14
Lower oxidation rate pyrite	74	117	43
Higher dissolution rate PCE & lower oxidation rate pyrite	73	58	15
Instantaneous reactions	74	56	18

Calcium – indicator
The high dissolution scenarios show a sequence of increasing and decreasing calcium concentration. First the calcium concentration decreases as only pyrite and organic matter oxidize upstream of the source zone. This results in an increase in pH and calcite to precipitate. Once pyrite is depleted and $PCE_{(aq)}$ starts to oxidize the pH decreases and calcite starts to dissolve, resulting in an increase of calcium concentration. Because of the released carbonate ions, as well as the ongoing organic matter oxidation, $PCE_{(aq)}$ oxidation is buffered and pH increases: calcite starts to precipitate again. Until organic matter is totally depleted from the domain and all calcite starts to dissolve due to $PCE_{(aq)}$ oxidation.

The indicators, as well as the efficiency graphs show that the kinetic rate constants have a significant influence on the outcome. By conducting the 'instantaneous scenario', the effect of the defined kinetic oxidation reactions is demonstrated.
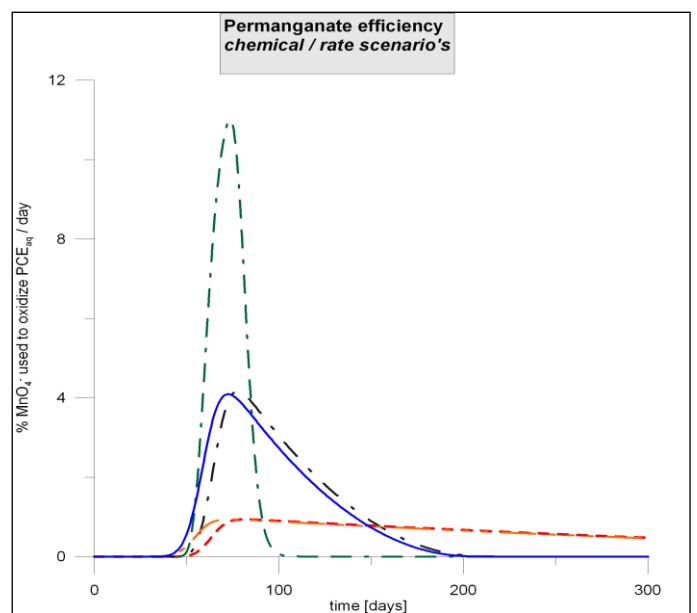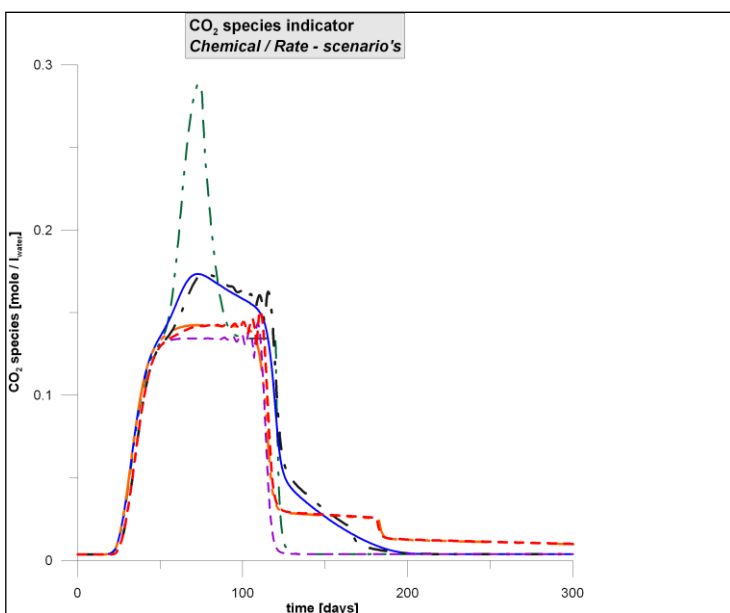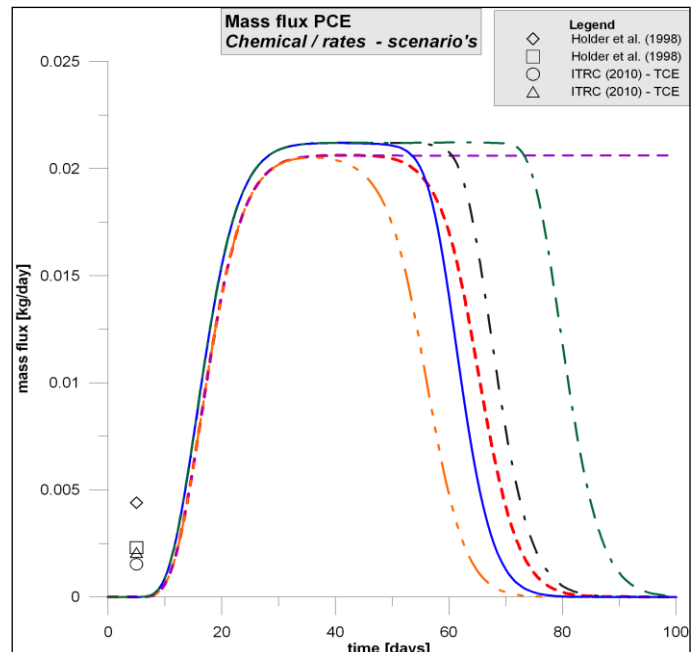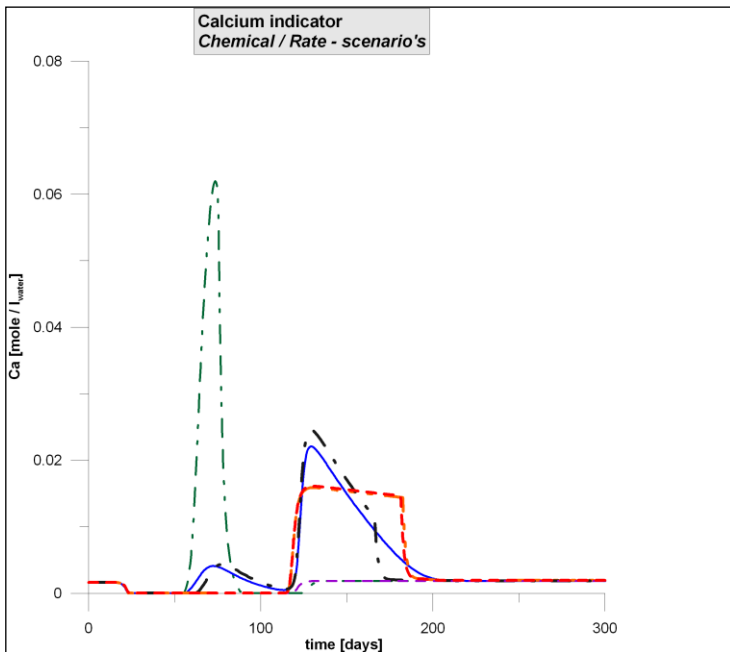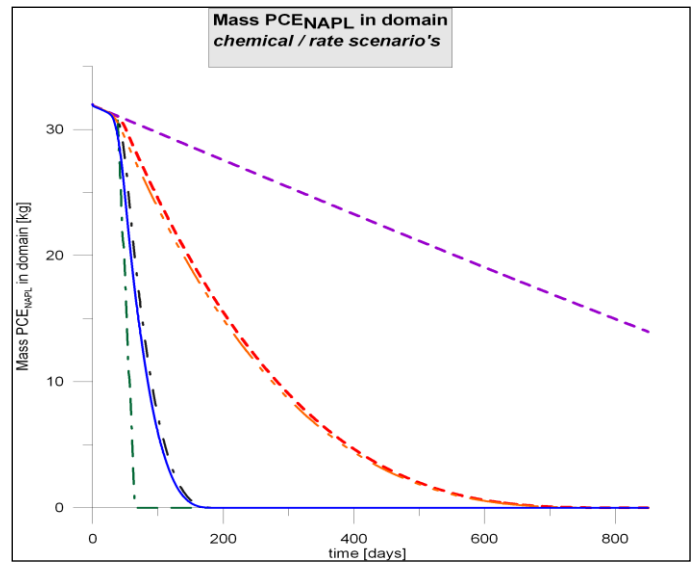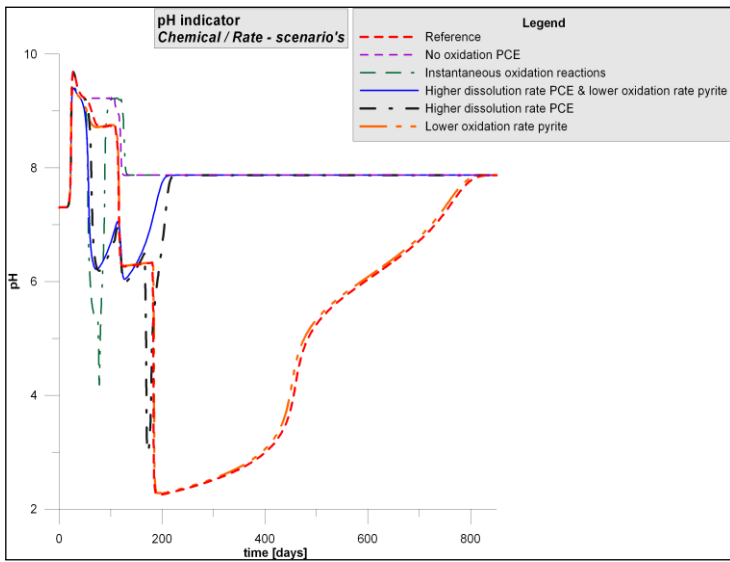
Figure 5.11   *Chemical / rate scenarios*

5.4.4 Remediation techniques scenarios

These graphs are presented mainly to show the influence of different remediation techniques on the efficiency of the ISCO process. However, again the indicator graphs are presented too, to see how these graphs match with he calculated efficiency.

Remediation efficiency
Compared to the efficiency presented in the graphs so far, the differences in this graph are more distinct (see also the overall efficiency in Appendix E). The highest efficiency is obtained when a lower concentration permanganate is added. This is also expected, as from the reference results it is known that a significant part of the injected permanganate flows out of the domain unaffectedly (~9% of injected permanganate reacts with reductants). This again traces back to the slow dissolution rate of PCE, as it is shown in the previous subparagraph that if the dissolution rate increased the efficiency increases too.

Lower permanganate injected: This scenario illustrates three nods in the curve. In fact, the curve seems to consist of three stapled curves. These correspond to the three succeeding cells in which PCE_{NAPL} is situated. When permanganate encounters the first cell in which PCE_{NAPL} is present it will first reacts with pyrite and organic matter due to the 'preference' of permanganate for the NOD. But once the NOD starts to get depleted permanganate becomes available for the oxidation of $PCE_{(aq)}$: the efficiency increases. When permanganate enters the next cell this process repeats itself: first oxidation of NOD, efficiency decreases, then oxidation of PCE: efficiency increases.

Considering the overall efficiency: almost 100% of injected permanganate is involved in oxidation reactions. Although peak efficiency is considerably larger than the reference scenario, the overall efficiency shows that still ~3% of the permanganate which is involved in oxidation reactions, reacts with $PCE_{(aq)}$.

Lower flow velocity: Instead of injecting a lower concentration and thus increasing efficiency by decreasing the injected permanganate flux, the efficiency also increases if the oxidation reactions are given more time. Because the residence time for permanganate increases, more permanganate can react with $PCE_{(aq)}$. Decreasing flow velocity can for example be achieved by injecting and pumping in the opposed direction relative to the natural background flow.

Segmented injection: Another method to decrease the total injected permanganate flux is by injecting permanganate more 'targeted': only at the depth of the source zone. This technique can be applied by using a segmented well and, for example, indicator measurements to determine the depth of the contamination.

Mass flux
Lower permanganate injected: The graph in which the mass flux is presented again shows the 'step' effect: When permanganate reaches the first cell, the mass flux decreases due to oxidation of PCE. The little remaining permanganate continues to the next cell, slightly decreasing the mass flux (first plateau). Once in the first cell all PCE is oxidized and more permanganate 'enters' the second succeeding cell the mass flux decreases at higher pace. Because the preceded permanganate already decreased the amount of PCE available in the second cell, more permanganate precedes into the third cell. The process repeats again for the third cell.

Indicator - pH
First it is noted that the 'segmented injection' scenario shows similar results when compared to the 'reference scenarios' because the concentrations are observed in the fifth layer. The only difference between the 'segmented injection scenario' and the 'reference scenario' is the fact that in the 'segmented injection scenario' permanganate is only injected at the fourth and fifth layer. This reflects in the efficiency graph.

Lower permanganate injections: Fluctuations in all the indicator graphs can be seen for this scenario. These are caused by the relative quick oxidation processes when compared to permanganate replenishment. Within one cell the incoming permanganate oxidizes pyrite and (as long as pyrite is present to a less amount) organic matter. This causes pH to go up. As permanganate replenishment cannot 'keep up' with the oxidation pH tends to go down,
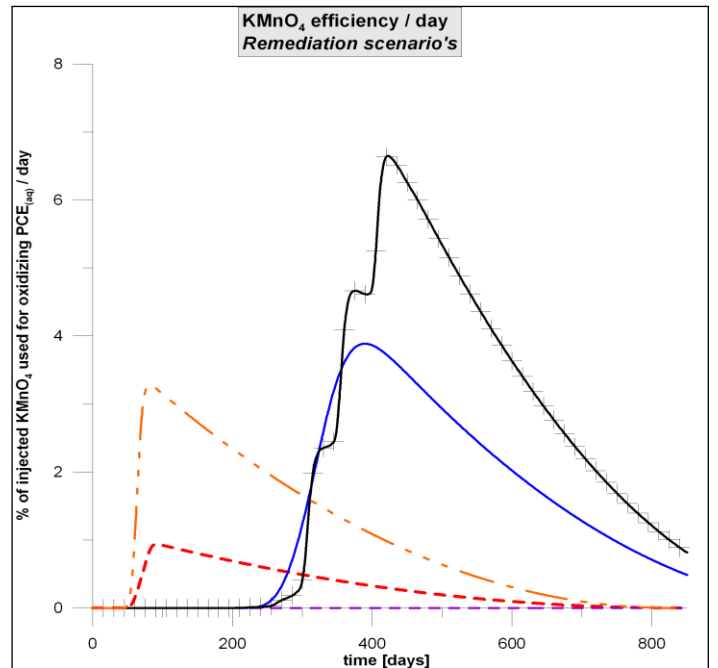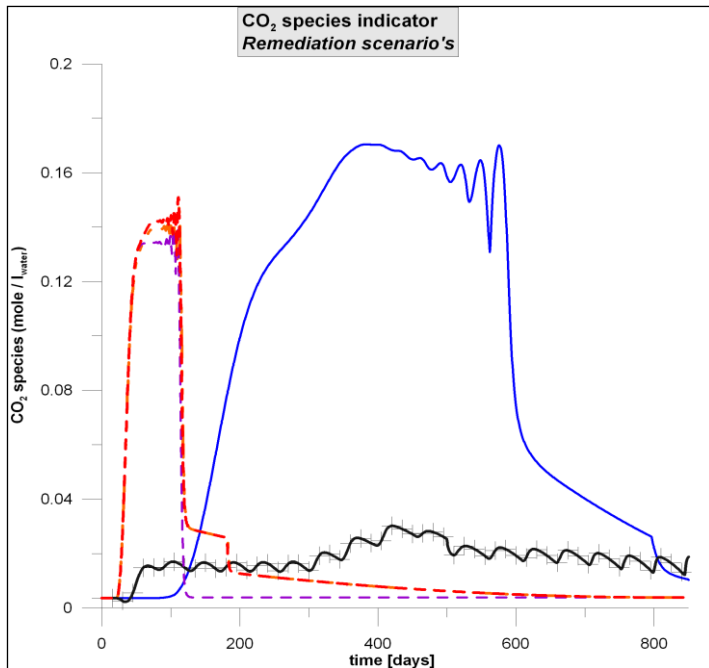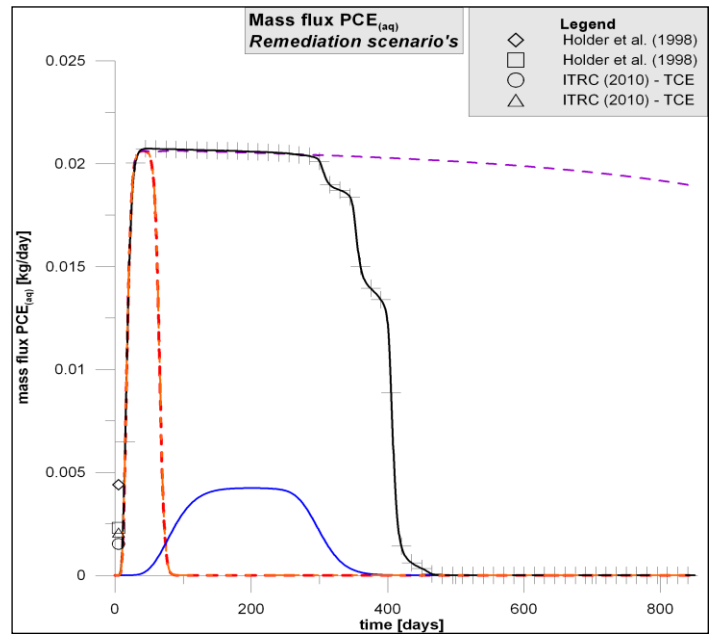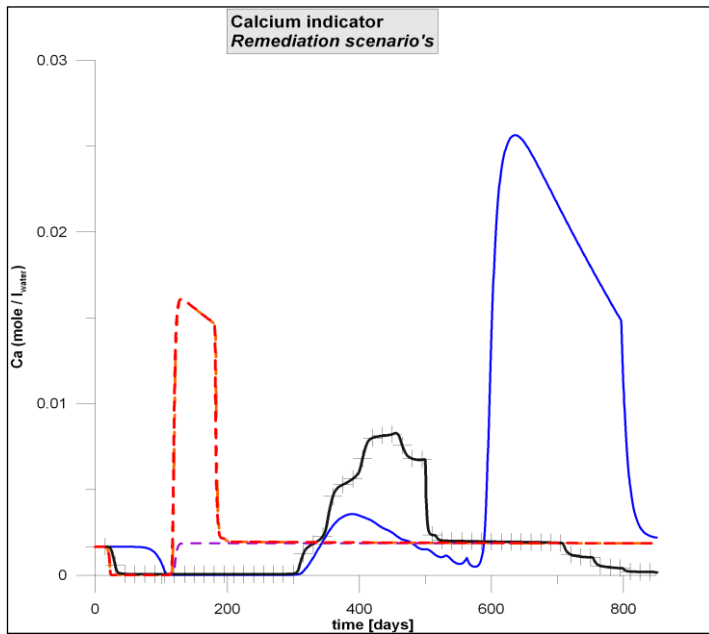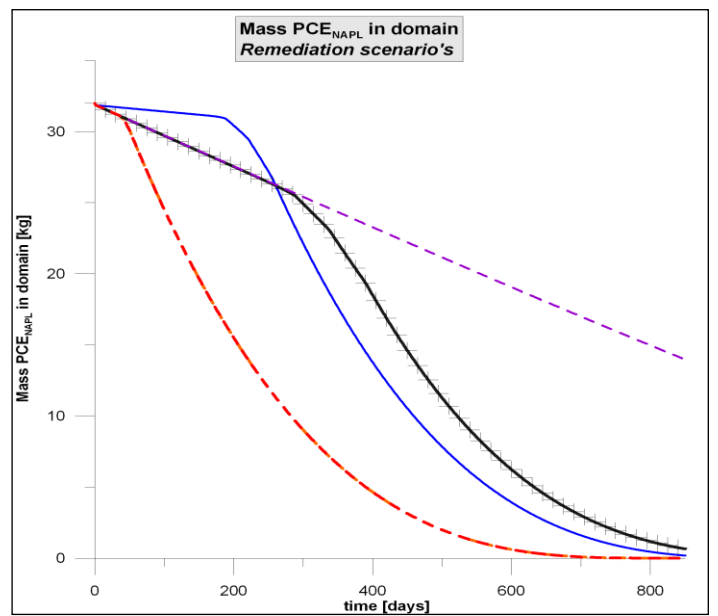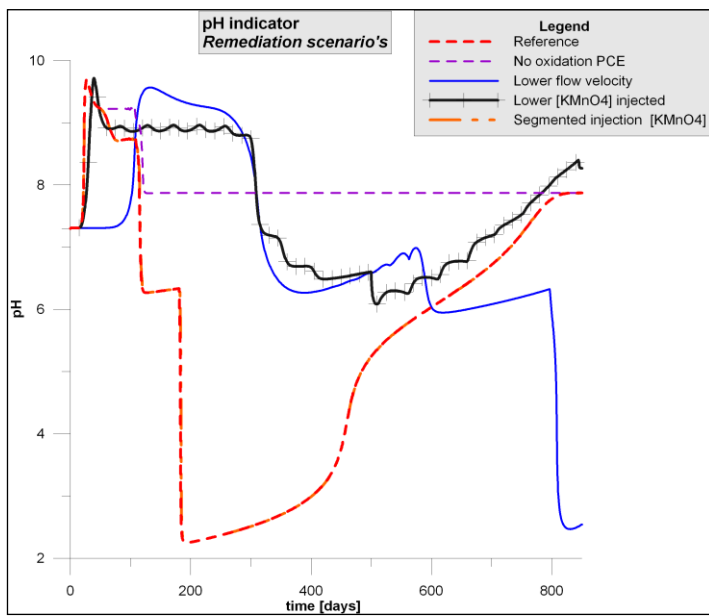
Figure 5.12   *Remediation scenarios*

towards its background value. As the water moves through the cells it experiences this alternation every cell, resulting in the fluctuations visible in the graphs.

The pH graph clearly illustrates that the moment at which pH < $pH_{initial}$ corresponds to the moment at which highest efficiency is measured.

Table 5.10   *Maximum efficiency and pH for remediation model scenarios*

Scenario	Maximum efficiency reached at [days]	pH < $pH_{initial}$ [days]	Difference [days]
Reference	81	116	35
Lower flow velocity	389	317	-72
Lower permanganate injected	422	318	-104
Segmented injection	81	116	35

Indicator – calcium
Lower flow velocity: This scenario shows a similar sequence of calcite precipitation and dissolution as seen in the 'higher dissolution rates PCE scenarios'.

Indicator – CO_2 species
Lower flow velocity: As water flows with slower rate, residence time in each cell is longer. So more time is available for CO_2 to add to the passing groundwater.
Lower permanganate injected: None of the different reductants are totally oxidized by the end of this graph (850days). Because oxidation of both organic matter and PCE is ongoing, but in small amounts, the concentration of CO_2 species is relatively constant. Only when calcite dissolves (which reflects in the calcium graph through the increase calcium concentration) the CO_2 species concentration goes slightly up.

From these graphs it can be concluded that injecting a lower permanganate flux - either through lowering the concentration, flow velocity or location of injection - results in a significant increase of efficiency. Largest increase is obtained by lowering the input concentration. This has the disadvantage that the contaminated flux remains high for a longer period.

5.4.5 Combined batch model and flow model results

All figures discussed in this paragraph are obtained by the flow model. In the previous chapter it was shown that a 'type curve', in which the calcium concentration is plotted against the pH, can indicate the remediation efficiency. To see if such a type curve can be used in a 'field situation' the model results obtained by the flow model are plotted in the type curve. The result is shown in figure 5.12.

The flow model results presented are obtained from the 'low permanganate injected scenario', as in this scenario the same concentration of permanganate is added.. The flow model 'observations' are from the 5th layer of the model, at the end of the domain. Goal of figure 5.12 is to find the relevance of the 'type curves' for indicating the efficiency of the ISCO remediation process.

Beside the pH and calcium concentration one more indicator has been used. The presented observations are all taken at a moment in time at which chloride concentration was higher than the initial value. So it is known that $PCE_{(aq)}$ oxidation is ongoing.
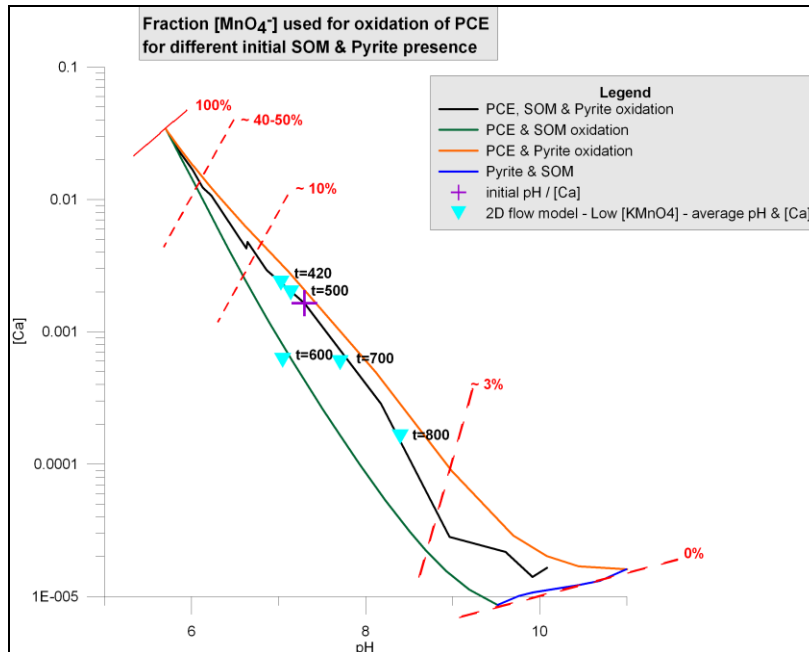
Figure 5.13   *Batch model results combined with 2D flow model results*

The efficiencies that can be read off figure 5.12 can be compared with the calculated efficiencies. In table 5.11 the results of both the type curve as well as the calculated efficiencies are presented.

Table 5.11   *efficiencies based on chloride flux and on type curve compared*

Time [days]	Calculated efficiency from chloride flux	Efficiency read off the type curve
420	6.6%	8%
500	5.3%	7%
600	3.6%	6%
700	2.3%	5%
800	1.2%	4%

Based on table it is assumed that – given a certain initial situation – type curves are useful in giving an indication of the remediation efficiency. Though values from the type curve exaggerate the efficiencies relative to the chloride measurements, values are in the same order of magnitude. As well, the decrease in efficiency reflects from the type curves. It must be known however if $PCE_{(aq)}$ oxidation is going on. This can be derived from chloride measurements.

6. Discussion

6.1 Important parameters

6.2.1 Reaction kinetics

All definitions of the kinetic oxidation reactions are based on Henderson et al. (2009), except the reaction kinetics for the oxidation of pyrite.
Four adjustments have been implemented relative to the kinetic definitions given by Henderson et al. (2009). These adjustments are (see as well Appendix A):

1) For the dissolution of PCE
   The definition of the dissolution of PCE in Henderson et al. (2009) accounts for rate decrease for decreasing PCE_{NAPL} saturation through a mass fraction ratio. In this study a surface relation is added to this ratio. This has been done because dissolution of PCE can only take place from the surface of the PCE_{NAPL}. PCE_{NAPL} is assumed to be present as residual droplets, and because the surface area of spherical shapes does not decrease linear with a decreasing volume a power of 2/3 is implemented.

2) For the oxidation of $PCE_{(aq)}$
   Like in Henderson et al. (2009) the oxidation of the aqueous phase contaminant is modeled as "a second order kinetic reaction with an overall reaction rate proportional to MnO_4^- and contaminant concentrations". The oxidation of $PCE_{(aq)}$ does not include for the ratio which is implemented in Henderson et al. (2009). The ratio is included by Henderson et al. (2009) to take account for decreasing reactivity for a decreasing aqueous concentration. But as the aqueous concentration is highly limited by the dissolution rate it is expected that this does not influence the results. Or, in other words: Because of the low dissolution rate, the aqueous concentration of PCE during the oxidation process is negligible.

3) For the oxidation of soil organic matter
   The reaction kinetics of the oxidation of soil organic matter, as defined by Henderson et al. (2009), includes a surface ratio. In this study, the surface ratio is excluded. This because it is assumed that the oxidation of organic matter is not surface controlled, unlike pyrite and $PCE_{(aq)}$.

4) Add the oxidation of pyrite
   The oxidation kinetics for the reaction of pyrite by permanganate has been implemented as a second order, surface controlled reaction. The mineral pyrite typically has a cubic shape. Therefore the volume of pyrite is converted to the surface of a cubic.
   Very little relevant information concerning the reaction kinetics for the oxidation of pyrite by potassium permanganate has been found in the available literature.

The significance of the defined kinetics is indicated in chapter 5, by the 'instantaneous model scenario'. In this scenario permanganate is divided over the different reductants by the stoichiometric relations. So, for every mole pyrite 5 moles of permanganate are 'reserved'. This results in a simultaneously oxidation of PCE, pyrite and organic matter.

6.2.2 Mass transfer rate PCE_{NAPL} to $PCE_{(aq)}$

From the 'chemical – rate scenarios' it is proved that especially the mass transfer rate constant for PCE is of crucial importance for the oxidation of PCE. From Henderson et al. (2009) it is adapted that oxidation only takes place from the aqueous phase. This assumption is based on the fact that potassium permanganate has negligible solubility in the nonaqueous phase NAPL. The relatively slow dissolution of PCE from the pure phase into the aqueous phase thus limits the amount of $PCE_{(aq)}$ available for oxidation. And although this parameter is found to be highly significant, only two studies have been found which specify the dissolution rate:

1) a model calibration parameter value by Henderson et al. (2009), and
2) a value resulting from an empirical relation originating from Mayer & Miller (1996), adapted from Langevoort (2009).

The value given by Henderson et al. (2009) has been used as the reference value, although this value actually applies for the mass transfer rate constant for TCE.

The majority of studies to permanganate based oxidation of PCE or TCE discuss the direct reaction between $PCE_{(aq)}$ and potassium permanganate without further specifying the mass transfer rate (a.o. Hood et al., 2000; Huang et al., 2002; Kao et al., 2008; Schnarr et al., 1998; Yan and Schwartz, 1999). This is because these studies either concern laboratory tests in which only aqueous $PCE_{(aq)}$ has been used or because they focus on the decrease of the mass flux (i.e. the plume).

6.2.3   Oxidation rate constants

$PCE_{(aq)}$
The oxidation rate constant that has been used is adapted from Henderson et al. (2009). Because this value indicates the oxidation rate constant for TCE the value obtained from Henderson et al. (2009) has been adjusted such that it is in the same order of magnitude as values found for PCE in other studies.

The oxidation rate constant which has been used in this study has initially been adapted from Henderson et al. (2009), although this actually is the oxidation rate constant for TCE. This value has initially been used, as the work of Henderson et al. (2009) is an important frame of reference for this research. The oxidation rate constant used by Henderson et al. (2009) differs an order of magnitude relative to the oxidation rate constants for the oxidation of $PCE_{(aq)}$ (table 2.2). However, later on in the modeling study the value has been changed such that it is in the same order of magnitude as the values given in table 2.2 (by decreasing the value used in Henderson et al. (2009) with one order of magnitude). The magnitude of the oxidation rate constant proved to be insignificant to the results within this research. This because the amount of $PCE_{(aq)}$ available to oxidize is highly limited by the dissolution rate.

Pyrite
All literature found about the oxidation of pyrite concern the oxidation by oxygen or other oxidizers but for potassium permanganate. This is confirmed by Chirita (2003): "Although the oxidation of pyrite by oxygen and ferric iron has been studied in detail, limited information is available on the reaction kinetics by other oxidants (like potassium permanganate), and rate parameters have not been established."

The values used in this research are actually rate constants for the oxidation of pyrite by Fenton's Reagent and are obtained from a laboratory study (Matta et al., 2007). In that study it is also shown that the oxidation rate of pyrite is highly dependent on pH: lower pH conditions give significant higher oxidation rates. Within this research this is not implemented, but considering the modeled pH range in this study a pH effect on pyrite oxidation could be significant. Further research to pyrite oxidation is needed to exclude uncertainties concerning pH dependence and oxidation rate constants.

Soil organic matter
Because SOM does not have a characteristic composition, it is difficult to find 'typical oxidation rate constants' for the oxidation reaction of organic matter by permanganate. The value given by Henderson et al. (2009) has been adapted in this study.

6.2   Remediation efficiency

The maximum efficiencies found in this model vary from ~0.8% up to ~10%. These rather low efficiencies are partly explained by the fact that permanganate is also injected in flow paths in which no contamination is situated. The maximum efficiency that can be reached is thus limited to 2/7th of the injected permanganate (for the reference scenario, in which two layers with PCE are present). Bypassing of the oxidant is as well mentioned by Heiderscheidt et al. (2008) as a reason of serious oxidant loss: "Only a small portion of the injected oxidant mass participated in oxidation of PCE mass. This was partly due to the oxidant delivery flow regime; less than 50% of the oxidant flushed through the tank was expected to pass through the source zone." As a potential solution 'alternative delivery methods' as well as 'lowering flow velocities are described by Heiderscheidt et al. (2008). In this study this is done by conducting the 'segmented injection scenario'. But even if permanganate is injected only in the contaminated flow paths, a peak efficiency of maximal ~3% is reached. This could be due to another factor influencing the efficiency: the relative distance between the upstream injection of the oxidant and the source zone. The larger this distance is, the more NOD is present upstream of the source zone which consumes oxidant.

Bypassing does not only occur through inaccurate source zone targeting, but as well due to the mass transfer rate limitations. Permanganate can flow through cells in which PCE is present, but due to the mass transfer limitation no oxidation takes place. Therefore, if more time is given per permanganate, or when concentration of injected permanganate is decreased, the highest efficiencies are obtained. The highest increase of maximum efficiency is obtained when the permanganate concentration is reduced (in Appendix E it can be seen that in that case almost 100% of the injected permanganate is involved in oxidation reactions. However, of the part of the used permanganate which reacts with $PCE_{(aq)}$ remains ~3%).

Throughout this work efficiency is calculated as the 'amount of the (injected) permanganate that reacts with the target component: $PCE_{(aq)}$', as we are mainly concerned in the efficiency of the target compound oxidation. The results discussed in the report are presented as efficiency per day. The calculations are based on the chloride flux. In addition, results presented in Appendix E show the percentage of the total injected permanganate which is involved in oxidation reactions. As well the distribution of the used permanganate over the different reductants. From these results is can be seen that organic matter is the reductant which confiscates largest share of injected permanganate.

Henderson et al. (2008) find an overall 6% efficiency when no density assisted oxidant delivery is taken into account. As this study looks at a static situation (no flow) and a pulse injection, the low efficiency found by Henderson et al. (2009) confirm that the low efficiencies found in this study are not only due to bypassing of the oxidant.
The main reason for the low efficiency is the mass transfer rate of PCE. This is as well found by Heiderscheidt et al. (2008): "Another reason why only a small portion of injected oxidant mass participated in oxidation of PCE mass is because of limitations on mass transfer from the DNAPL to aqueous phase within sources or localized flow."

Several points of discussion concerning the efficiency of permanganate based chemical oxidation are:
▪ Kao et al. (2008) show that pH conditions influence the 'functioning' of permanganate as the oxidizing agent: "lower TCE removal efficiency under high initial pH conditions is caused by the reduction of MnO_4^- to MnO_4^{2-}, which is a less powerful oxidizing agent and also unstable under high pH conditions: it reacts with H^+ to form $MnO_{2(s)}$. The lower the pH condition, the lower this 'consumption' of MnO_4^- to $MnO_{2(s)}$ and thus the more MnO_4^- remains to oxidize TCE." However, Huang et al. (2002) find that the oxidation reaction for $PCE_{(aq)}$ by $KMnO_4$ is independent of pH within the range of 3 – 10.
    The effect of pH dependent permanganate functioning is not included in this study. Including this effect could lead to lower efficiencies.
▪ Another efficiency issue which has not been taken into account is the auto-decomposition of MnO_4 in water. In Henderson et al. (2009) it is stated that the auto-decomposition reaction is strongly acid-consuming resulting in significant increases of pH.   However,

an increase of pH due to auto-decomposition of MnO_4^- is not consistent with field observations. Since it is not consistent with field observations, following Henderson et al. (2009), the effect of auto-decomposition is neglected in this study.

- It is known from stoichiometry that the mineral manganese is a product of the different oxidation reactions. The formation of manganese affects the aquifer permeability. Especially in the source zone, where most oxidation occurs, this may result in loss of permeability due to pore blocking. This will increase oxidant bypassing. However, Heiderscheidt et al. (2008) state that the effect depends on the source zone characteristics: "The configuration of the discrete DNAPL soure zones partly determined the effects. A pool with little or no residual around it, in a relatively homogeneous flow field, appeared to benefit from the development of MnO_2 pore-blocking." Because the effect is not unambiguously this effect is neglected.

- Henderson et al. (2009) show in their modeling results that density assisted oxidant delivery can increase remediation efficiency up to 60%, whereas without the density assistance a efficiency of 6% was obtained. In this study no density differences have been considered.

6.3 Indicator functioning

6.3.1 pH

In the results of this study the pH showed to be an effective indicator, although affected by the buffer capacity of calcite. The pH graphs presented in this study clearly indicate the dominant oxidation process and for all different scenarios it holds that a pH drop below the initial pH indicates predominant $PCE_{(aq)}$ oxidation. However, this is only measured in observation point's right behind the source zone. As well, the decrease in pH is 'carried along' by the flowing groundwater, towards the observations points. If in a field situation more dispersion is expected to occur, for example due to heterogeneities of the aquifer hydrological characteristics. As a consequence, the lower pH groundwater will mix with initial pH groundwater. Therefore the effect of a pH decrease in a field situation will be less distinct.
Besides potential mixing, pH changes are very local. In the flow paths above and below the source zone, no pH decrease has been observed. In this model this is explained by the fact that vertical movements are negligible. Henderson et al. (2009) find as well that the effect of pH decrease due to oxidation of PCE is locally. In figure 6.1 it can be seen that already 15cm above the source zone interface the decrease of pH is relatively small compared with the pH decrease at the source zone boundary (graph most left). The measurements (grey squares) show a more distinct difference than the model results (black lines).
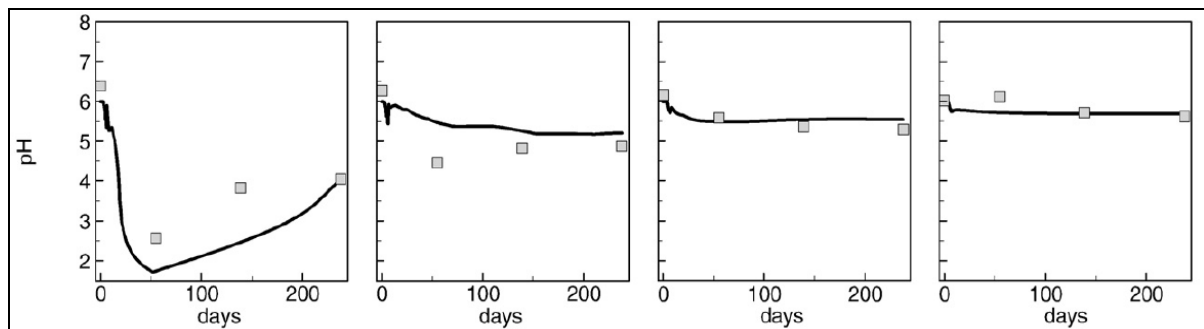
Figure 6.1 *pH measurements (squares) and model results (black line) from Henderson et al. (2009). The graphs represent a vertical profile from a multilevel sampler. Most left graph is at the source zone interface. Every graph towards the right is 15cm higher in the profile.*

6.3.2 Chloride

Chloride is the strongest indicator for the oxidation of the target compound. Once produced through oxidation of $PCE_{(aq)}$ it can be considered a conservative tracer. As mixing is negligible in this study, the concentration measured in the observation well could be used to determine the moles of $PCE_{(aq)}$ oxidized. This can be done by using the stoichiometric relation. In this report all efficiency calculations are based on chloride observations.
Henderson et al. (2009) mention that "chloride concentrations provide an additional mechanism to estimate the amount of TCE oxidized by permanganate". Which indicates that it can be used for both TCE and PCE contaminated sites. In a (small scale) field study conducted by Schnarr et al. (1998) it is proved that remediation progress of a homogeneous PCE contaminated source zone, as well as a heterogeneous PCE/TCE source zone, can be monitored by measuring chloride fluxes. In figure 6.2 the chloride flux of the reference scenario is compared to the chloride fluxes as modeled by Henderson et al. (2009) and measured by Schnarr et al. (1998).
The main disadvantage of using chloride concentration as indicator for the efficiency of contaminant oxidation has to do with the fact that background concentration of chloride is present in groundwater. It depends on the magnitude and fluctuations in the background concentrations whether or not the added chloride concentration due to $PCE_{(aq)}$ oxidation is significant. The background concentration in groundwater depends on natural as well as anthropogenic sources. Examples of anthropogenic chloride sources are road-de-icing salts,

fertilizers, animal feeds and industrial effluents. The most important natural source in (the western part) of the Netherlands is seawater intrusion. To indicate the significance of the measured and modeled values from the different studies, target values for ground- and drinking water are shown too in figure 6.2.
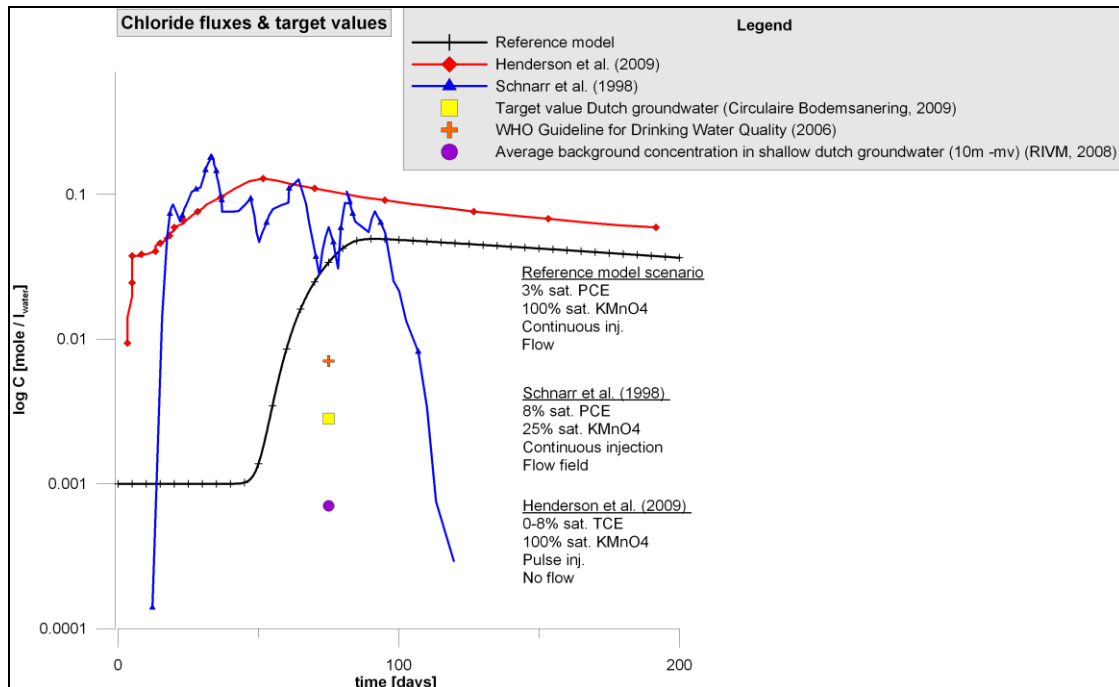
Figure 6.2   *Chloride fluxes & target values. On the logarithmic y-axis the chloride concentration in mole per*

                    liter water is indicated.

The average fresh groundwater concentration for the Netherlands is considerably low (25 mg Cl^-/l), as can be seen in figure 6.2. However, a study conducted by the Dutch Institute of Public Health and Environment (RIVM, 2010) showed that especially in the western part of the Netherlands large areas exceed the target value. The magnitude of the natural and anthropogenic caused fluctuations in background chloride concentration depends heavily on the location (in the Netherlands). This indicates that the applicability of the chloride concentration to indicate the remediation efficiency depends on the location too.

6.3.3   Calcium and CO_2 species

These indicators are considered less effective as their concentrations are not only dependent on the oxidation reactions, but as well on geochemical processes. However, in this study calcium concentration did indicate the moment at which $PCE_{(aq)}$ oxidation was ongoing. But since the calcium concentration depends on the presence of calcite, initial calcium presence, pH and $p[CO_2]$ the reliability as indicator is low compared to chloride and pH.
Calcite dissolution showed a stronger reaction to an increase in $p[CO_2]$ (as result of organic matter and $PCE_{(aq)}$ oxidation) than to a decrease of pH. Therefore the applicability of the calcium concentration indicator for aquifers which are in contact with atmosphere is lower.
The CO_2 species concentration proved to be less indicative to the remediation efficiency. As both target and non-target compounds produce CO_2, and the concentration is influenced by calcite concentration, the concentration is too indistinct.

6.4 Feedback driven remediation

In this study it is found that the efficiency of the oxidation reactions can be improved by adjusting the flow velocity through the sources and/or by adjusting the oxidant concentration. The efficiency can as well be increased by injecting permanganate more targeted. However, in field situations the source zone characteristics are often not exactly known. Usually the size of the source zone can only be estimated from the mass flux it produces. Also the exact location is often not known, due to migration through the subsurface and/or because the location where the contamination got spilled is not exactly known. In this study it is shown that indicators can be used to determine the location more precisely. As well it is shown that using pH measurements it can be determined when oxidation is near its maximum efficiency (pH < $pH_{iinitial}$).

This 'rule of thumb' has been applied to adjust the injection of permanganate during a model run. The 'adjustment' which has been applied is to decrease the injected permanganate concentration. This because lowering the injected concentration proved to result into the highest efficiency, and it is expected that this interference is most easily to realize in a field situation. The result shown in figure 6.3 indicates that the maximum efficiency increased up to ~9% (where ~0,8% was the maximum). The total clean up time was not affected, and a mass decrease of 80% was established.

It is noted here that the extent to which pH can be used to make an intervention decision depends on the distance from the source zone. The closer to the source zone, the more effective the intervention can be.
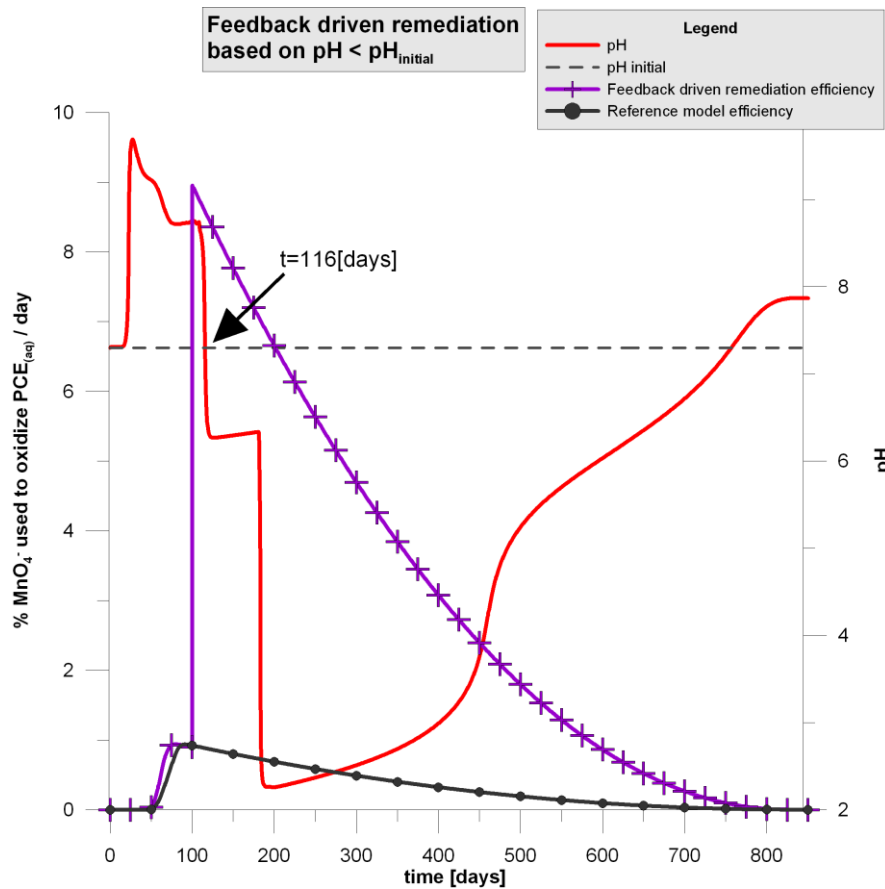
Figure 6.3   *Results feedback driven remediation scenario*

7.   Conclusions and recommendations

In this study the use of indicators to increase insight in the efficiency of an ISCO remediation process has been investigated. A PCE_{NAPL} contaminated site is simulated using the PHT3D/MODFLOW model packages. First, using a no flow – batch model the interaction between different oxidation reactions and the reflection on different indicators has been studied. Secondly, the selected indicators have been studied in a more realistic, field scale, two dimensional flow model. The main conclusions from the model results are:

Conclusions
- Considerably low remediation efficiencies are found, with maxima ranging from 0.8% - 10%.
- The main reason for the low efficiency is the limiting mass transfer rate constant of PCE.
- Due to the low mass transfer rate it is possible that a breakthrough of permanganate is measured, while the source zone is not completely oxidized. Only a small part of the injected permanganate reacts with $PCE_{(aq)}$. Thus, $PCE_{(aq)}$ breaking through does not automatically imply that no $PCE_{(aq)}$ oxidation is taking place.
- Within this study it is found that efficiency can most effectively be increased by lower the concentration of injected oxidant. As only the aqueous PCE reacts with permanganate and the availability of aqueous PCE is limited by the low mass transfer rate, bypassing of injected permanganate is the main cause of low remediation efficiency. The results of the Reference model show that only 14% of the injected permanganate reacts with one of the reductants.
- Chloride and pH are the most effective indicators to determine whether or not $PCE_{(aq)}$ oxidation is ongoing.
- From chloride measurements the efficiency can be determined exactly, through stoichiometric relation.
- From pH measurements the prevailing oxidation process can be determined. As well, using (depending on the distance from the source zone) the rule of thumb pH < $pH_{initial}$ proved to effectively indicate that $PCE_{(aq)}$ oxidation by permanganate is near its maximum efficiency.
- For certain initial conditions a type curve can be created. Using such type curves can give an indication of remediation efficiency. Therefore the calcium, pH and chloride concentrations are needed.
- For aquifers rich in calcite the calcium concentration proved to be an effective indicator too: as $PCE_{(aq)}$ oxidizes, calcite starts to dissolve resulting in a strong increase of the calcium concentration.

Recommendations
The following characteristics are equal for all modeled scenarios:
   o   a homogeneous aquifer (porosity, permeability, conductivity);
   o   similar groundwater composition (initial pH; concentrations);
   o   homogeneous flow field;
   o   source zone (only residual, no pool);
   o   homogeneous contaminant source (only PCE_{NAPL});

In order to increase insights in the applicability of the described indicator heterogeneities should be included for each of these categories. Including heterogeneities could best be done by simulating a real field situation, of which sufficient data is available to be able to calibrate the model results. This study lacks calibration, which makes the results less robust.
In the discussion of this study a result of a 'feedback driven remediation modeling scenario' is given. Next step could be to include for inverse modeling.

References

Appelo, C.A.J., B. Drijvere, R. Hekkenberg and M. de Jonge (1999). "Modeling In Situ Iron Removal from Ground Water." Groundwater, Vol. 37, No. 6, pp. 811 – 817.

Appelo, C.A.J. and D. Postma (1994). "Geochemistry, Groundwater and pollution." A.A. Balkema Publishers, Rotterdam. pp. 536.

Bethke, C.M. (2008). "Geochemical and Biogeochemical Reaction Modeling." Cambridge University Press, Cambridge. pp. 543.

Chandra, A.P. and A.R. Gerson (2010). "The mechanisms of pyrite oxidation and leaching: A fundamental perspective." Surface Science Reports, Vol. 65, pp. 293 – 315.

Chiang, W.H. (2007). "Processing Modflow – A simulation system for modeling groundwater flow and transport processes." PMWIN Pro – version 8.0 Manual. pp. 399.

Chirita, P. (2003). "Kinetics of Aqueous Pyrite Oxidation by Potassium Dichromate – An experimental study." Turk J Chemistry, Vol. 27, pp. 111 – 118.

Faure, G. (1998). "Principles and applications of Geochemistry – A comprehensive textbook for Geology Students." Prentice Hall, Inc., New Jersey. pp. 600.

Fetter, C.W. (2008). "Contaminant Hydrogeology - second edition." Waveland Press, Inc., Illenois. pp. 500.

Gerken, M. (2005). "Introduction to the Chemistry of the Elements – Lecture notes." Document available on website University of Lethburg, Canada (http://classes.uleth.ca/200501/chem2810a/).

Goltz, M.N., S. Kim, H. Yoon and J. Park (2007). "Review of Groundwater Contaminant – mass flux measurement. "Environmental Engineering Research, Vol. 12, No. 4.

Hammack, R.W. and G.R. Watzlaf (1990). "The effect of oxygen on pyrite oxidation." Paper presented at the 1990 Mining and Reclamation Conference and Exhibition, Charleston, West Virginia, April 23-26, 1990

Harbaugh, A.W. (2005). "MODFLOW-2005, The U.S. Geological Survey Modular Ground-Water Model – the groundwater flow process." U.S. Geological Survey, Reston, Virignia.

Hartog, N., J. Griffioen and C.H. Van der Weijden (2002). "Distribution and reactivity of O_2-reducing components in sediments from a layered aquifer." Environmental Science and Technology, Vol. 36, No. 11. pp. 2338 – 2344.

Hassanizadeh, S.M. (2007) – Summary Lecture Notes 'Hydrogeological Transport Phenomena'. Department of Earth Sciences, Utrecht University, Utrecht. pp. 40.

Hassanizadeh, S.M. (2010) - Lecture notes Hydrogeological Transport Phenomena & Environmental Hydrogeology. Master courses participated at University Utrecht, 2010.

Heiderscheidt, J.L., R.L. Siegrist, T.H. Illangasekare (2008). "Intermediate-scale 2D experimental investigation of in situ chemical oxidation using potassium permanganate for remediation of complex DNAPL source zones." Journal of Contaminant Hydrology, Vol. 102, pp. 3 – 16.

Henderson, H.T., K.U. Mayer, B.L. Parker and T.A. Al (2009). "Three-dimensional density

dependent flow and multicomponent reactive transport modeling of chlorinated solvent oxidation by potassium permanganate." Journal of Contaminant Hydrology, Vol. 106, pp. 195 – 211.

Hønning, J. (2007). "Use of in situ chemical oxidation with permanganate in PCE-contaminated clayey till with sand lenses." Ph.D. Thesis. Institute of Environment & Resources, Technical University of Denmark. pp. 61.

Hood, E.D., N.R. Thomson, D. Grossi and G.J. Farquhar (2000). "Experimental determination of the kinetice rate law for the oxidation of perchloroethylene by potassium permanganate." Chemosphere, Vol. 40, pp. 1383 – 1388.

Huang, K-C., G. E. Hoag, P. Chheda, B.A. Woody, G.M. Dobbs (2002). "Kinetics and mechanism of oxidation of tetrachloroethylene with permanganate." Chemosphere, Vol. 46, pp. 845 – 825.

Interstate Technology & Regulatory Council (ITRC) (2010). "Use and Measurement of Mass Flux and Mass Discharge." MASSFLUX-1. Washington, D.C.: Interstate Technology & Regulatory Council, Integrated DNAPL Site Strategy Team. www.itrcweb.org.

Kao, C.M., K.D. Huang, J.Y. Wang, T.Y. Chen, H.Y. Chien (2008). "Application of potassium permanganate as an oxidant for in situ oxidation of trichloroethylene-contaminated groundwater: A laboratory and kinetics study." Journal of Hazardous Materials, Vol. 153, pp. 919 – 927.

Kim, K. and M.D. Gurol (2005). "Reaction of Nonaqueous Phase TCE with Permanganate." Environmental Science & Technology, Vol. 39, No. 23, pp 9309 – 9308.

Knauss, K.G., M.J. Dibley, , R.N. Leif, D.A. Mew and R.D. Aines (2000). "The aqueous solubility of trichloroethene (TCE) and tetrachloroethene (PCE) as a function of temperature." Applied Geochemistry, Vol. 15, No. 4, pp. 501 - 512.

Kono, L., M. Nishigaki, M. Komatsu (eds) (2003). "Groundwater Engineering – Recent Advances." Swets & Zeitlinger, Lisse, the Netherlands. pp. 625.

Langevoort, M.(2009). "Multiphase flow and enhanced biodegradation of dense non-aqueous phase liquids." Dissertation at Faculty of Geosciences, University Utrecht, Utrecht. pp. 236.

Matta, R., K. Hanna and S. Chiron (2007). " Fenton-like oxidation of 2,4,6-trinitrotoluene using different iron minerals." Science of the Total Environment, Vol. 385, pp. 242 – 251.

Mayer, A.S. and C.T. Miller (1996). "The influence of mass transfer characteristics and porous media heterogeneity on nonaqueous phase dissolution." Water Resources Research, Vol. 32, No. 6. pp. 1551 – 1567.

Mayer, A.S. and S.M. Hassanizadeh (2005). "Soil and Groundwater Contamination: Nonaqueous Phase Liquids – Principles and Observations." American Geophysical Union, Washington, DC. pp. 216.

Newell, J.C., S. K. Farhat, D.T. Adamson and B.B. Looney (2010). "Contaminant Plume Classification System Based on Mass Discharge." Ground Water, published online (2011), pp. 1 – 6.

Pankow, J.F. and Cherry, J.A. (1996). "Dense Chlorinated Solvents and other DNAPLs in Groundwater." Waterloo Press. Portland, USA.

Parkhurst, D.L. and C.A.J. Appelo (1999). "Users Guide to PHREEQC (version 2) – A

computer program for speciation, batch-reaction,one-dimensional transport and inverse geochemical calculations." Water Resource Investigations Report 99-4259. U.S. Geological Survey. pp. 312.

Prommer, H., D.A. Barry, W.H. Chiang and C. Zheng (2001). "PHT3D – A MODFLOW/MT3DMS-based reactive multi-component transport model." MODFLOW 2001 and Other Modeling Odysseys – Conference Proceedings. pp. 477 – 483.

Prommer, H. and V. Post (2010). "PHT3D – A Reactive Multicomponent Transport Model for Saturated Porous Media." User's Manual v2.10, august 2010. pp. 186.

RIVM (2008). "Afleiding van milieurisicogrenzen voor chloride in oppervlaktewater, grondwater, bodem en waterbodem." RIVM Rapport 711701075/2008, pp. 76.

RIVM (2010). "De kwaliteit van ondiep en middeldiep grondwater in Nederland in het jaar 2008 en de verandering daarvan in 1984-2008." RIVM-rapport 680721005/2010, pp. 199.

Schnarr, M., C. Truax, G. Farquhar, E.Hood, T. Gonullu and B. Stickney (1998). "Labaratory and controlled field experiments using potassium permanganate to remediate trichloroethylene and perchloroethylene DNAPLs in porous media." Journal of Contaminant Hydrology, vol. 29, pp. 205 – 224.

Simcore Software (2010). "Processing Modflow – An integrated modeling environment for the simulation of groundwater flow, transport and reactive processes." Processing Modflow Manual. pp. 413.

UPSOIL proposal (2009) - Seventh Framework Programme Theme 6 "Environment (Including Climate Change)", Annex 1 – Description of Work. pp. 115.

Urynowicz, M.A., B. Balu and U. Udayasankar (2008). "Kinetics of natural oxidant demand by permanganate in aquifer solids." Journal of Contaminant Hydrology, Vol. 96, pp. 187 – 194.

U.S. Environmental Protection Agency (EPA) (*year unknown)*. "A citizens guide to Soil and Groundwater Remediation Methods. pp. 43.

Van Gaans, P., N. Hartog and J. Valstar (2011). "Deliverable 2.3: Methodology of parameters that determine effectiveness, efficiency, and rates of contaminant remediation." *Confidential document only available for members of the UPSOIL consortium.* pp. 27.

VROM (2009). "Circulaire bodemsanering 2009 Streefwaarden en interventiewaarden bodemsanering." Document available on website http://wetten.overheid.nl/BWBR0025649/Bijlage1/geldigheidsdatum_27-06-2011.

Xu, X. and N.R. Thomson (2006). "Oxidant fate in the subsurface environment: From batch to column system." Proceedings of the 5th International Conference on Remediation of Chlorinated and Recalcitrant Compounds, Monterey, CA, May 22-25, 2006.

Xu, X. and N.R. Thomson (2008). "Estimation of the maximum consumption of permanganate by aquifer solids using a modified chemical oxygen demand test." Journal of Environmental Engineering, Vol. 353.

Yan, Y.E. and Schwartz, F.W. " Oxidation of chlorinated solvents by permanganate." Proceedings of the First International Conference on Remediation of Chlorinated and Recalcitrant Compounds, Monterey, California, pp. 403 – 408.

Yan, Y.E. and F.W. Schwartz (1999). "Oxidative degradation and kinetics of chlorinated ethylenes by potassium permanganate." Journal of Contaminant Hydrology, Vol. 37, pp. 343 – 365.

Zeng, C. and P. Wang (1999). "MT3DMS – A Modular Three-Dimensional Multispecies Transport Model." Documentation and User's Guide. pp. 239.

Appendices

A. Reactions, rate expressions and rate constants

Reaction [a]	Rate expression	Rate constant
(1) $C_2HCl_{3(DNAPL)} \rightarrow C_2HCl_{3(aq)}$	$R_{tce}^{diss} = -k_{tce}^{diss}\left([C_2HCl_{3(aq)}]_{sat} - [C_2HCl_{3(aq)}]\right)\left(\frac{\varphi_{C_2HCl_5}}{\varphi_{C_2HCl_3,0}}\right)$	3.4×10^{-6} [b]
(2) $C_2HCl_{3(aq)} + 2MnO_4^- + 2H_2O \rightarrow 2MnO_{2(am)} + 3Cl^- + 2CO_3^- + 5H^+$	$R_{tce}^{ox} = -k_{tce}^{ox}[C_2HCl_{3(aq)}][MnO_4^-]\left[\frac{[C_2HCl_{3(aq)}]}{K_{tce}^{ox} + [C_2HCl_{3(aq)}]}\right]$	0.65 [c]
(3) $3CH_2O + 4MnO_4^- \rightarrow 4MnO_{2(am)} + 3CO_3^{2-} + 2H^+ + 2H_2O$	$R_{CH_2O}^{ox} = -k_{CH_2O}^{ox}[MnO_4^-]\left(\frac{\varphi_{CH_2O}}{\varphi_{CH_2O,0}}\right)^{\frac{2}{3}}$	5.0×10^{-5} [d]
(4) $4MnO_4^- + 4H^+ \rightarrow 3O_2 + 2H_2O + 4MnO_{2(am)}$	$R_{H_2O}^{ox} = -k_{H_2O}^{ox}[MnO_4^-]$	1.0×10^{-8} [e]

[a] Reactions are written in terms of aqueous components, reaction and product species are subject to aqueous complexation.
[b] Model calibration parameter, $mol \cdot L^{-1}$ bulk s^{-1}.
[c] From Yan and Schwartz (1999), $mol^{-1} \cdot L^2 H_2O \, L^{-1}$ bulk s^{-1}.
[d] Model calibration parameter, $L H_2O \, L^{-1}$ bulk s^{-1}.
[e] Model calibration parameter, $L H_2O \, L^{-1}$ bulk s^{-1}.

Stoichiometric relation	Rate expression	Rate constant(s)
1. Dissolution of nonaqueous PCE into the aqueous phase : $C_2Cl_{4(DNAPL)} \rightarrow C_2Cl_{4(aq)}$	$r_{diss}^{PCE} = \kappa^{PCE}\left(\left[C_2Cl_{4(aq)}\right]_{sat} - \left[C_2Cl_{4(aq)}\right]\right)\left(\frac{\left[C_2Cl_{4(DNAPL)}\right]}{\left[C_2Cl_{4(DNAPL)}\right]_{t=0}}\right)^{\frac{2}{3}}$	(1) 0.98 [day^{-1}][a] (2) 5.2 [day^{-1}][b]
2. Oxidation of aqueous phase PCE by permanganate: $3C_2Cl_{4(aq)} + 4MnO_4^- + 4H_2O$ $\quad \rightarrow 6CO_{2(aq)} + 12Cl^- + 4MnO_{2(s)} + 8H^+$	$r_{ox}^{PCE} = k_{ox}^{PCE}\left[C_2Cl_{4(aq)}\right][MnO_4^-]$	5620 [M^{-1} day^{-1}][a]
3. Oxidation of soil organic matter by permanganate: $CH_2O + 12H^+ + 12MnO_4^- \rightarrow 12MnO_{2(s)} + 9CO_2$	$r_{ox}^{SOM} = -k_{ox}^{SOM}[CH_2O][MnO_4^-]$	4.32 [M^{-1} day^{-1}]
4. Oxidation of pyrite by permanganate: $FeS_2 + H^+ + 5MnO_4 \rightarrow 5MnO_{2(s)} + 2SO_4^{2-} + FeOOH_{(s)}$	$r_{ox}^{pyrite} = -k_{ox}^{pyrite}[MnO_4^-]6\left([FeS_2]_{t=t}\right)^{\frac{2}{3}}$	(1) 108 [Mole dm^{-2} day^{-1}] (2) 0.128 [Mole dm^{-2} day^{-1}]

B. PHT3D & PHREEQC-2 input files

Basic Transport Package file (descriptions from Zheng & Wang, 1999):

```
a)         7         1        20         1        20         9
b)     T   L   M
c)   T T T F T T
d)   3 3 3 3 3 3
e)         0         .5                              -1 A7. DELR(NCOL)
                   0          1                      -1 A8. DELC(NROW)
                   0          0                      -1 A9. HTOP(NCOL,NROW); Top of the first layer
                   0   .7142857                      -1 A10. Thickness of layer  1
                   0         .3                      -1 A11. Effective porosity of layer 1
f)                 0          1                      -1 A12. ICBUND matrix of Layer 1
g)                 0          0                      -1 A13. Starting concentration in layer  1 for species # 1Pcesolute
                   0          0                      -1 A13. Starting concentration in layer  1 for species # 2Permanganate
                   0       .001                      -1 A13. Starting concentration in layer  1 for species # 3Cl
                   0  9.990E-04                      -1 A13. Starting concentration in layer  1 for species # 4K
                   0    .001646                      -1 A13. Starting concentration in layer  1 for species # 5Ca
                   0    .003622                      -1 A13. Starting concentration in layer  1 for species # 6C(4)
                   0     .00001                      -1 A13. Starting concentration in layer  1 for species # 7S(6)
                   0          0                      -1 A13. Starting concentration in layer  1 for species # 8Na
                   0          0                      -1 A13. Starting concentration in layer  1 for species # 9Br
                   0      7.297                      -1 A13. Starting concentration in layer  1 for species # 10pH
                   0       10.4                      -1 A13. Starting concentration in layer  1 for species # 11pe
                   0          1                      -1 A13. Starting concentration in layer  1 for species # 12Dummypcenapl
                   0          1                      -1 A13. Starting concentration in layer  1 for species # 13Dummysom
                   0          1                      -1 A13. Starting concentration in layer  1 for species # 15Dummypyrite
                   0          0                      -1 A13. Starting concentration in layer  1 for species # 16Pcenapl
                   0          0                      -1 A13. Starting concentration in layer  2 for species # 16Pcenapl
                   0          0                      -1 A13. Starting concentration in layer  3 for species # 16Pcenapl
                 100          1(5G14.0)              -1  A13. Starting concentration in layer  4 for species # 16Pcenapl
              0          0          0          0          0
              0        .09        .09        .09          0
              0          0          0          0          0
              0          0          0          0          0
                 100          1(5G14.0)              -1  A13. Starting concentration in layer  5 for species # 16Pcenapl
              0          0          0          0          0
              0        .09        .09        .09          0
              0          0          0          0          0
              0          0          0          0          0
              0          0                           -1 A13. Starting concentration in layer  6 for species # 16Pcenapl
              0          0                           -1 A13. Starting concentration in layer  7 for species # 16Pcenapl
              0          0                           -1 A13. Starting concentration in layer  1 for species # 17Pyrolusitee
              0        .01                           -1 A13. Starting concentration in layer  1 for species # 18Calcite
              0        .01                           -1 A13. Starting concentration in layer  1 for species # 19Som
              0        .01                           -1 A13. Starting concentration in layer  1 for species # 20Pyritee
h)      1E+30        .05
i)          1          0          0          0       T
j)         30
              0         30         60         90        120        150        180        210
            240        270        300        330        360        390        420        450
            480        510        540        570        600        630        660        690
            720        750        780        810        840        850        780        790
            800        810        820        830        840        850
k)         12          1
l)          5          1          2
            5          1          4
            5          1          6
            5          1          7
            5          1          8
            5          1          9
            5          1         10
            5          1         12
            5          1         14
            5          1         16
            5          1         18
            5          1         20
m)          T          1
n)        850       1700          1
o)          0      50000          1          0
```

a) | #Layers **|** #Rows **|** #Columns **|** #Stress periods **| #**Chemical species included **|** #Mobile species included

b) | Units time **|** Unit length **|** Unit mass |

c) Logical flags indicating which processes are involved:
    | Advection | Dispersion | Sink & Sources **|** Adsorption | Chemical reactions | GCG Solver|

d) Type of model layers:
    0 = confined
    1 = unconfined
    2 = Confined/unconfined (transmissivity constant)
    3 **=** Confined/unconfined (transmissivity varies)

e) Cell/grid characteristics

f) *ICBUND:* Concentration boundary condition shared by all species:
    0 = inactive concentration
    -1 = constant concentration
    1 = active concentration

g) *SCONC:* Initial concentration in domain

h) | *CINACT:* Value awarded inactive concentration cells | *THKMIN:* Minimum saturated thickness in a cell |

i) (logical) flag indicating whether the …. should be printed as output file:
    | *IFMTCN:* Calculated concentration | *IFMTNP:* Number of particles in each cell | *IFMTRF:* Model-calculated retardation factor | *IFMTDP:* Model-calculated, distance weighted dispersion coefficient | *SAVUCN:* Concentration solution (.UCN files) |

j) *TIMPRS:* Frequency of output (times at which .UCN files are written)

k) | *NOBS:* Number of observation points at which the concentration of each specie will be saved in .OBS files | *NPROBS:* Frequency with which .OBS files are saved (1= every 1 timestep) |

l) | *KOBS:* Layer | *IOBS:* Row | *JOBS:* Column of observation points |

m) | *CHKMAS:* Logical flag indicating if .MAS files are to be printed | *NPRMAS:* Frequency at which .MAS files are to be printed |

n) | *PERLEN:* Length of stress period |*NSTP:* Number of time steps in the stress period | *TSMULT:*

o) | *DT0:* Transport step size within each time step of the flow solution. If GCG solver is used (i.e. for implicit solutions), this value is the initial transport step size. If it is zero, a model-calculated value based on the Courant number in the Advection Package is used | *MXSTRN:* Maximum number of transport steps allowed within one time step of the flow solution. | *TTSMULT:* Multiplier for successive transport steps within a flow time step | *TTSMAX:* Maximum transport stepsize allowed (0 = no maximum limit) |

Advection Package file:

```
a)        2         1        5000         0
b)        3        .5
c)        1         0          15
```

a) | *MIXELM:* Integer flag specifying the advection solution:
   0 = standard finite difference method
   1 = forward-tracking method of characteristics (MOC)
   2 = backward-tracking modified method of characteristics (MMOC)
   3 = hybrid method of characteristics (HMOC). Switches automatically between MOC and MMOC.
   -1 = third order TVD scheme (ULTIMATE)
   | *PERCEL:* Courant number. The number of cells advection will be allowed in any direction in one transport step. 1= advection 'brings' a particle one cell length. Particle tracking methods, as the used MMOC, determine the location of a particle based on where that particle was one timestep before.
   | *MXPART:* Maximum total number of moving particles allowed. Only used when advection solution scheme is MOC or HMOC.
   | *NADVFD:* Weighting scheme which should be used:
   0 or 1 = Upstream Weightening (is default)
   2 = central in space weighting. |
b) | *ITRACK:* Flag indicating which particle tracking algorithm is selected for the Eulerian-Lagrangian methods:
   1 = First order Euler algorithm.
   2 = Fourth-order Runge-Kutta algorithm is used (computationally demanding, only needed when Courant
       number > 1.
   3 = Hybrid 1st and 4th order algorithm are both used; Runga-Kutta algorithm is used in sink/source cells and next to sinks/source cells (where changes are largest), while Euler algorithm is used elsewhere.
   | *WD*: Concentration weighting factor. Default value = 0,5.
c) | I*NTERP*: Flag indicating the concentration interpolation method for use in the MMOC scheme. 1=linear.
   | *NLSINK*: Flag indicating whether the random or fixed pattern is selected for initial placement of particles to approximate sink cells in the MMOC scheme.
   0 = the random pattern is selected. This implies that particles are randomly distributed in both the horizontal and vertical directions by calling a random number generator. This option is usually preferred as it leads to smaller mass balance discrepancies.
   | *NPSINK*: number of particles used to approximate sink cells in the MMOC scheme.

Dispersion Package file:

```
a)     100        1(5G14.0)                    -1  C1. Longitudinal dispersivity of layer  1
         .01           .01           .01           .01            .01
         .01           .01           .01           .01            .01
         .01           .01           .01           .01            .01
         .01           .01           .01           .01            .01
       100        1(5G14.0)                    -1  C1. Longitudinal dispersivity of layer  2
         .01           .01           .01           .01            .01
         .01           .01           .01           .01            .01
         .01           .01           .01           .01            .01
         .01           .01           .01           .01            .01
       100        1(5G14.0)                    -1  C1. Longitudinal dispersivity of layer  3
         .01           .01           .01           .01            .01
         .01           .01           .01           .01            .01
         .01           .01           .01           .01            .01
         .01           .01           .01           .01            .01
       100        1(5G14.0)                    -1  C1. Longitudinal dispersivity of layer  4
         .01           .01           .01           .01            .01
         .01           .01           .01           .01            .01
         .01           .01           .01           .01            .01
         .01           .01           .01           .01            .01
       100        1(5G14.0)                    -1  C1. Longitudinal dispersivity of layer  5
         .01           .01           .01           .01            .01
         .01           .01           .01           .01            .01
         .01           .01           .01           .01            .01
         .01           .01           .01           .01            .01
       100        1(5G14.0)                    -1  C1. Longitudinal dispersivity of layer  6
         .01           .01           .01           .01            .01
         .01           .01           .01           .01            .01
         .01           .01           .01           .01            .01
         .01           .01           .01           .01            .01
       100        1(5G14.0)                    -1  C1. Longitudinal dispersivity of layer  7
         .01           .01           .01           .01            .01
         .01           .01           .01           .01            .01
         .01           .01           .01           .01            .01
         .01           .01           .01           .01            .01
b)     100        1(5G14.0)                    -1  C2. TRPT=(horizontal transverse dispersivity) / (Longitudinal dispersivity)
         0.1           0.1           0.1           0.1            0.1
         0.1           0.1
c)     100        1(5G14.0)                    -1  C3. TRPV=(vertical transverse dispersivity) / (Longitudinal dispersivity)
         0.1           0.1           0.1           0.1            0.1
         0.1           0.1
d)     100        1(5G14.0)                    -1  C4. effective molecular diffusion coefficient [L^2/T]
           0             0             0             0              0
           0             0
```

a) | *AL*: The longitudinal dispersivity for every cell of the model grid (unit is Length). |

b) | *TRPT:* Real array defining the ratio of the horizontal transverse dispersivity to the longitudinal dispersivity.

c) | *TRPV:* The ratio of the vertical transverse dispersivity to the longitudinal dispersivity.

d) | *DMCOEF:* The effective molecular diffusion coefficient (unit L^2T^{-1})

Sink & Source Mixing Package file:

```
a)   F F F F F F
b)      2014
c)         7
d)         1         1         1         0         1         0       .25       .001
           2         1         1         0         1         0       .25       .001
           3         1         1         0         1         0       .25       .001
           4         1         1         0         1         0       .25       .001
           5         1         1         0         1         0       .25       .001
           6         1         1         0         1         0       .25       .001
           7         1         1         0         1         0       .25       .001
```

a) Logical flags for: | Well option | Drain option | Recharge option | Evapotranspiration option | River option | General-Head-Dependent-Boundary option |
If one of these options is set True, this must correspond with the data created by MODFLOW and written to MT3D.FLO file. If not PHT3D automatically adjust the logical flags of the SSM file to equal value as the MT3D.FLO file.

b) | *MXSS:* Maximum number of all point sinks and sources included in the flow model.

c) | *NSS:* The number op point sources whose concentrations need to be specified.

d) | *KSS | ISS | JSS:* layer, row and column of the point source for which a concentration needs to be specified.
| *CSS:* specified source concentration or mass loading rate. Not used for multi-species simulation, thus 0).
| *ITYPE:* integer indicating the type of the point source. 1 = constant head cell.
| *CSSMS(n):* input concentrations of all species for the defined source zone. In the file shown above, the concentration of only three components are shown. This because of the length of the file.

Generalized Conjugate Gradient Solver Package file:

```
a)        1        50         1         0
b)        1    .00001         0
```

a) | *MXITER:* Maximum number of outer iterations.
| *ITER1:* Maximum number of inner iterations.
| *ISOLVE:* type of preconditioners to be used with the acceleration scheme. 1= Jacobi.
| *NCRS:* integer flag for treatment of dispersion tensor cross terms. 0 = lump all dispersion cross terms to the right-hand side. This option is far less memory intensive as the alternative, to include the full dispersion tensor.

b) | *ACCL:* Relaxation factor for the SSOR option, not used in this model (as Jacobi is selected). Therefore default value of 1 is remained.
| *CCLOSE:* Convergence criterion in term of relative concentration.
| *IPRG:* Interval for printing the maximum concentration changes of each iteration. 0 = default for printing at the end of each stress period.

Chemical Reactions Package file:

```
a)        0         0         2         0
```

b) | *ISOTHM:* Flag indicating which type of sorption is simulated. 0 = No sorption is simulated.
| *IREACT:* Flag indicating which type of kinetic rate reaction is simulated. 0 = No kinetic rate reaction is simulated.
| *IRCTOP:* Integer flag indicating how reaction variable are entered. Is not relevant, as no sorption reactions included.
| *IGETSC:* Integer flag indicating that no initial concentration for sorbed or immobile phase has to be read (since no sorption).

Pht3d_ph file (descriptions from Prommer and Post, 2010):

```
a)    2 1   0                 25 0            1E-10          .001 4000
b)    0
c)    10
d)    5
e)    0    0
f)    0
g)    1              0               0               4
h)    0              0
i)    Pcesolute       2
            .979
            .3
      -formula Pcesolute 1.0 Pcenapl -1.0
j)    Permanganate
      Cl
      K
      Ca
      C(4)
      S(6)
      Na
      Br
      pH
      pe
k)    Dummypcenapl    1
                  0
      -formula Pcenapl -1.0 Permanganate- -1.33333 Cl- 4.0 Pyrolusitee 1.3333 H+ 2.66667 CO2 2.0
      Dummysom        2
                  4.32
                  3.333333E-02
      -formula Som -1.0 H+ -12.0 Permanganate- -12.0 Pyrolusitee 12.0 CO2 9.0
l)    Dummypce        1
                  5620
      -formula Pcesolute -1.0 Permanganate- -1.33333 Cl- 4.0  Pyrolusitee 1.3333 H+ 2.66667 CO2 2.0
m)    Dummypyrite     2
                  108
                  3.333333E-02
      -formula Pyritee -1.0 H+ -1.0 Permanganate- -5.0 Pyrolusitee 5.0  SO4-2 2.0 goethite 1.0
n)    Pcenapl
      Pyrolusitee
      Calcite
      Som
      Pyritee
```

a) |*OS:* Operating Splitting scheme;
2 = Sequential operator-splitting scheme with reactions calculated only after flow time steps.
|*TMP_LOC:*
|*RED_MOD:*
|*TEMP*= Temperature

|*ASBIN*: output: 0 = binary files only.
|*EPS_AQU*: activation/deactivation criteria.
|*EPS_PH:* activation/deactivation criteria.
|*PACK_SZ*:

b) |*NR_XXX_COMP:* Number of exchange components.
c) |*NR_INORG_COMP_EQU:* Number of aqueous components which are assumed to be in chemical equilibrium.
d) |*NR_MIN_EQU:* Number of mineral components which are assumed to be in chemical equilibrium.
e) |*NR_ION_EX:* Number of Exchange (Master) Species for which cation exchanging reactions should be considered.
f) |*NR_SURF:* Number of Surface (Master) Species.
g) |*NR_MOB_KIN:* Number of mobile components for which a rate expression is defined in the database file and the local equilibrium assumption is assumed to be invalid.
    |*NR_MIN_KIN:* Number of minerals for which a rate expression is defined in the database file and the local equilibrium assumption is assumed to be invalid.
    |*NR_SURF_KIN:* Kinetic surface-complexation reactions.
    |*NR_IMOB_KIN:* Number of immobile components for which a rate expression is defined in the database file and the local equilibrium assumption is assumed to be invalid.
h) |*NR_OUTSP_SPEC:*
    |*PR_ALKALINITY_FLAG:*
i) |*NR_MOB_KIN*: Mobile kinetic component.
    |*NR_KIN_PARM:* number of parameters needed by the kinetic rate expression as defined in the database file. If >0, values are defined below.
j) |*NR_INORG_COMP_EQU:* Aqueous components which are assumed to be in chemical equilibrium.
k) |*NR_IMOB_KIN:* Immobile kinetic component.
    |*NR_KIN_PARM:* Number of parameters needed by the kinetic rate expression as defined in the database file. If >0, values are defined below.
    |*FORMULA:* Stoichiometric relation.
l) *See k)*
m) *See k)*
n) *NR_MIN_EQU:* Immobile equilibrium components.

C. Database definitions of kinetic rate expressions for Reference scenario

Process	Description in database
| 1. Dissolution of nonaqueous PCE into the aqueous phase | ```
Pcesolute
-start
40   mPcenapl = equi("Pcenapl")
50   if (mPcenapl <=1e-8) then goto 200
60   solub_Pce = 0.0011928
70   mPcesolute = tot("Pcesolute")
80   rate = parm(1) * (solub_Pce - mPcesolute)   *
             (((mPcenapl)^(2/3))/((parm(2))^(2/3)))
90   moles = rate * time / 86400
100  if (moles > mPcenapl) then moles = mPcenapl
200 SAVE moles
-end
``` |
| 2. Oxidation of aqueous phase PCE by permanganate | ```
Dummypce
-start
1  rate = parm(1)
5  mPce = mol("Pcesolute")
20  if (mPce <= 1e-10) then goto 200
30  mPermanganate = mol("Permanganate-")
60  if (mPermanganate <= 1e-10) then goto 200
90  moles = rate * mPce * mPermanganate * time/86400
200 SAVE moles
-end
``` |
| 3. Oxidation of soil organic matter by permanganate | ```
Dummysom
-start
1  rate = parm(1)
10  mSom = equi("Som")
20  if (mSom <= 1e-10) then goto 200
30  mPermanganate = mol("Permanganate-")
40  ratio = (mSom / parm(2))^(2/3)
60  if (mPermanganate <= 1e-10) then goto 200
80  moles = rate * mSom * mPermanganate * time/86400
200 SAVE moles
``` |

| 4. Oxidation of pyrite by permanganate | ```
-end
Dummypyrite
-start
10  mPyrite = equi("Pyritee")
20  if (mPyrite <= 1e-10) then goto 200
30  mPermanganate = mol("Permanganate-")
60  if (mPermanganate <= 1e-10) then goto 200
70  rate = parm(1) * mPermanganate * 6 * (mPyrite)^(2/3)
80  moles = rate * time/86400
200 SAVE moles
-end
``` |

D. Database definitions of kinetic rate expressions for Instantaneous scenario

Process	Description in database
| 1. Dissolution of nonaqueous PCE into the aqueous phase | ```
Pcesolute
-start
40  mPcenapl = equi("Pcenapl")
50  if (mPcenapl <=1e-8) then goto 200
60  solub_Pce = 0.0011928
70  mPcesolute = tot("Pcesolute")
80  rate = parm(1) * (solub_Pce - mPcesolute) *
              (((mPcenapl)^(2/3))/((parm(2))^(2/3)))
90  moles = rate * time / 86400
100  if (moles > mPcenapl) then moles = mPcenapl
200 SAVE moles
-end
``` |
| 2. Oxidation of aqueous phase PCE by permanganate | ```
Dummypce
-start
1  rate = parm(1)
5  mPce = mol("Pcesolute")
10  mSom = equi("Som")
20  if (mPce <= 1e-10) then goto 200
30  mPermanganate = mol("Permanganate-")
40  mPcenapl = equi("Pcenapl")
45  mPyrite = equi("Pyritee")
50  oxydizerdemand = mPcenapl * 4/3 + mSom * 12 + mPyrite *5
60  if (mPermanganate <= 1e-10) then goto 200
70  if (mPermanganate <= oxydizerdemand) then goto 200
80  overdosepermanganate = mPermanganate - oxydizerdemand
90  moles = overdosepermanganate * 4/3   * rate * time/86400
200 SAVE moles
-end
``` |
| 3. Oxidation of soil organic matter by permanganate | ```
Dummysom
-start
1  rate = parm(1)
10  mSom = equi("Som")
20  if (mSom <= 1e-10) then goto 200
``` |

```
30  mPermanganate = mol("Permanganate-")
40  mPcenapl = equi("Pcenapl")
45  mPyrite = equi("Pyritee")
50  oxydizerdemand = mPcenapl * 4/3 + mSom * 12 + mPyrite *5
60  if (mPermanganate <= 1e-10) then goto 200
70  if (mPermanganate >= oxydizerdemand) then goto 150
80  moles = mSom * 12 /oxydizerdemand * mPermanganate /12 * rate * time/86400
130 goto 200
150 moles = mSom * rate * time/86400
200 SAVE moles
-end
```

4. Oxidation of pyrite by permanganate

```
Dummypyrite
-start
1   rate = parm(1)
10  mPyrite = equi("Pyritee")
20  if (mPyrite <= 1e-10) then goto 200
30  mPermanganate = mol("Permanganate-")
40  mPcenapl = equi("Pcenapl")
45  mSom = equi("Som")
50  oxydizerdemand = mPcenapl * 4/3 + mSom * 12 + mPyrite * 5
60  if (mPermanganate <= 1e-10) then goto 200
70  if (mPermanganate >= oxydizerdemand) then goto 150
80  moles = mPyrite * 5/ oxydizerdemand * mPermanganate/5 * rate * time/86400
130 goto 200
150 moles = mPyrite * rate * time/86400
200 SAVE moles
-end
```

E.   Permanganate use and distribution over the different reductants.

Field characteristic scenarios
% of total injected permanganate used in oxidation reactions

Field characteristics scenarios
Distribution of the used permanganate over the different reductants

Remediation scenarios
% of total injected permanganate used in oxidation reactions

Remediation scenarios
Distribution of the used permanganate over the different reductants

- % used for oxidation SOM
- % used for oxidation Pyrite
- % used for oxidation PCE